

MECHANICAL BEHAVIOR OF DIP-BRAZED ALUMINUM SANDWICH PANELS

By

Brian P. Hohmann

B.S., Ceramic Engineering (2004)
Rutgers University

Submitted to the Department of Materials Science and Engineering in partial fulfillment
of the requirements for the degree of

Master of Science
in Materials Science and Engineering

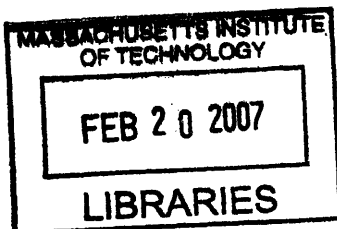
At the
Massachusetts Institute of Technology
February 2007

© Massachusetts Institute of Technology
All rights reserved

Signature of Author.....
Department of Materials Science and Engineering
January 16, 2007

Certified by.....
Thomas W. Eagar
Professor of Materials Engineering and Engineering Systems
Thesis Supervisor

Accepted by.....
Samuel M. Allen
POSCO Professor of Physical Metallurgy
Chair, Departmental Committee on Graduate Students



ARCHIVES

This page intentionally left blank

MECHANICAL BEHAVIOR OF DIP-BRAZED ALUMINUM SANDWICH PANELS

By

Brian P. Hohmann

Submitted to the Department of Materials Science and Engineering on January 16, 2007
in partial fulfillment of the requirements for the Degree of Master of Science
in Materials Science and Engineering

Abstract

An experimental study was carried out to determine the mechanical behavior of sandwich panels containing cellular cores of varying shape. Compression and four point bend tests were performed on sandwich panels with square and triangular honeycomb cores. These honeycombs were made of perforated aluminum sheet of repeating diamond and hexagonal patterns. The sandwich panel assemblies were joined via dip brazing. Defects were introduced into some panels to quantify the effect on strength and stiffness. Hybrid sandwich panels, consisting of foam material in the void spaces of the square and triangular cells were evaluated for the effect on the defect tolerance of the structures.

The results showed that sandwich panels with diamond shaped cores had compressive strengths approximately four times greater than hexagonal shaped cores. In four point bending the diamond cores were approximately twice as stiff as cores made from hexagonal patterned sheet. The introduction of defects lowered strength by about 30% for diamond cores in compression, and about 15% for hexagonal cores. In four point bending this strength reduction was not as significant due to shear stresses damaging periodicity at a faster rate than in compression. The use of foam within the cells resulted in higher absolute peak compression and flexure loads, however the Load/Density ratios demonstrated cases where the added weight of the foam did not result in a better panel. A difference of nearly an order of magnitude between the highest and lowest compressive and flexure loads is evident when the presence of defects and foam are taken into account.

Thesis Supervisor : Thomas Eagar

Title : Professor of Materials Engineering and Engineering Systems

Acknowledgements

I have many people to thank since my arrival at MIT. First and foremost I must thank my parents for their continuous support in all my efforts. They have always told me to reach for my dreams, and without them I would not be the man I am today. Much love also goes to my sisters, Jennifer and Colleen, for always being there to support their baby brother.

Besides my family, the most important person to influence my life since I came to MIT has been my thesis advisor, Thomas Eagar. I am forever grateful for the respect, guidance, and leadership he has shown me since we first met.

I must thank all the staff members of the Welding and Joining Lab, including Jeri Hill, Harold Larson, and Don Galler for their support and assistance over the years.

I would not have kept my sanity if not for my fellow group members. Particular thanks go to Joel Williams and Chris Musso for helping get through my first year of grad school. Thanks also goes to Neil Jenkins, Vee, and my partner in crime Dave Fischer for keeping the office an enjoyable place to come to every day.

To my friends, especially Jay Trelewicz and Trey Holzwarth, thanks for giving me a reason to leave the lab and go enjoy the sights (and bars) of Boston.

Finally I'd like to thank all of the UROPs, in particular Gene Settoon, and everyone else who helped make this possible.

Table of Contents

Abstract	3
Acknowledgements	4
Table of Contents	5
List of Figures	8
List of Tables	10
Chapter 1 : Introduction	11
1.1 Scope of Thesis	11
1.2 Overview of Thesis	12
Chapter 2 : Background	14
2.1 Cellular Materials	14
2.2 Sandwich Panel Design	18
2.2.1 <i>Honeycombs</i>	20
2.2.2 <i>Metal Foams</i>	28
2.2.3 <i>Truss Structures and Lattice Block Materials (LBM)</i>	33
2.2.4 <i>Failure Mechanisms and Optimal Designs</i>	39
2.3 Material Selection	43
2.3.1 <i>Aluminum Alloys</i>	43
2.3.2 <i>Relation between material selection and application</i>	45
2.4 The Dip-Brazing Process	49
Chapter 3 : Experimental Procedure	52
3.1 Procedure for laboratory samples	52
3.1.1 <i>Materials</i>	52
3.1.2 <i>Dip Bath Preparation</i>	54
3.1.3 <i>Sample Preparation</i>	56
3.2 Procedure for procured samples	60
3.3 Microscopy	66
3.3.1 <i>Scanning Electron Microscopy</i>	67
3.3.2 <i>Light Optical Microscopy</i>	69
3.4 Mechanical Testing	69
3.5 Simulations	69
Chapter 4 : Experimental Results	73
4.1 Mechanical Testing Results	73
4.1.1 <i>Compression results</i>	73
4.1.2 <i>Four point bend results</i>	83
4.2 Metallographic analysis	89
4.3 Simulation Results	91
Chapter 5 : Conclusions	93
Appendix A : Background on the Importance of Welding and Joining	97
Appendix B : Background on Aluminum Alloys	101

Appendix C : Data from Mechanical Tests	103
Appendix D : Time Lapse Photography of Mechanical Tests	108
References	158
About the Author	161

This page intentionally left blank

List of Figures

	Page
Figure 2.1 : Example of a) honeycomb [2] and b) open cell foam [3].....	14
Figure 2.2 : a) Square and b) Triangular repeating 2-D cells.....	15
Figure 2.3 : Example of a hybrid sandwich panel.	15
Figure 2.4 : Packing of 2-D cells to fill space. (from [1])	17
Figure 2.5 : Schematic of a typical sandwich panel (from [4])	18
Figure 2.6 : The HOBE manufacturing process (from [11])	21
Figure 2.7 : Loading directions for hexagonal honeycomb (from [1])	22
Figure 2.8 : In plane compressive behavior of metallic honeycombs (from [12])	22
Figure 2.9 : Elastic buckling of hexagonal cell. (from [1])	24
Figure 2.10 : Young’s modulus as a function of direction for square, triangular, and hexagonal honeycombs (from [1])	25
Figure 2.11 : Effect of randomly located defects on (a) modulus and (b) strength of intact Voronoi honeycombs (•), and defective hexagonal (■) and Voronoi (♦) honeycombs (from [13])	27
Figure 2.12 : The process steps used in the manufacture of (a) Alporas ® and (b) Duocel ® (from [6])	30
Figure 2.13 : Bending dominated mechanism in an open cell foam (from [4])	30
Figure 2.14 : Formation of plastic hinges in an open cell foam (from [4])	32
Figure 2.15 : Five lattice truss topologies (from [20])	33
Figure 2.16 : Schematic of perforation and deformation shaping process (from [20])	34
Figure 2.17 : Asymmetric response of truss loaded in 3-point bend. (from [24])	35
Figure 2.18 : Compressive stress-strain response for solid and hollow pyramidal lattice truss sandwich structures (from [21])	36
Figure 2.19 : Compressive stress- strain response of diamond and square hollow truss lattices made from 304 SS (from [25])	37
Figure 2.20 : Compressive curves for (a) annealed core and (b) age hardened core of aluminum tetrahedral lattice truss structures (from [20])	38
Figure 2.21 : Failure modes in sandwich panels (from [6])	39
Figure 2.22 : Sandwich panel loaded in four point bending (from [27])	40
Figure 2.23 : Mode A and Mode B core shear under loading (from [27])	40
Figure 2.24 : The energy absorption capabilities of metal foams (from [4])	42
Figure 2.25 : The U.S. Navy’s “Sea Fighter” (concept drawing courtesy U.S. Navy)	47
Figure 2.26 : Typical dip brazing process (from [31])	49
Figure 3.1 : Specifications of the (a) diamond perforated and (b) hexagonal perforated sheet for laboratory experiments (from [44])	53
Figure 3.2 : High temperature furnace [45]	54
Figure 3.3 : Laboratory cleaning and dip brazing assembly.....	55
Figure 3.4 : EDM cutting of samples.....	56
Figure 3.5 : Deformation shaped sandwich core.....	57
Figure 3.6 : Wrapping with Chromel ® wire.....	58
Figure 3.7 : Size difference between procured panels and laboratory panels.....	61
Figure 3.8 : Closed and open cell metallic foams.[46]	62
Figure 3.9 : Polymeric foam filled sandwich panel.....	63
Figure 3.10 : Metal-metallic foam hybrid sandwich panel produced in laboratory.....	63
Figure 3.11 : a) Panel filled with Alporas ® b) Panel filled with Duocel ® c) Close-up of metal foam filler snugness.	65
Figure 3.12 : a) Triangular core defect b) Square core defect.....	66
Figure 3.13 : SEM image of brazed joint from laboratory produced sample.....	68
Figure 3.14 : Polymer/Metal interface.....	68
Figure 3.15 : CAD drawings of shaped perforated cores.....	70
Figure 3.16 : CAD drawing of sandwich panel with foam filler.....	71
Figure 3.17 : Assembly of hexagonal square cell sandwich panel	72
Figure 4.1 : Load-extension curve for three samples of a diamond square pattern with polymeric foam and no defects.....	75

	Page
Figure 4.2 : Crushing occurs in (a), while buckling occurs in (b)	77
Figure 4.3 : Load-extension curve for two samples of hexagonal square core, no foam, no defects...	78
Figure 4.4 : Polymer filled diamond triangular panels (a) without defects and (b) with defects.....	79
Figure 4.5 : Polymer filled hexagonal square panels (a) without defects and (b) with defects.....	80
Figure 4.6 : Hexagonal Triangular sandwich panel cores, filled with Alporas. There is no significant difference due to the presence of defects for this cell architecture.	81
Figure 4.7 : Flexure load-extension curves for (a) no foam, no defects and (b) polymeric foam, no defects for diamond triangular core panels.....	84
Figure 4.8 : Sandwich panels with polymeric foam filling, no defects and (a) diamond square core and (b) diamond triangular core.....	85
Figure 4.9 : Effect of metallic foam on load-extension curves. (a) diamond square core and (b) hexagonal triangular core.....	87
Figure 4.10 : Comparison of microstructures of (a) laboratory panel and (b) procured panel. All scales are in terms of mm.....	89
Figure 4.11 : Silicon interdiffusion into bulk aluminum brazed joint. Mag=50x. Scale in mm.	90
Figure 4.12 : Needle like Mg ₂ Si phase in the procured sample. Mag =200x . Scale in mm.	90
Figure 4.13 : Stress simulation results for diamond square sandwich panels.....	91
Figure A.1: Oxyacetylene welding process schematic [48] (figure courtesy of Granta Design, Cambridge UK)	98
Figure A.2 : Typical brazing process schematic [48] (figure courtesy of Granta Design, Cambridge UK)	99

List of Tables

	Page
Table 2.1 : Features of cellular metals and quality criteria on a macroscopic scale (from [5])	16
Table 2.2 : Properties of isolated cells (adapted from[1])	17
Table 2.3 : Theoretical in-plane mechanical properties of various periodic honeycomb cell structures (from [12])	26
Table 2.4 : Properties of commercial metal foams (from [6])	29
Table 2.5 : Comparison between monolithic AA6061-T6 and Steel	45
Table 2.6 : Advantages and Limitations of Molten Salt [40]	50
Table 3.1 : Pre-cleaning procedure for laboratory samples	58
Table 3.2 : Observations of different dipping parameters	59
Table 3.3 : Post cleaning procedure for laboratory produced samples	60
Table 4.1 : Effect of defects and polymeric foam for each core type	74
Table 4.2 : Load/Density Ratios for Hexagonal and Diamond perforations	76
Table 4.3 : Effect of Metal Foam Filler on Load/Density Ratio	78
Table 4.4 : Effect of Defects when No Foam, Polymeric Foam, and Alporas foam were used as filler	82
Table 4.5 : Percentage change in the Load/Density ratio for four point bend tests	83
Table 4.6 : Ratio of Hexagonal to Diamond patterned Load/Density values	86
Table 4.7 : Metal foam filler effect on Load/Density ratios	86
Table 4.8 : Defect/No Defect ratios on Load/Density values for experiments	88
Table 5.1 : Maximum and minimum peak compressive loads attained for each core type	93
Table 5.2 : Maximum and minimum peak flexural loads attained for each core type	93
Table A.1 Comparison of Welding, Brazing, and Soldering Processes (adapted from [4])	100
Table B.1 : Aluminum Alloy Designations	101
Table B.2 : Tempers of Aluminum Alloys	102
Table B.3 : Common solution heat treated tempers	102

Chapter 1 : Introduction

1.1 Scope of Thesis

Structural cellular materials provide the dual benefit of light weight and high strength. Both weight and strength are directly related to the cell shape and orientation of the structural cellular solid. Any defect in the periodicity of the cellular material, be it missing cell members or the deformation of the cell shape result in significant deterioration of the material properties of the entire structure. The ability to withstand loads yet maintain structural integrity is essential for materials used in critical applications.

Sandwich panels consist of two thin facesheets bonded to a lightweight core. Structurally, sandwich panels are very efficient and achieve both high strengths and high stiffnesses. Because of this, sandwich panels are promising substitutes for monolithic materials in naval vessels. In particular, the ability to use aluminum sandwich panels instead of steel can result in significant weight savings and allow for faster operating speeds. Significant challenges exist that must be addressed before aluminum sandwich panels could become a feasible alternative to steel. With expected operating lives of fifty years in naval vessels, sandwich panels will need to maintain their mechanical properties without deforming. A robust joining method to assemble the sandwich panels is a necessity, and adhesive bonding could not be used as a long term solution. The complex shapes of the cellular materials would further constrain the choices of joining method. Finally, as the introduction of defects in the structure is inevitable with such lengthy service lives, the ability to tolerate defects without significant deterioration of properties is not only desirable but necessary.

This thesis has investigated the mechanical properties of two dimensional cellular sandwich panels. The cores of these panels consisted of square and triangular honeycombs. These honeycombs were made up of perforated aluminum sheet of repeating hexagonal and diamond patterns. Compressive and four point bend tests evaluated the mechanical response of these sandwich panels, and additional experiments were performed to quantify the utility of hybrid sandwich panels. The hybrid panels contained foam in the void spaces of the square and triangular cells. Polyurethane foam, open cell metallic foam, and closed cell metallic foam were analyzed. Finally, panels with defects intentionally introduced into the core were tested to determine the defect tolerance of these varying structural panels.

1.2 Overview of Thesis

This thesis contains five chapters as well as appendices. This chapter has served to define the scope of the thesis as well as to outline the remaining chapters. Chapter 2 contains background on the properties of cellular materials, the design of sandwich panels, material selection, and the dip brazing joining process. The experimental procedure of this thesis is discussed in detail in Chapter 3 for both experiments performed in the lab to determine the feasibility of dip brazing and the mechanical tests performed on procured sandwich panels. Chapter 4 contains the results and discussion from the mechanical tests performed. Chapter 5 identifies conclusions based upon these results. Appendix A provides a discussion on the significance of the system design on selection of the joining process. Appendix B provides background on the varying options possible for aluminum alloy selection. Appendix C contains mechanical test data while

Appendix D includes time lapse photography from both the compressive tests and bending tests.

Chapter 2 : Background

2.1 Cellular Materials

This thesis involves the integration of cellular materials in three distinct aspects of the design process, therefore it is critical to clearly define all terms to avoid confusion. A cellular solid is an assembly of cells packed together to fill space. For this thesis the terms cellular solid and cellular material are interchangeable. Cellular materials which pack to fill space in two dimensions are called honeycombs while cellular materials that fill space in three dimensions are called foams [1]. Open cell foams contain cells that connect through open faces such that only the edges of the foam are solid, while in a closed cell foam the edges and faces are solid and each cell is sealed off from neighboring cells [1]. Figure 2.1 shows examples of both honeycombs and foams.

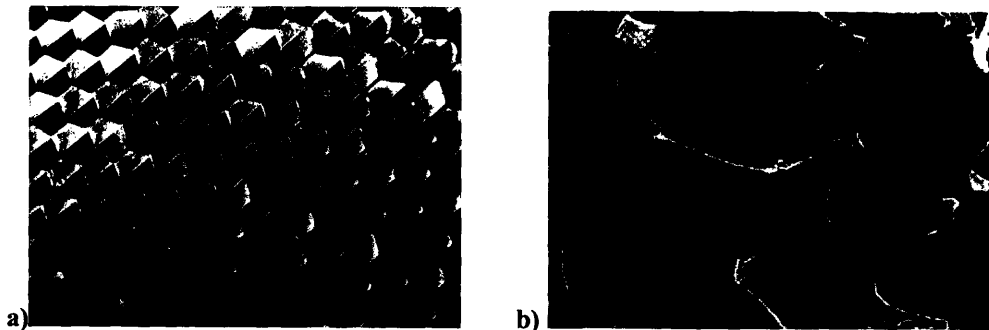
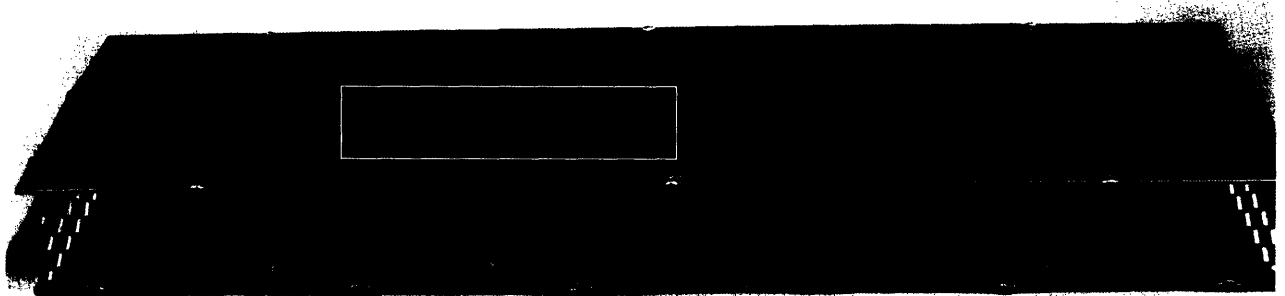


Figure 2.1 : Example of a) honeycomb[2] and b) open cell foam [3]

Throughout this thesis, the term honeycomb will refer to repeating 2-D cells, however honeycomb will not necessarily refer to a six sided polygon. A diamond honeycomb will refer to a 2-D repeating diamond pattern, and hexagonal honeycomb will be used for a 2-D repeating hexagonal pattern. Open cell and closed cell metallic foam as well as polyurethane foam will be discussed in this thesis. The term periodic repeating

cell will refer to the cell shape of the cores of the sandwich panels analyzed. Square and triangular periodic repeating cells, seen in Figure 2.2, have been examined. When a foam

(a)



(b)

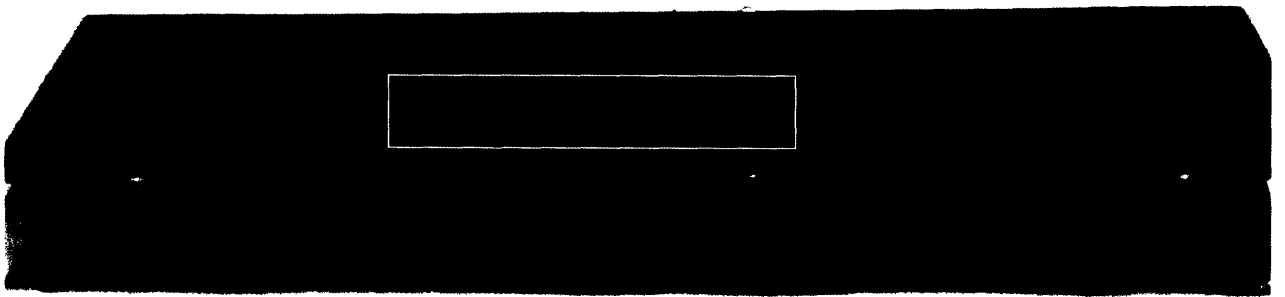


Figure 2.2 : a) Square and b) Triangular repeating 2-D cells

material is used to fill the void space of the periodic repeating cells, as shown in Figure 2.3, the resulting sandwich panel core will be referred to as hybrid [4]. An analysis of truss and lattice block structures, which fall under the category of periodic cellular structures, will also be made. Finally, the term defect will refer to any non-uniformity in the periodicity of the repeating cellular structure. When discussed in the context of foams, “defect” will refer to irregularities in cell features such as pore size and shape.

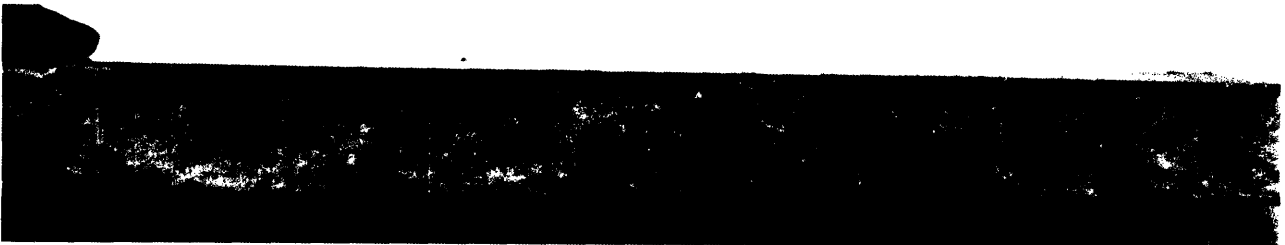


Figure 2.3 : Example of a hybrid sandwich panel. This particular hybrid contains a core consisting of metallic triangular repeating cells with polymeric foam filling the void space.

The properties of cellular materials in both two and three dimensions depend directly on the shape and structure of the cells. The relative density of a cellular solid, ρ^*/ρ_s , where ρ^* is the density of the cellular material and ρ_s is the density of the solid monolithic material from which it is made, is an extremely important structural characteristic [1]. Most mechanical properties depend weakly on cell size, however the cell shape is a much more important characteristic [1]. Small deviations in the cell shape can result in large differences in mechanical properties due to the resulting anisotropy. This is especially important for foams which have a random cell orientation in three dimensions. Table 2.1 lists features of cellular metals and corresponding quality criteria. Mechanical properties can also be profoundly affected for particular loading directions.

Table 2.1 : Features of cellular metals and quality criteria on a macroscopic scale (from [5])

<i>Features</i>	<i>Quality goals</i>	<i>Quality criteria</i>	<i>Defect evidence</i>	<i>Quality testing</i>
Cell architecture	Reproducible and similar throughout the sample	Reproducible processing parameters	Unsatisfactorily controlled parameters	Process records, assessment of relevant parameter variations
Dimensional accuracy	Tolerances of outer dimensions achieved	Specified variations in lengths and radii	Dimensions beyond tolerances	Contour measurements
Surfaces	Reproducible surface features	Properties, roughness, open porosity	Dents and blisters Surface porosity index	Roughness measurement, Dye penetrant tests, Chemical analysis, hardness
Metal matrix	Defined chemical composition	Uniform solid properties	Scatter in chemical analysis of different positions	Chemical analysis of ingredients and product
Mass distribution	Reproducible density	Apparent mass density within specifications	Scatter in average mass density; asymmetry of mass distribution	Density measurements, Determination of centers of gravity of shape and mass
Properties	Properties unambiguously related to structural quality	Property values within specifications	Scatter beyond specifications	Representative tests, Correlation to structure, Service performance

Even when the cell shape is held constant, different stacking methods can result in structures with different properties based on the varying connectivity of the cell edges in two dimensions [1]. Figure 2.4 represents the varying ways cells can be stacked to fill space. The edge connectivity is defined as the number of edges which meet at a vertex

and is represented by Z_e . Typically this value is three in honeycombs and four in foams, but other values are also possible based on stacking methods [1]. Table 2.2 lists the geometric properties of particular cell shapes.

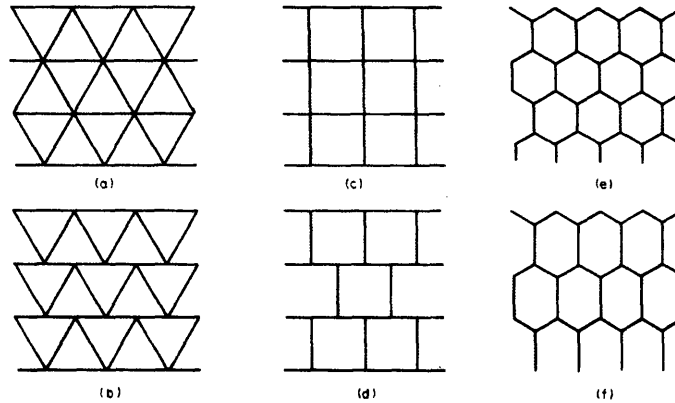


Figure 2.4 : Packing of 2-D cells to fill space. In (a) $Z_e=6$, (b) $Z_e=4$, (c) $Z_e=4$, (d) $Z_e=3$, (e) regular hexagons (f) irregular hexagons [from [1]]

Table 2.2 : Properties of isolated cells (adapted from[1])

Cell Shape	# of faces	# of edges	# of vertices	Cell Volume	Surface Area
Tetrahedron	4	6	4	$0.118l^3$	$\sqrt{3} l^2$
Triangular prism	5	9	6	$(\sqrt{3}/4) l^3 A_r$	$(\sqrt{3}/2) l^2 (1+2\sqrt{3} A_r)$
Square prism	6	12	8	$l^3 A_r$	$2l^2 (1+2A_r)$
Hexagonal prism	8	18	12	$((3\sqrt{3})/2) l^3 A_r$	$(3\sqrt{3}) l^2 (1+2A_r/\sqrt{3})$

(Note : A_r is the aspect ratio)

The influence of the relative density and cell architecture on mechanical properties is complex. In contrast to fully dense monolithic materials which have definitive material constants such as Young's and shear moduli, cellular solids have *effective* material constants that are dependant on cell architecture [5]. The determination of these effective properties becomes even more complex for hybrids. An understanding of these properties is necessary to adequately describe the deformation mechanisms that take place in honeycombs, foams, and hybrids. The deformation mechanisms are

intrinsically related to how defects affect the cell architecture, by either reducing the edge connectivity or altering the cell shape. A thorough analysis of the deformation mechanisms of the sandwich panels examined in this research will be made.

Cellular materials have applications across multiple industries. These applications include thermal insulation, packaging, and structural. In each of these industries the properties of the cellular solid is tailored to the desired application. This thesis is limited to analyzing sandwich panels. Sandwich panels are multifunctional and can be used as heat exchangers, as lightweight airplane components, and as blast absorbers in ballistics to name a few. This thesis is only concerned with the structural capabilities of sandwich panels, and therefore light weight and high stiffness are the two most important parameters.

2.2 Sandwich Panel Design

A sandwich panel, as seen in Figure 2.5, consists of two identical facesheets of thickness t bonded to a core of thickness c . Sandwich panels offer high stiffness at low weight, which make them very attractive for structural applications. Commonly,

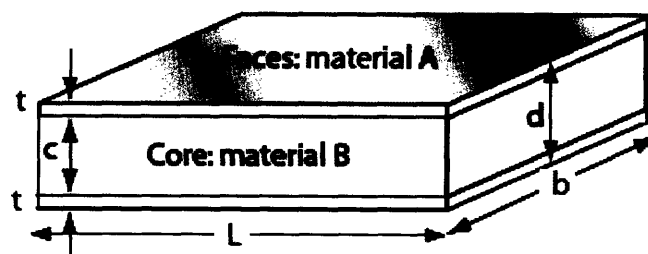


Figure 2.5 : Schematic of a typical sandwich panel (from [4])

the cores of such panels are made of balsa wood, foamed polymers, or glue bonded aluminum[6]. These materials have drawbacks which preclude their use as structural materials in naval vessels. In particular, their properties are moisture dependant and they cannot generally be used above room temperature [6]. For this reason, novel core designs including metallic foams, trusses, and lattice block materials have recently gained attention.

Many theoretical calculations on the mechanical properties of sandwich panels have been made. Experimental results have not achieved these theoretical expectations however, and “knock-down” factors ranging from 2 to 100 have been seen on commercially available cellular metals [7]. There are two reasons why theoretical estimates of strength are unattainable. The first is that theoretical calculations assume a perfectly bonded interface between the core and facesheets of a sandwich panel [6]. However most sandwich panels are adhesively bonded, which can never result in a perfect bond since surface contaminants are not removed in this joining process [8]. The second reason has to do with the role defects play in both the manufacture of the panels and on the onset of deformation. Since the mechanical properties of cellular structures depend on cell shape, any deviation from the nominal repeating pattern will diminish overall properties [7]. Reducing defects is necessary in minimizing these knock down factors and optimizing sandwich panel design.

Sandwich panels are by no means a new technology. The first aircraft sandwich panel was fabricated in 1919, and manufacture of modern structural honeycombs began in the late 1930's [9]. Mike Ashby, one of the leading modern material scientists, has said, “Innovation in engineering often means the clever use of a new material—new to a

particular application, but not necessarily new in the sense of recently developed.” [10]

This thesis is unique from previous sandwich panel research for two reasons; the first being dip brazing as the method of joining the sandwich panel together. Appendix A contains a background on the importance of welding and joining in the design process. The second, and most important reason, involves the use of cellular materials in multiple levels of the core design. The sandwich panels fabricated for this research have a core consisting of two dimensional periodic repeating cells, but the innovation comes in the fact that these cells themselves are made up of cellular materials in a perforated pattern. This type of design allows an even greater weight savings without sacrificing structural integrity. The utility of this design can only be determined after a discussion of competing sandwich panel technologies.

2.2.1 Honeycombs

Hexagonal honeycombs are the most recognizable structural sandwich panel design, and a greater amount of research has been done on honeycombs than any of the other competing core designs. Hexagonal honeycombs are usually fabricated by an expansion manufacturing process, as seen in Figure 2.6. This honeycomb before expansion, or HOBE process for short, works well for low density honeycombs with thin webs [11]. The result is a cost effective process, however adhesives are used to achieve bonding in this process. For this research, adhesive bonding was precluded as a method

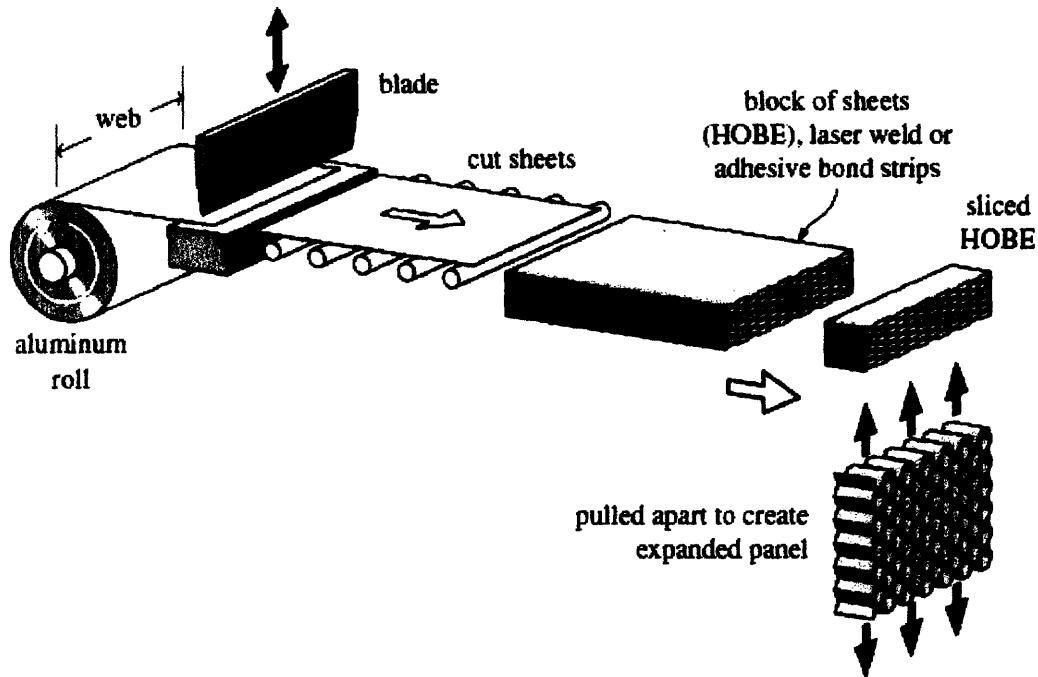


Figure 2.6 : The HOBE manufacturing process (from [11])

of joining the cellular core to the facesheets. Laser welding is an option for this type of honeycomb, however the cost effectiveness of the process is lost due to the complex geometry.

The properties of hexagonal honeycombs vary greatly depending on whether loading is in plane or out of plane. In plane loading is defined as loading in the X_1 - X_2 plane, while out of plane loading is in the X_3 direction. Figure 2.7 represents these loading directions for a hexagonal honeycomb. The in plane stiffness and strength are the lowest because stresses in this plane make the cell walls bend, while the out of plane stiffness and strength are larger due to the required axial compression of the cell walls [1].

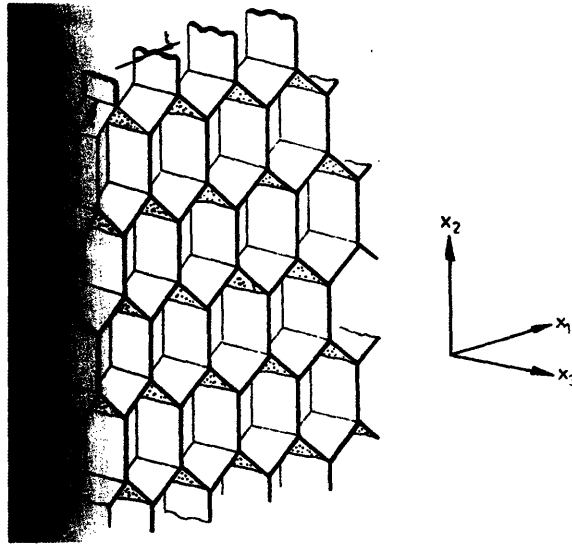


Figure 2.7 : Loading directions for hexagonal honeycomb (from [1])

The in plane analysis highlights the mechanisms by which the cellular material will deform and fail, while the out of plane analysis describes the stiffness of the honeycomb.

Figure 2.8 shows the mechanical response of honeycombs under in plane compression. The compressive stress-strain behavior is characterized by three regimes.

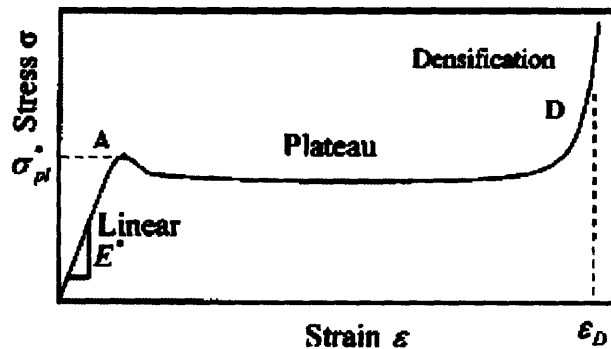


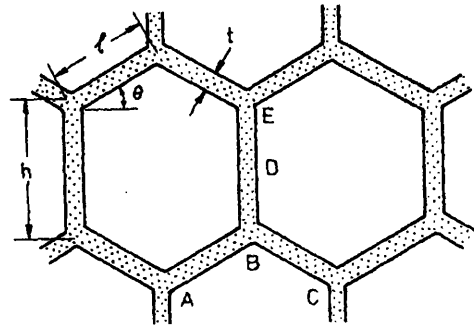
Figure 2.8 : In plane compressive behavior of metallic honeycombs (from [12])

The first regime shows a linear elastic response, followed by a plateau regime of roughly constant stress, and finally a densification regime of steeply rising stress following significant crushing [12]. Each regime is associated with a mechanism of deformation. Upon loading, the cell walls bend, leading to a linear elastic regime. Beyond a critical

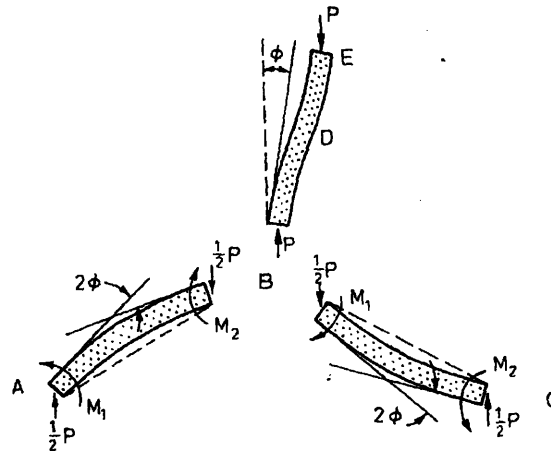
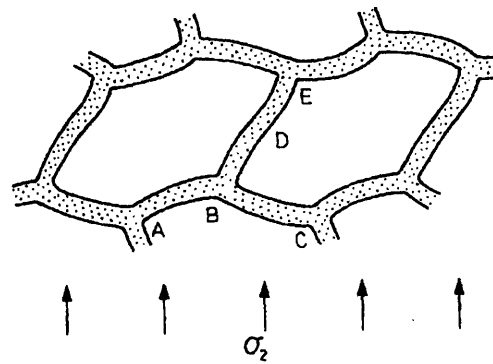
stress (point *A* in Figure 2.8) the cells begin to collapse either by elastic buckling, plastic buckling, or brittle fracture depending on the nature of the cell wall material [1]. At high strains the opposing cell walls have collapsed to the point of touching, and further deformation leads to densification (point *D*) of the material resulting in a steep increase in stiffness [12].

Out of plane deformation for a hexagonal honeycomb results in a similarly looking stress-strain curve as in Figure 2.8. The initial linear elastic regime for out of plane deformation involves significant shear of the cell walls [1]. Sandwich panels loaded in bending are a good example of this out of plane shear. For out of plane compression the linear elastic regime is truncated due to buckling and final failure is by tearing or crushing [1]. Figure 2.9 shows the elastic buckling of a hexagonal cell.

It is useful to compare the deformation mechanisms of hexagonal honeycombs with other two dimensional honeycomb cell shapes. The in plane elastic constants for square and triangular honeycombs differ in a fundamental way from hexagonal cells because in certain directions of loading the bending moments of the cell walls equal zero [1]. This results in a typical increase in moduli by a factor of $(l/t)^2$ in these directions as compared with directions where bending is possible. Figure 2.10 shows how the Young's modulus varies with direction for square and triangular cells. From this figure it is apparent that triangular and hexagonal cells are isotropic, but triangular cells are much stiffer. Square cells on the other hand are very anisotropic, with two stiff directions and two compliant directions. It should be noted that any imperfection in these cell shapes increases the bending contribution to the deformation and decreases the modulus [1].



(a)



(b)

Figure 2.9 : Elastic buckling of hexagonal cell. In (a) the cell is undeformed. In (b) the buckling mode in uniaxial loading as well as the associated forces and moments are represented (from [1])

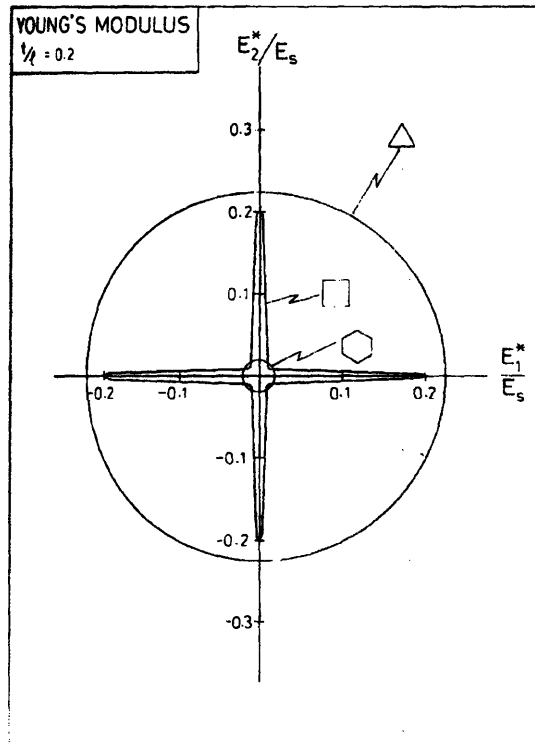
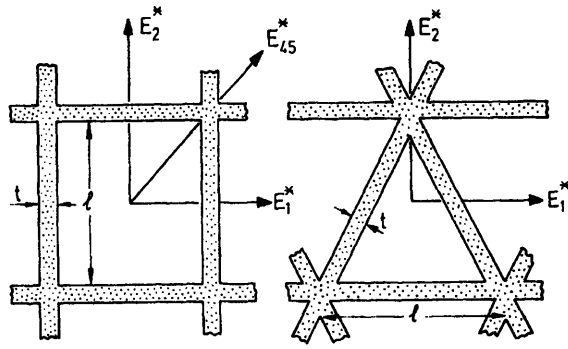
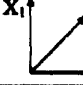
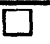








Figure 2.10 : Young's modulus as a function of direction for square, triangular, and hexagonal honeycombs (from [1])

Wang and McDowell [12] investigated the in plane mechanical properties of seven different cell types of two dimensional honeycombs. Their results are summarized in Table 2.3. Simple beam/column theory was used to derive these first order mechanical

Table 2.3 : Theoretical in-plane mechanical properties of various periodic honeycomb cell structures (from [12])

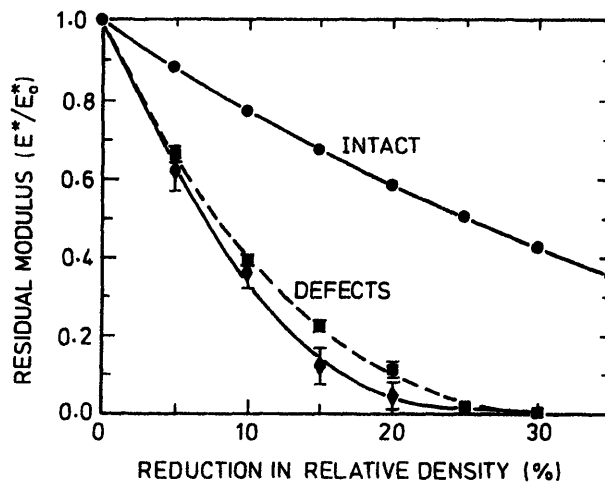
	Relative density $r = \rho^* / \rho_s$	E_1^* / E_s or E_2^* / E_s	G_{12}^* / E_s	ν_{12}^*	σ_n^* / E_s	σ_μ^* / σ_n	τ_μ^* / σ_n	E_{shear}^* / E_s	$\frac{(\sigma_\mu^*)_{max}}{\sigma_n}$	r_{crit}
Square Cell 	$2/1$	$0.5r$	$0.0625r^3$	$0.5\nu_s, r$	$0.103r^3$	$0.5r$	$0.125r^2$	$0.25r^3$	$0.25r^2$	0.0698
Hexagonal Cell 	$(2/\sqrt{3})/1$	$1.50r^3$	$0.375r^3$	1.0	$0.143r^3$	$0.5r^2$	$0.217r^2$	—	—	0.0035
Triangular Cell 	$2\sqrt{3}/1$	$0.333r$	$0.125r$	0.333	$0.0914r^3$	$0.5r$ $0.333r$	$0.289r$	—	—	0.0604
Mixed Cell 	$(2+\sqrt{2})/1$	$0.369r$	$0.104r$	0.146	$0.0292r^3$	$0.369r$	$0.207r$	$0.293r$	$0.293r$	0.0594
Kagome Cell 	$\sqrt{3}/1$	$0.333r$	$0.125r$	0.333	$0.366r^3$	$0.5r$ $0.333r$	$0.289r$	—	—	0.0301
Diamond Cell 	$(5/\sqrt{3})/1$	$0.4r$ $0.2r$	$0.15r$	0.333	$0.0789r^3$	$0.6r$ $0.2r$	$0.346r$	—	—	0.0502
Rectangular Cell 	$\frac{at_2 + bt_1}{ab}$	t_1/a t_2/b	$t_1^2 t_2^2$ $ab(at_1^2 + bt_2^2)$	$\nu_{12} = \nu_s \frac{t_1}{a}$ $\nu_{21} = \nu_s \frac{t_2}{b}$	$\frac{\pi^2 t_1^2}{12 ab^2}$ $\frac{\pi^2 t_2^2}{12 a^2 b}$	t_1/a t_2/b	$\frac{1 t_2^2}{2 ab}$	$\frac{(a^2 + b^2)^2 t_1^2 t_2^2}{a^3 b^3 (at_1^2 + bt_2^2)}$	$\frac{t_2^2 (a^2 + b^2)}{2 a^2 b^2}$	—

Note: The elastic buckling values are calculated in the directions of the lowest buckling load for each honeycomb, and are based on a ratio of yield strength to Young's modulus of 0.001 (see Appendix 1). The rectangular cell has aspect ratio a/b , where a is the length in the X_2 direction, and b is the length in the X_1 direction, and the cell wall thicknesses are t_1 and t_2 for cell edges of lengths b and a , respectively; typically, $t_1 > t_2$.

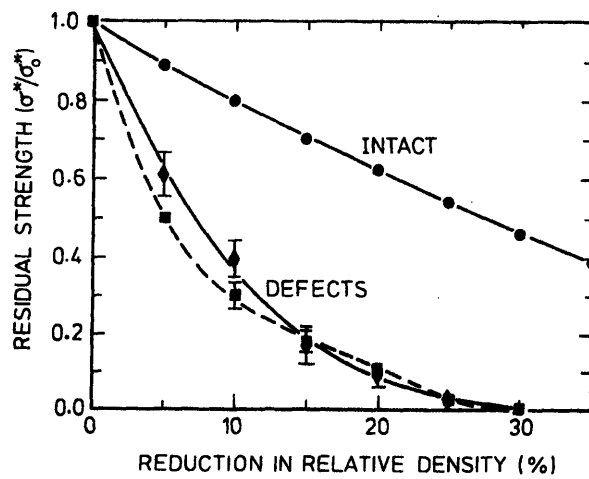
properties. Wang and McDowell determined the diamond cell had a higher effective shear and Young's moduli than the hexagonal cell, as well as a higher initial yield strength and shear yield strength [12]. These results, combined with the ease of fabricating these two particular cells as compared with mixed cells or the Kagome cell, led to the decision to use a diamond repeating pattern and hexagonal repeating pattern for the perforated core of the samples analyzed in this thesis. These repeating 2-D patterns were then deformation shaped into the square and triangular repeating cells shown in Figure 2.2.

Silva and Gibson [13] analyzed the effects of non periodic microstructure and defects on the compressive strength of 2-D cellular solids. They determined that Voronoi

honeycombs with random cell arrangement were approximately 30% weaker than periodic hexagonal honeycombs of the same density [13]. Silva and Gibson also noted that defects in the periodicity, introduced by removing cell walls at random locations, caused a significant decrease in effective mechanical properties of both the Voronoi and hexagonal honeycombs [13]. Figure 2.11 shows that a removal of only 5% of the cell walls results in modulus and strength reductions of over 30%. When 35% of the cell



(a)



(b)

Figure 2.11 : Effect of randomly located defects on (a) modulus and (b) strength of intact Voronoi honeycombs (•), and defective hexagonal (■) and Voronoi (◆) honeycombs (from [13])

walls have been removed the mechanical properties degrade completely as expected from percolation theory [1]. These results show the influence of fractured or removed cell walls in a periodic honeycomb have a 2-3 times greater effect than an equivalent reduction in density by simply thinning the cell walls but maintaining overall periodicity [5]. By filling the void spaces of defective cells with foam, this thesis hypothesized that the *defect tolerance* of the entire sandwich structure could significantly be improved, despite the weight increase associated with the foam filling.

2.2.2 *Metal Foams*

Certain requirements exist for the core material of a sandwich panel. The core material must be low density, provide good shear strength and good stiffness, and prevent buckling of the facesheets [14]. Metal foams have a variety of attractive features that apply to sandwich panel design. In particular, metal foams generally are light, strong, energy absorbing, vibration and noise absorbing, non-toxic, and recyclable [15]. Metal foams are a relatively new class of materials and as such, challenges exist. Metal foams are not fully characterized and a lack of understanding of the basic mechanisms of foaming exists, as well as the inability to make foams of constant quality with pre defined parameters on a large scale [16]. Recently a great deal of research has been done on the mechanics of metal foams. An understanding of these mechanics is necessary to describe the deformation mechanisms which take place in sandwich panels with a metal foam core.

Table 2.4 shows the typical mechanical properties of commercial metallic foams. The metal foams used in this research were the closed cell Alporas ® and the open cell

Table 2.4 : Properties of commercial metal foams (from [6])

<i>Property, symbol [units]</i>	<i>Cymat</i>	<i>Alulight</i>	<i>Alporas</i>	<i>ERG</i>	<i>Inco</i>
Material	Al-SiC	Al	Al	Al	Ni
Relative density, ρ/ρ_0	0.02–0.2	0.1–0.35	0.08–0.1	0.05–0.1	0.03–0.04
Structure	Closed cell	Closed cell	Closed cell	Open cell	Open cell
Young's modulus, E [GPa]	0.02–2.0	1.7–12	0.4–1.0	0.06–0.3	0.4–1.0
Poisson's ratio, ν	0.31–0.34	0.31–.34	0.31–0.34	0.31–0.34	0.31–0.34
Compressive strength, σ_{pl} [MPa]	0.04–7.0	1.9–14.0	1.3–1.7	0.9–3.0	0.6–1.1
Tensile elastic limit, σ_y [MPa]	0.04–7.0	2.0–20	1.6–1.8	0.9–2.7	0.6–1.1
Tensile strength, σ_{UTS} [MPa]	0.05–8.5	2.2–30	1.6–1.9	1.9–3.5	1.0–2.4
Endurance limit, σ_c^c [MPa]	0.02–3.6	0.95–13	0.9–1.0	0.45–1.5	0.3–0.6
Densification strain, ϵ_D	0.6–0.9	0.4–0.8	0.7–0.82	0.8–0.9	0.9–0.94
Tensile ductility, ϵ_{UTS}	0.01–0.02	0.002–0.04	0.01–0.06	0.1–0.2	0.03–0.1
Fracture toughness, K_{IC}^c [MPa.m ^{1/2}]	0.03–0.5	0.3–1.6	0.1–0.9	0.1–0.2	0.6–1.0
Thermal conductivity, λ [W/m.K]	0.3–10	3.0–35	3.5–4.5	6.0–11	0.2–0.3
Resistivity, R [$10^{-8}\Omega\cdot m$]	90–3000	20–200	210–250	180–450	300–500

ERG Duocel ®. The properties of metal foams are a direct result of the foaming process, which is unique to each of the commercially available foams. Figure 2.12 shows the different process steps used to make Alporas ® and Duocel ®. The processes are inherently different, with Alporas ® using TiH₂ as a foaming agent while Duocel ® relies on an investment casting method followed by burnout.

A second difference between open and closed cell foam is whether it deforms by a bending or stretching mechanism. In the linear elastic regime, open cell foam structures

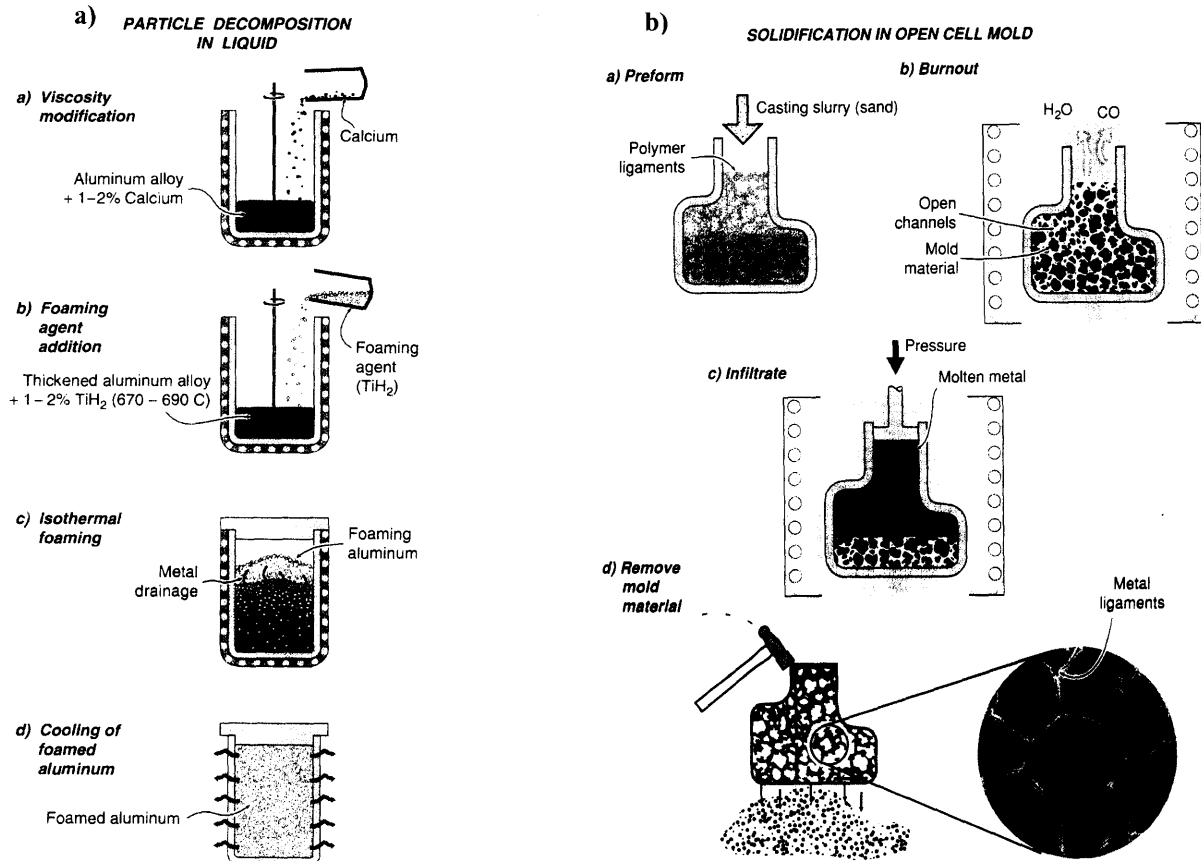


Figure 2.12 : The process steps used in the manufacture of (a) Alporas ® and (b) Duocel ® (from [6])

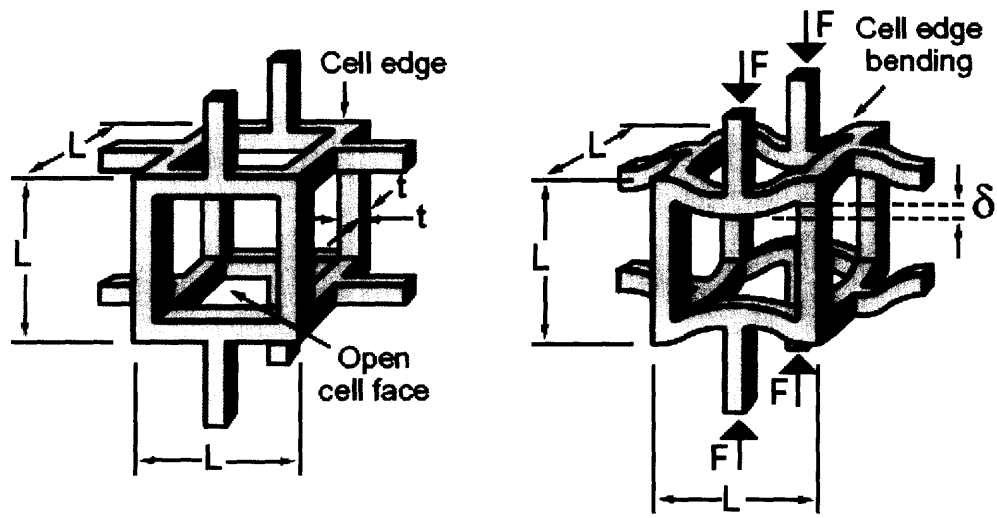


Figure 2.13 : Bending dominated mechanism in an open cell foam (from [4])

exhibit a bending mechanism, as shown in Figure 2.13. Upon compressive loading, a stress σ exerts a force proportional to σL^2 on the cell edges, where L is the cell edge length [4]. This causes the cells to bend and a deflection δ as shown in Figure 2.13. For an open cell foam the bending deflection scales as

$$\delta \propto (FL^3/E_s I)$$

Where E_s is the modulus of the solid from which the foam is made and I is the second moment of inertia which equals $I=t^4/12$ [4]. The modulus of the foam, E^* , then scales as

$$E^*/E_s \propto (\rho^*/\rho_s)^2$$

for bending dominated behavior [1].

Plastic collapse occurs when the moment exerted by the force F exceeds the fully plastic moment of the cell edges. This is the plateau regime in the stress-strain curve. The formation of *plastic hinges* is evident for metal foams in this regime [1]. Figure 2.14 shows the formation of plastic hinges at the corners of an open cell foam. The failure strength, σ^*_{pl} , is then determined to be

$$\sigma^*_{pl}/\sigma_{y,s} = C (\rho^*/\rho_s)^{3/2}$$

where $\sigma_{y,s}$ is the yield strength of the solid from which the foam is made and C is a constant of proportionality determined to be approximately $C=0.3$ [4]. It should be noted that honeycombs deform primarily by bending of the cell edges, therefore the stress-strain curve for in plane compressive behavior of honeycombs in Figure 2.8 is also what the stress-strain curve for open cell foams looks like.

Closed cell foams, on the other hand, deform by a stretching mechanism due to the fact that their cell faces are filled. Deshpande et. al [17] determined foams that are stretching dominated are more efficient from a weight standpoint. A stretch

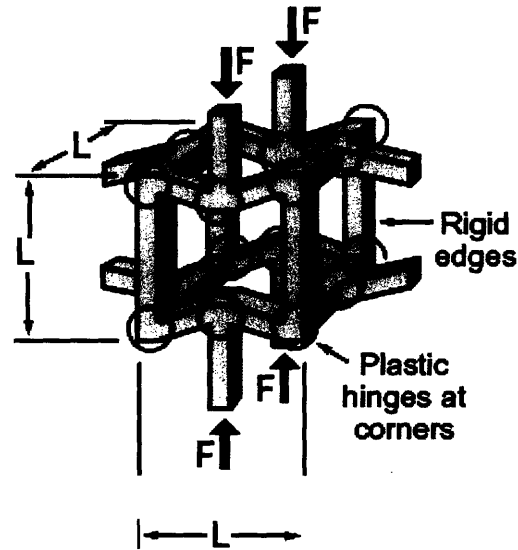


Figure 2.14 : Formation of plastic hinges in an open cell foam (from [4])

dominated foam is expected to be about ten times as stiff and about three times as strong as a bending dominated foam for a relative density $\rho^*/\rho_s = 0.1$ [17]. Sanders [18] noted that although this theoretical performance of closed cell foams far exceeds that of open cell foams, processing defects result in commercially available material that behaves similar to open cell foams at low relative densities. These processing defects can reduce mechanical properties by an order of magnitude [18]. Simone and Gibson [19] attributed these defects to the presence of curvature and corrugations in the cell faces. These structural imperfections have an impact on the stiffness of the structure as well as the strength [5]. In terms of weight efficiency, structural sandwich panels using low density metallic foam cores are inferior to other core designs including honeycomb and truss [19]. Although metal foam cores alone cannot compete with these other designs, by combining metal foams with honeycombs and trusses, hybrid sandwich structures can be developed. It is hypothesized that these hybrid structures may offer better properties than any individual core design.

2.2.3 Truss Structures and Lattice Block Materials (LBM)

Truss structures have been evaluated both in the cores of sandwich panels and as stand alone structures without facesheets. Figure 2.15 shows some of these structures.

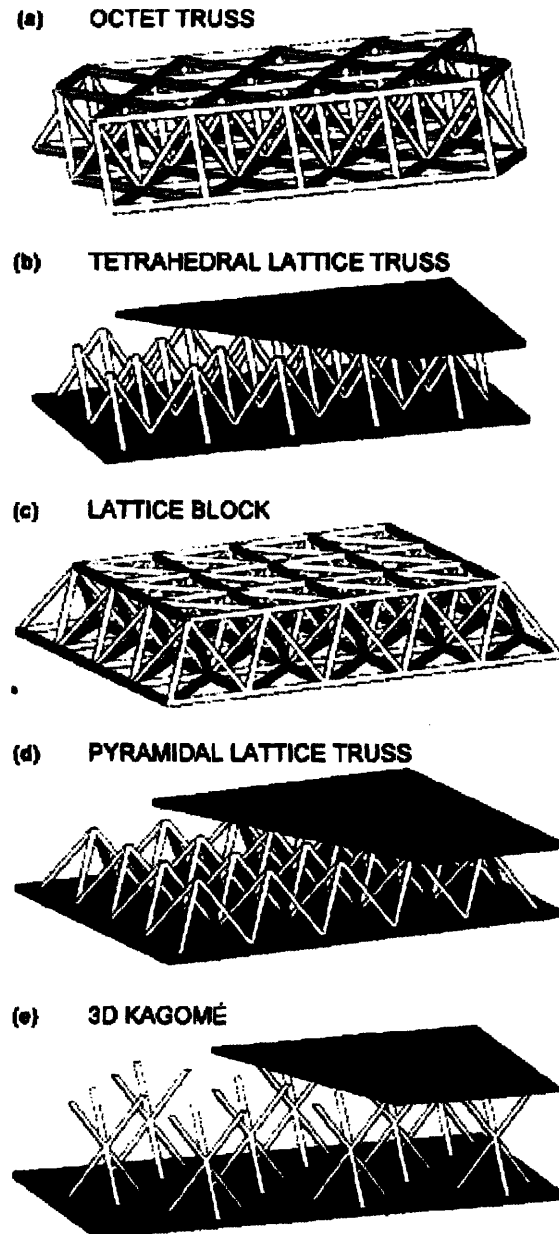


Figure 2.15 : Five lattice truss topologies (from [20])

Trusses have an advantage over stochastic metal foams in that their properties are stretch dominated. The members of stretch dominated structures carry both tension and

compression when loaded, making them highly structurally efficient as compared to bending structures [4]. The octet truss and lattice block topologies of Figure 2.15 are two examples of stand alone structures; these trusses require no facesheets. Analyzing the fabrication techniques for these truss structures as well as a comparison with other viable sandwich panel structures is important in determining an optimum design.

The tetrahedral and pyramidal lattice truss structures of Figure 2.15 are fabricated via a deformation shaping process similar to that seen in Figure 2.16. Queheillalt and

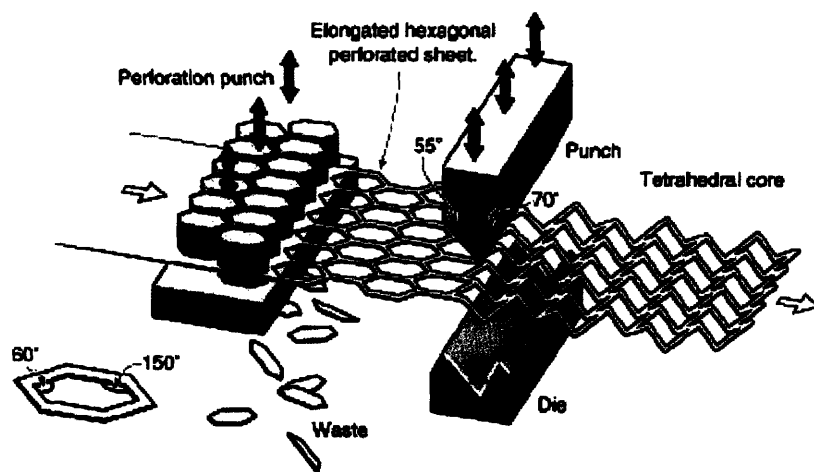


Figure 2.16 : Schematic of perforation and deformation shaping process (from [20])

Wadley [21] describe a vacuum brazing process to join the lattice truss structures to 304L stainless steel face sheets. A similar process is described by Kooistra et al. [20] which involved brazing of aluminum alloy (AA6951 sheets clad with AA4343) sheets in a muffle furnace. Subsequent to furnace brazing, the aluminum truss sandwich panels were both annealed and age hardened. Investment casting methods have also been used to successfully fabricate the tetragonal and pyramidal truss structures, however casting defects resulted in a strength knockdown [22]. While the brazing method described by Kooistra et al. works for aluminum alloys, silicon interdiffusion from the AA4343 cladding may lead to joint weakening if the truss structure is heated for too long [20].

The dip brazing method employed in the present research leads to more uniform joint quality throughout the sandwich structure.

Research on the deformation of lattice truss structures provides insight into the viability of these structures in sandwich panel design. Wicks and Hutchinson [23] performed a theoretical analysis of sandwich panels with truss cores and determined optimized sandwich panels of this design compare favorably with the most efficient stringer stiffened plates in compression. They also noted that the weights of optimized sandwich plates with truss cores are very similar to honeycomb cores, which are regarded as the lightest weight plate structures [23]. Chiras et al. [24] experimentally confirmed the predictions of Wicks and Hutchinson using an investment casting technique. These experimental results also found that in three point bending an asymmetrical structural response arose due to the fact that bending behavior is dependant on truss orientation [24]. Figure 2.17 clearly shows this asymmetric response. Plastic hinges are evident

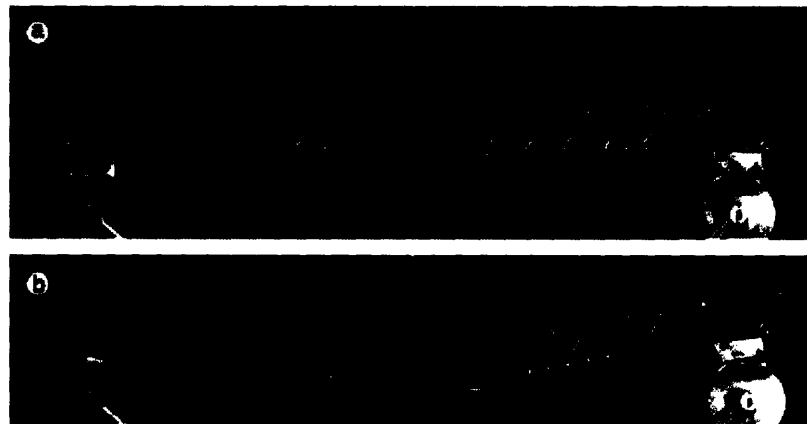


Figure 2.17 : Asymmetric response of truss loaded in 3-point bend. In (a) the truss is undeformed and in (b) the truss has been deformed. (from [24])

on the left hand side of Figure 2.17(b) as a result of large core shear strains, however the right side of the truss does not show evidence of plastic hinges.

Queheillalt and Wadley [21] analyzed pyramidal lattice truss structures made from 304L stainless steel and found that structures with both solid and hollow truss members exhibited characteristics of typical cellular structures. As seen in Figure 2.18, this compressive response included a region of nominally elastic response, yielding, plastic strain hardening to a peak strength, followed by a plateau region and finally a densification regime [21]. For both solid and hollow trusses of this type, they found peak

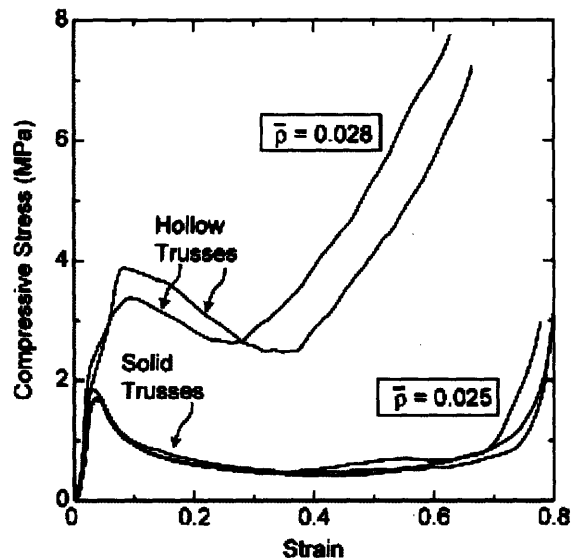


Figure 2.18 : Compressive stress-strain response for solid and hollow pyramidal lattice truss sandwich structures (from [21])

strength to be governed by inelastic truss buckling, however hollow trusses exhibited a compressive strength approximately twice that of solid trusses [21]. This increased strength can be attributed to the higher second moment of inertia of the hollow truss.

An analysis of the compressive response of square and diamond patterned lattice trusses has also been reported [25]. These patterned truss structures showed a compressive response similar to the pyramidal truss. Figure 2.19 shows these compressive results at varying relative densities. The peak compressive strengths for

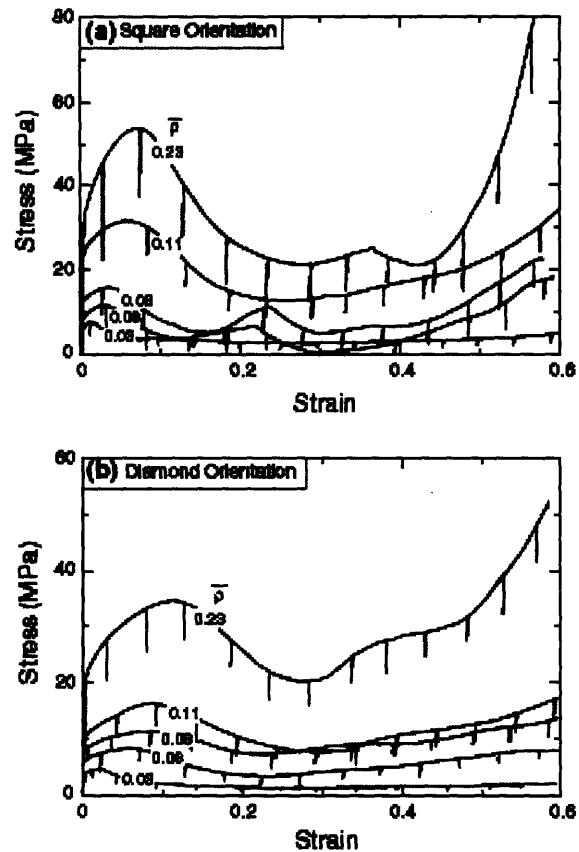


Figure 2.19 : Compressive stress- strain response of diamond and square hollow truss lattices made from 304 SS (from [25])

both these topologies was controlled by plastic buckling, however the square truss lattice had twice the stiffness of the diamond truss lattice [25].

Kooistra et al. [20] analyzed the compressive behavior of tetrahedral lattice truss structures made from aluminum. The response of these aluminum truss structures also exhibited linear elastic, plateau, and densification regimes. Figure 2.20 shows the compressive stress-strain response for annealed and age hardened cores. The compressive response of the age hardened cores exhibits a softening after reaching peak stress, evident by the downward slope of the curve as opposed to the steady plateau stress of the annealed cores. This softening is a result of the formation of plastic hinges in the middle of the truss members [20]. The tetrahedral lattice core is competitive with

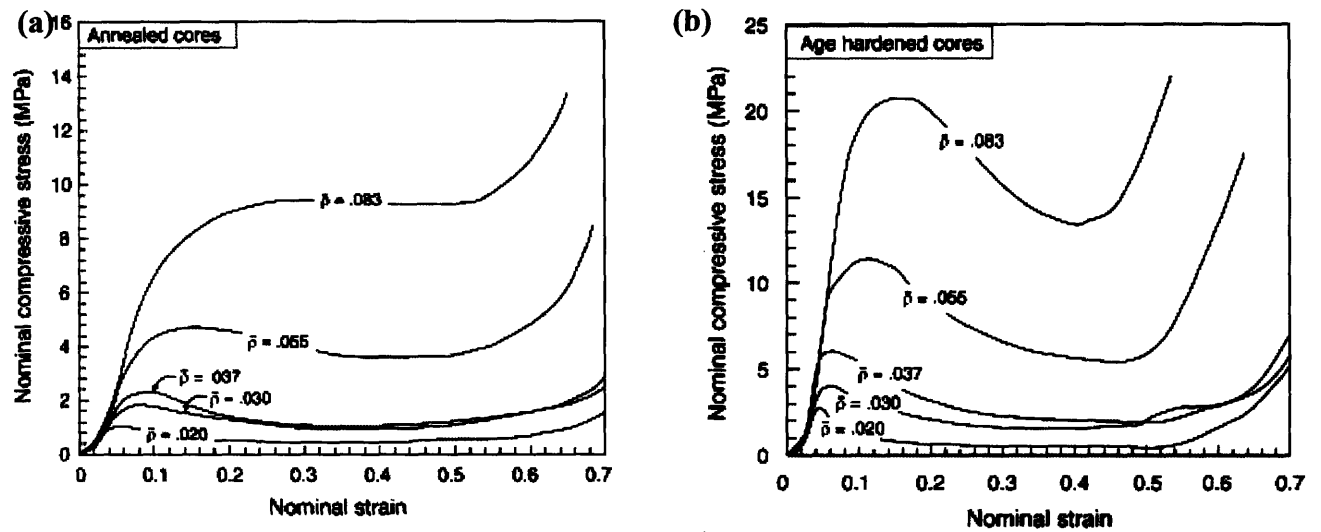


Figure 2.20 : Compressive curves for (a) annealed core and (b) age hardened core of aluminum tetrahedral lattice truss structures (from [20])

honeycomb cores and is superior to open cell foams in terms of compressive strength.

The sensitivity of a 3D truss structure to defects was analyzed by Wallach and Gibson [26]. The truss structure looked similar to the lattice block structure of Figure 2.15(c). The effect of randomly removing truss members on the Young's modulus and compressive strength of the structure was determined. It was determined that the Young's modulus decreased linearly with increasing fraction of missing members, with a 17% decrease in modulus for every 10% reduction in density [26]. The strength decreased at about the same rate. Randomly removing truss members decreased the modulus much more rapidly than when an equivalent density reduction was made by simply thinning the truss members [26]. This results from the reduced connectivity of the structure, and is analogous to results obtained for both honeycombs and foams. When compared with an open cell Voronoi foam (Duocel ® is one), the truss material was found to be much less sensitive to defects than the foam [26].

2.2.4 Failure Mechanisms and Optimal Designs

The preceding sections have thoroughly explained the deformation mechanisms of competing core designs in sandwich panels. When used in the cores of sandwich panels, cellular materials of all topologies can be used to design panels with high bend resistance, excellent strength and shear stiffness [11]. The ultimate choice of core material for a sandwich panel must be made after consideration of the panel's application. The failure mechanism of the panel will depend on the forces applied and the nature of the load. The possibility of fatigue and creep after multiple loading cycles is also an important characteristic to consider in the design process. Only after thorough diagnosis of the possible failure mechanisms should a final design be chosen.

Identification of constraints on failure and deflection are necessary in optimizing sandwich panel design. Figure 2.21 schematically shows the failure modes in sandwich panels. The most common failure modes for sandwich panels containing a cellular

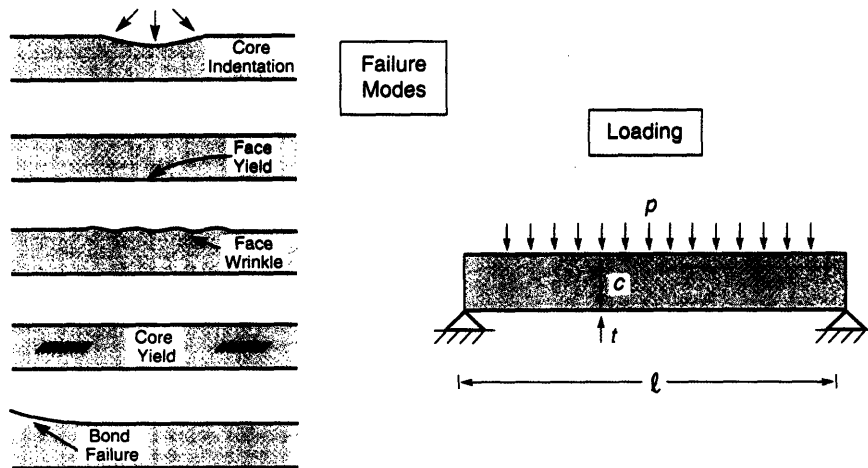


Figure 2.21 : Failure modes in sandwich panels (from [6])

metallic core are face yield, core yield, and core indentation. Face wrinkling and bond failure cannot be neglected, especially if the panel is loaded in bending and a weak interfacial bond between core and facesheet is present.

Figure 2.22 is a schematic of a sandwich panel loaded in four point bending. The subscripts f and c stand for facesheet and core. Core shear typically results from this type of loading, and Figure 2.23 shows two particular modes of core shear for sandwich panels. Mode A involves plastic hinge formation under the inner rollers with shear

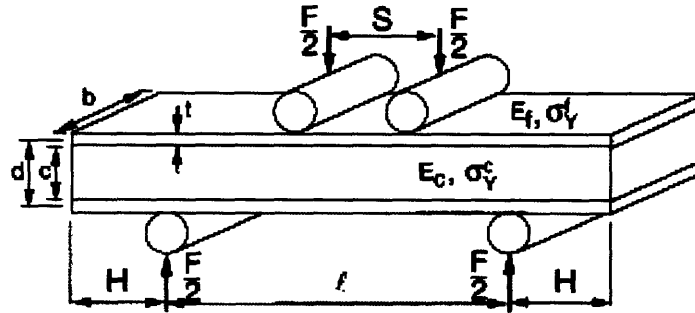
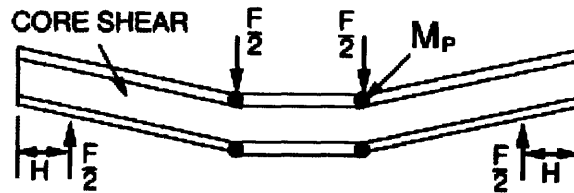


Figure 2.22 : Sandwich panel loaded in four point bending (from [27])

MODE A



MODE B

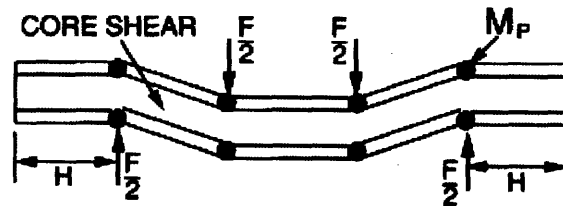


Figure 2.23 : Mode A and Mode B core shear under loading (from [27])

yielding of the core, while Mode B consists of plastic hinge formation at both the inner and outer supports [27]. The length of the sandwich panel overhang H beyond the outer rollers determines whether Mode A or Mode B will dominate.

The fatigue response of sandwich panels with metallic foam cores under compression includes three distinct types of behavior. The mechanism of fatigue is thought to be a combination of cracking of cell walls and cyclic ratcheting, which eventually lead to the crushing of the cells [6]. In Type 1 behavior uniform strain accumulates in the foam, without the formation of crush bands. Crush bands form at random non-adjacent sites in Type 2, resulting in increased strain [6]. Type 3 behavior involves the broadening of a single crush band with increasing fatigue cycles. This type of behavior has been observed for Alporas[®] foam, resulting in a significant drop in the elastic modulus [6]. This decrease in modulus under fatigue is similar to the decrease that occurs under static loading, as both are a result of geometric changes in the strained cellular material.

When load capacity governs the sandwich panel design, it has been determined that foam core sandwich panels are not competitive on a performance basis [28]. Honeycomb core panels are always lighter for the same performance, for flat sandwich panels subject to bending. However, metal foams may still provide an important benefit in the design of hybrid sandwich panels. This is because metal foams have very good energy absorption characteristics. The area under the stress-strain curve is the energy absorbed, shown in Figure 2.24 as the shaded region [4]. For honeycombs and trusses the onset of buckling in the cell members leads to a significant decrease in mechanical properties. It is hypothesized that by filling the void spaces of these open sandwich panel

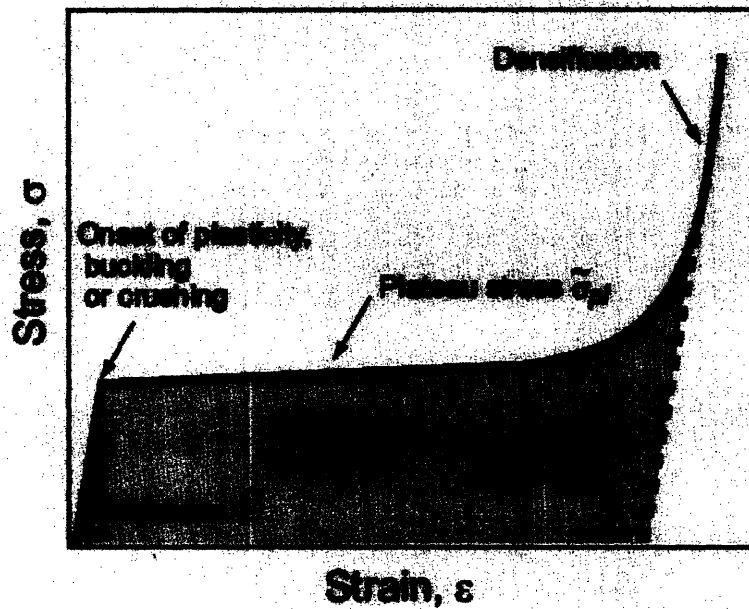


Figure 2.24 : The energy absorption capabilities of metal foams (from [4])

cores with metallic foam, the onset of buckling can be impeded. An additional weight gain would naturally arise, but if the foam could absorb energy otherwise absorbed by the honeycomb or truss members overall performance could be improved. One of the goals of this thesis is to quantify the effect metal foams have on impeding failure in sandwich structures containing periodic repeating cellular cores.

2.3 Material Selection

Material selection is critical to successful systems design. As has been stated, the application presumed for this research was a structural naval material. This application for military use strongly influenced the utility of parameters such as cost, weight, and structural stability. Ultimately selection of aluminum alloy was made.

A second caveat involved selection of the core of the sandwich panel. Defect tolerance, defined as how robust a design is to defects, became a primary concern. This led to an examination of different core shapes and different perforated sheet patterns. Hexagonal and diamond patterned perforated sheet, deformation shaped into square and triangular core cells, were chosen due to their ease of fabrication and lower cost than more exotic shapes such as Kagome or mixed cell.

The selection of aluminum immediately constrained the choice of joining processes available. The complex shape of the sandwich panel cores further limited potential joining techniques. Dip brazing was chosen because it was the most capable technique given the system constraints.

2.3.1 *Aluminum Alloys*

Aluminum is commercially available in a multitude of alloys. These alloys cover a wide range of compositions. The result is that different series of aluminum alloys have very different mechanical and physical properties. These differences are made more complex by the choice of temper chosen. Appendix B provides a background on these various alloys and tempers. The varieties of properties are apparent when the aluminum

foil used to wrap food is compared to the aluminum body on an automobile.

Specification of both alloy and temper are essential for proper material selection.

Aluminum alloy 6061-T6 was selected as the material to use in the diamond and hexagonal perforated sheet core for multiple reasons. The general characteristics in Table B.1 apply. Typical mechanical properties for monolithic AA6061-T6 include an ultimate tensile strength of 45 ksi and yield strength of 40 ksi [29]. This alloy is the best of the heat treatable alloys for brazing and welding, and is widely used for structural aluminum applications [30]. The corrosion resistance of aluminum is beneficial for naval vessels that operate in corrosive marine environments. There are no limitations on the availability of this material, leading to lower material costs than other potential alloys. Finally, dip brazing of this alloy has been performed commercially on complexly shaped heat exchangers for many years [31]. If this technology were to be implemented, the knowledge gained from dip brazing of heat exchangers could be transferred to this application. The thickness of the diamond and hexagonal sheets was specified at 0.040 inch.

Ideally the same material chosen for the core of the sandwich panels would be chosen for the facesheets. The use of dissimilar alloys could result in brittle intermetallic phases due to compositional differences among varying alloy series. For the mechanical tests performed in this thesis however, Brazing Sheet #21-F was specified as the facesheet material. This particular brazing sheet consists of AA6951-F with an AA4343 cladding on one side. The cladding is 10% of the sheet thickness and aids in surface wetting. This results in better brazed joints due to silicon interdiffusion into the fillet region of the joint. AA6951-F has a yield strength of 33.4 ksi and a tensile strength of

38.4 ksi, which is slightly lower than AA6061-T6. Due to the complexity of the core shapes the decision to use Brazing sheet #21-F was made. It should be noted that AA6061-T6 could also have been used as the facesheet material. The sole determinant in the decision was the complex core shape.

2.3.2 Relation between material selection and application

Most naval vessels are made of steel, so a comparison between aluminum alloy 6061-T6 and steel is required. Table 2.5 provides a comparison between these two materials for particular parameters related to this application. As seen from the table,

Table 2.5 : Comparison between monolithic AA6061-T6 and Steel

Parameter	AA6061-T6	HSLA Steel
Material Cost	1.5-2.0 USD/lb	0.25-0.50 USD/lb
Weight	Approx. 0.1 lb/cu. in	Approx. 0.28 lb/cu. in.
Maintenance	Corrosion resistant. Little maintenance required.	Maintenance required. In particular regular painting required.
Yield Strength	40 ksi	Min. 80 ksi
Elastic Modulus	10,000 ksi	29,700 ksi

steel is much cheaper but weighs more. Global use of aluminum is increasing significantly, from 5.5 billion pounds in 1991 to 12 billion pounds in 2006 for the auto industry alone [32]. It could therefore be expected that the price per pound of aluminum will decrease in the future since usage of a material in pounds per annum is inversely related to its cost per pound, however this decrease would occur gradually over a long time period[33]. Steel also is about three times stiffer than the aluminum alloy with a yield strength about twice as high. The fact that aluminum requires much less maintenance than steel should be factored into life cycle costs. The values in this table

are for monolithic AA6061-T6 and are not applicable for the hybrid sandwich panels used in this research. Effective properties of these panels would have to be determined from mechanical tests and theoretical derivations.

Table 2.5 shows there are trade-offs between aluminum alloy and steel. Not included are any values for composite materials. This thesis defines composite material to be a polymer based material with an added strengthening agent, such as epoxy or fiber. Glass fiber reinforced plastic (GFRP) and carbon fiber reinforced plastic (CFRP) are two particular composite materials that have been evaluated for naval hulls [34]. While composites have been used on marine vessels, in particular the Visby class which has a CFRP hull, composites were excluded in this analysis due to their high cost, poor flammability ratings, and difficulty in joining to metal. Polyurethane foam was included in the mechanical tests performed in this thesis simply to provide a comparison with metallic foam. Hybrid materials, generally considered a subset of composites, are distinguished from composites in this thesis. The hybrid materials analyzed in this thesis included sandwich panels of varying core shape and perforated pattern, filled with either polyurethane, closed cell metallic, or open cell metallic foams.

Military applications must also adhere to governmental regulations. Standards, such as the Guide for Aluminum Hull Welding, determine material qualification requirements [35]. Flexure and rigidity are not normally an issue for steel, so steel is designed to a yield point criteria. Aluminum, however, is designed to a deflection criteria to account for the fact that it is not as stiff as steel [36]. Fire resistance standards are very strict for marine vessels, but the 6xxx series of aluminum alloys are the most spark resistant [37]. When built to the same standards, an aluminum hull structure can weigh

approximately 35-45% less than a steel hull [36]. When governmental regulations which must be met are taken into account, aluminum alloy still provides certain benefits over steel.

Finally, aluminum was chosen as the material for this thesis because the U.S. Navy has mandated that its next generation of littoral combat ships (LCS) be faster and more fuel efficient than its current fleet. This makes the substitution of lightweight structural materials highly advantageous. The faster an object moves, the greater the value of weight saved [33]. As the operational lives of these vessels increase, each pound of weight saved can result in significant life cycle savings, and will permit faster vessels. Also the top-side weight of naval aircraft carriers increase by 250 tons each year as more equipment is brought on-board, therefore it is imperative to make as lightweight a structure as possible before the vessel enters service [38]. The U.S. Navy recently took possession of its fastest ship ever, a 262 foot catamaran titled “Sea Fighter”. Pictured in Figure 2.25, the “Sea Fighter” is a 1,600 ton aluminum catamaran capable of going 50 knots per hour [39]. The “Sea Fighter” cost \$50 million to build and was completed in



Figure 2.25 : The U.S. Navy’s “Sea Fighter” (concept drawing courtesy U.S. Navy)

under two years [39]. Future LCS ships still under development carry an estimated price tag of \$250 million per ship, and destroyers and carriers cost billions of dollars each, therefore weight savings gained by changing from steel to aluminum can lead to significant life cycle cost savings [39]. Aluminum alloys appear to be the material of the future for the U.S. Navy.

2.4 The Dip-Brazing Process

The dip brazing process was selected for joining the aluminum sandwich panels.

Figure 2.26 depicts a typical dip brazing process. Dip brazing was selected

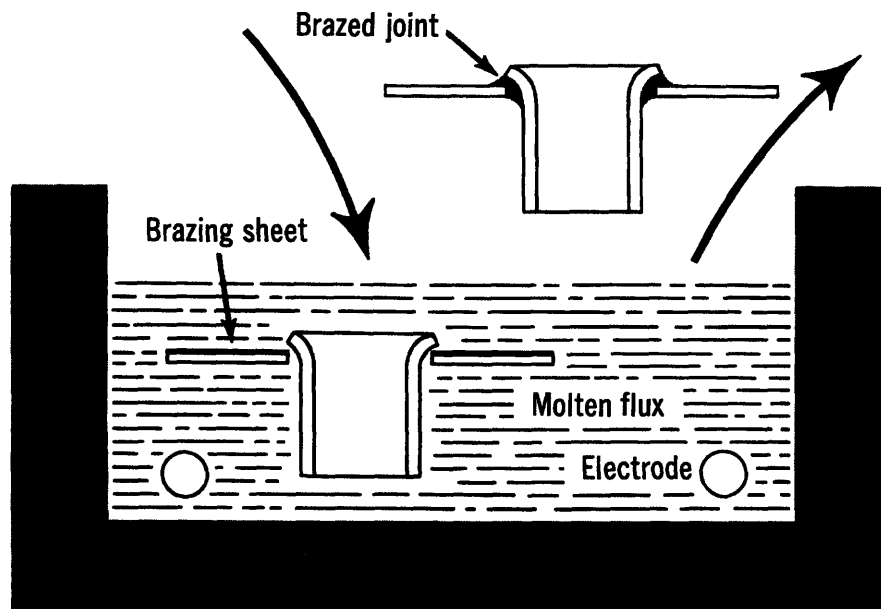


Figure 2.26 : Typical dip brazing process (from [31])

primarily because it is an extremely reliable way of joining complex aluminum parts.

There are, however, benefits and deficiencies associated with the choice of any joining process.

Dip brazing is by no means a new process, and it has been employed in particular industries as the preferred method of joining for decades. In dip brazing, the part to be joined is completely immersed in a heated bath which may consist of molten salt or molten metal [40]. The samples prepared in this project were all made using molten salt. The molten salt acts as both a provider of heat as well as a fluxing agent [41]. Table 2.6 details the advantages and limitations of molten salt.

Table 2.6 : Advantages and Limitations of Molten Salt [40]

Advantage	Limitation
1) Time required for heating is ¼ that of controlled-atmosphere furnaces.	1) Generally requires salt bath furnace to be constantly heated with no down time.
2) Selective brazing of partially immersed joints is possible.	2) Workpieces must be completely dry
3) High production volume possible, limited only by size and heating capacity of salt bath.	3) Shape of part must be designed to avoid trapping of molten salt, as it causes corrosion if not removed.
4) Molten salts protect from scaling	4) Part cleaning may be difficult
5) Salts reduce the likelihood of distortion of metal upon heating.	5) Salt fumes are hazardous and require proper ventilation.

Although molten flux dip brazing is possible with many metals, it is most notable for aluminum alloys. Aluminum alloys have a tenacious oxide layer, therefore pre-cleaning is essential [31]. After pre-cleaning has occurred, the proper brazing time must be determined. When only thin-section parts are to be brazed, the immersion time may be as short as one minute [42]. The combination of short braze time and high possible production volume makes dip brazing very attractive for certain applications. Dip brazing has enjoyed remarkable success in the manufacture of complex aluminum heat exchanger units [31].

Certain considerations must be taken into account with dip brazing. Since the molten salts are very corrosive, the salt bath furnace must be very corrosion resistant. Ongoing maintenance is required on the salt bath furnace as well. The furnace must be run 24 hours a day because if the molten salts become cool for any extended period of time they absorb moisture and become concrete hard [43]. On the other hand, dip brazing requires less tooling than other processes such as casting. The ability to “jig” parts that are to be dip brazed has contributed to this lower tooling cost and the ability to achieve close tolerances [43]. Tolerances as tight as +/- 0.002 in. have been maintained

in regular production via dip brazing [31]. When dealing with small scale parts, this ability to form strong joints with tight tolerances is very important.

As with every joining process, comparisons can be made between the utility of dip brazing versus other processes. The material selection of aluminum combined with the use of complexly shaped parts favored dip brazing. The ability to form multiple joints with the same properties at the same time was a big advantage in specifying the use of dip brazing in this research. Despite the limitations of dip brazing, it was the best possible process for the brazing of aluminum sandwich panels.

Chapter 3 : Experimental Procedure

The experimental procedure chapter consists of a section describing how the laboratory samples were prepared. The laboratory experiments showed dip brazing would be a feasible process to successfully join the facesheets and core of the sandwich panels together. There were two major shortcomings of the laboratory set up however. Panels could not be joined on the desired length scale, and multiple panels could not be dipped simultaneously which resulted in non-uniform properties between panels. It was determined procuring samples from a professional dip brazing facility would be the easiest way to overcome these obstacles. Mechanical tests were performed on these samples. The second section of this chapter deals with the preparation of these samples for mechanical testing, including defect introduction and foam filling.

3.1 Procedure for laboratory samples

3.1.1 Materials

For the laboratory experiments conducted, perforated aluminum sheets were purchased from McMaster-Carr (Dayton, NJ). These perforated sheets were available in hexagonal and diamond patterns at a reasonable price. Figure 3.1 shows the specifications for the diamond perforated sheet. As can be seen from Figure 3.1, these sheets were made from Aluminum Alloy 3003.

The facesheets used in these experiments were purchased through Lynch Metals (Union, NJ). The facesheets were brazing sheet #21-F. This brazing sheet is made from Aluminum Alloy 6951-F with a 10% nominal cladding of Alloy 4343 on one side. The

brazing sheets were 0.040 inch thick, and were made in accordance with AMS 4255 and AMS 20148 specifications.

The 3003 aluminum alloy is not a heat treatable alloy, and because dip brazing occurs near 600 degrees Celsius, a degradation of mechanical properties due to the brazing process was expected. Also, the use of 3000 and 6000 series alloys was not optimal. The goal of the laboratory experiments was to determine if complexly shaped cores of aluminum alloy could be joined via dip brazing.

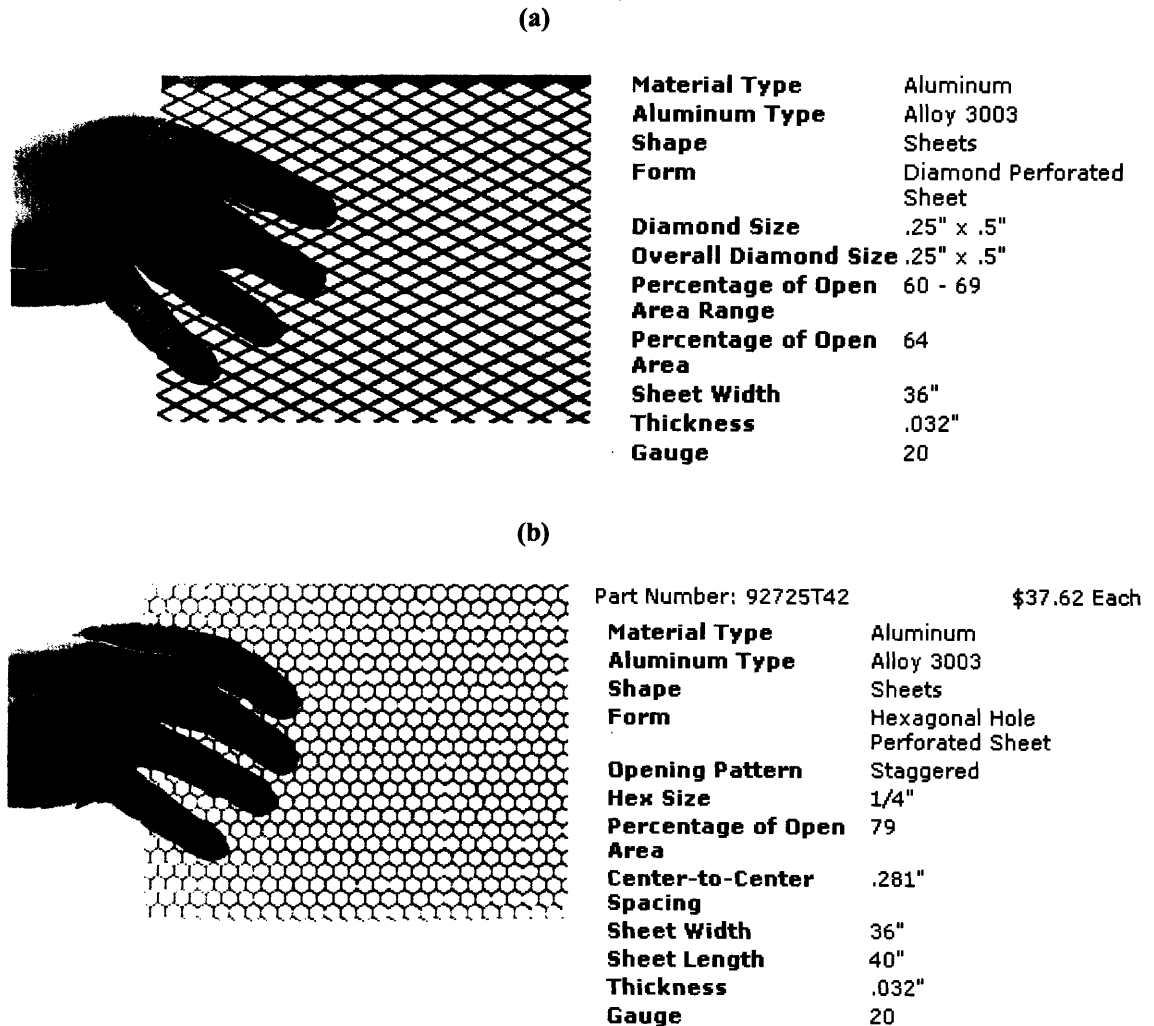


Figure 3.1 : Specifications of the (a) diamond perforated and (b) hexagonal perforated sheet for laboratory experiments (from [44])

3.1.2 Dip Bath Preparation

Equipment for dip brazing was purchased from Wenesco Inc. (Chicago). High temperature furnace Model MPM1C had a capacity of 100 liquid oz. as well as overall dimensions of 7x6x15 in. high [45]. This furnace reaches a maximum temperature of 1100 deg. C, and includes a removable graphite crucible. This furnace is shown in Figure 3.2.

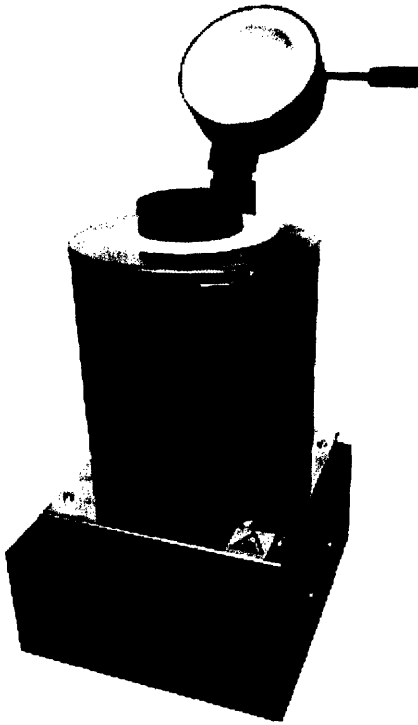


Figure 3.2 : High Temperature Furnace [45]

While this particular furnace is primarily used to melt gold and silver, it provided an economical and capable alternative to traditional dip furnaces which can cost many thousands of dollars.

The brazing salts used as the molten flux in the dip bath were purchased from Heatbath/ Park Metallurgical Corp. (Indian Orchard, MA). Alu-Braze 860 ® is primarily

a sodium fluoride salt. Its fluidity and braze characteristics made it an excellent choice for these laboratory experiments. However, the hazardous fumes emitted when these salts are heated, as well as their corrosive nature required a fume hood. The laboratory assembly used for this research is displayed in Figure 3.3.

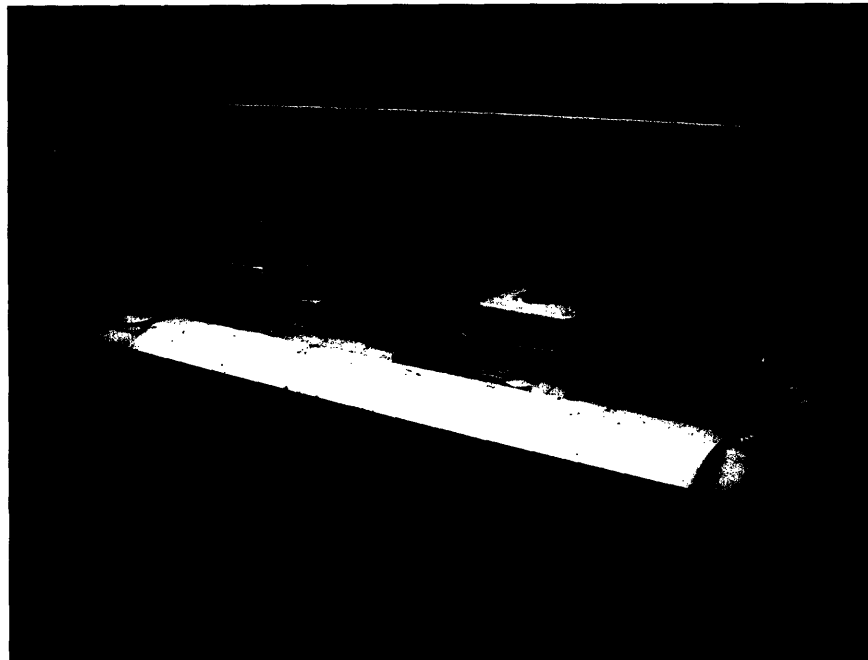


Figure 3.3 : Laboratory cleaning and dip brazing assembly

The brazing salts were pre-heated to 575 deg. C. No dipping occurred until all the salt had melted and reached a uniform temperature. After the required experiments had been performed, the brazing salts were allowed to cool. After cooling, the salts hardened like concrete due to a chemical reaction that occurs while cooling where the salts absorb a great deal of moisture. The graphite crucible containing the salts would be removed and a new crucible was placed in the furnace for each experiment. A method of quenching the salts with water in the crucible was developed that allowed for multiple use of individual crucibles. In this manner an economical method of performing the

experiments evolved, as the furnace did not need to remain heated continuously and graphite crucibles became reusable.

3.1.3 *Sample Preparation*

Having acquired both the raw materials as well as the equipment required, the only step remaining was the sample preparation. The sample preparation consisted of multiple steps, including sheet bending, sample lay-up, and cleaning operations.

The perforated sheets as well as the brazing facesheets were cut to size using an Electrical Discharge Machine (EDM). Samples 1 in. wide by 5 in. long were EDM cut on the Robofil 240 (Charmilles Tech., Chicago) as seen in Figure 3.4. The sheet bending

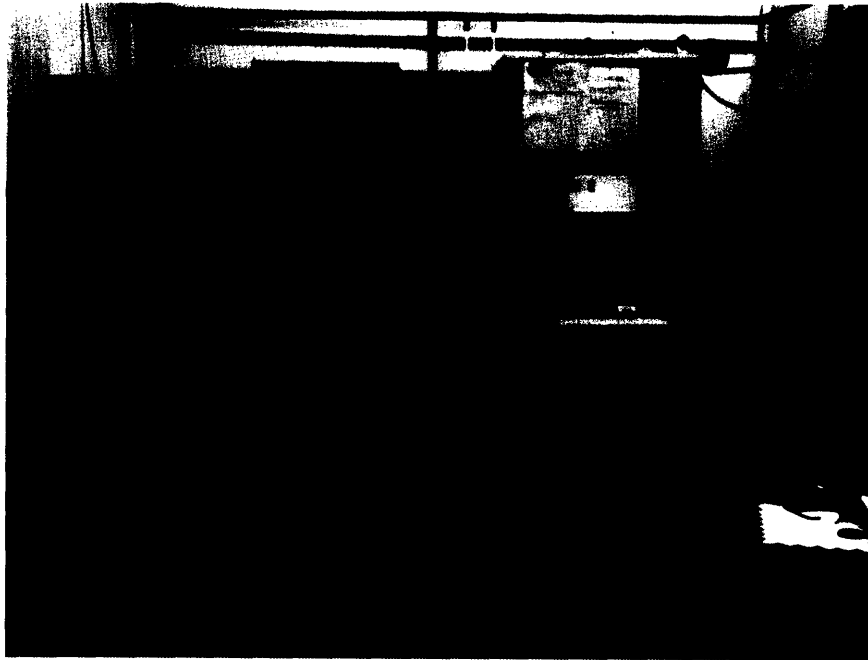


Figure 3.4 : EDM cutting of samples

operation consisted of first determining where to bend the perforated sheets based on the geometrical pattern and then the deformation shaping process. Figure 3.5 is a deformation shaped core of triangular repeating cell type.

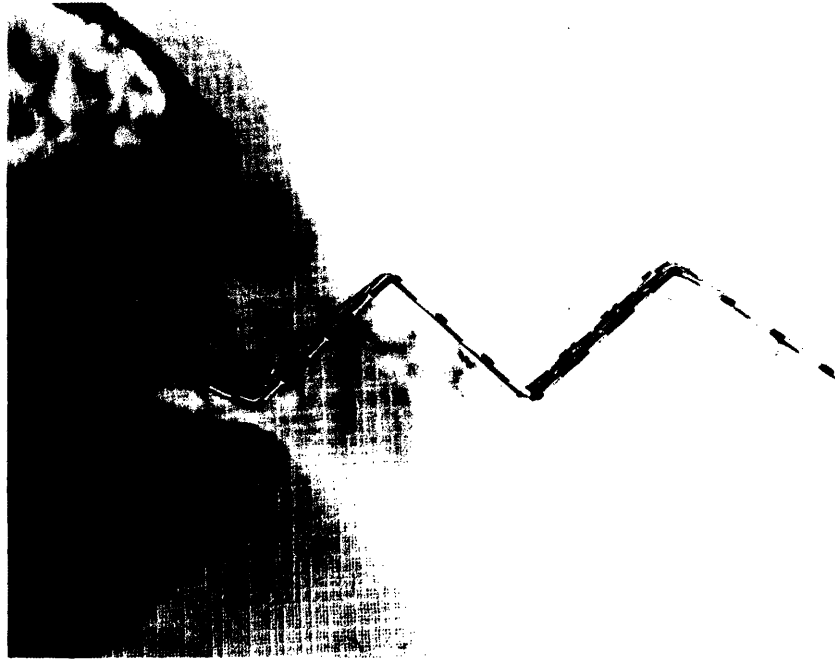


Figure 3.5 : Deformation shaped sandwich core

Prior to dipping the sample, the parts to be brazed were assembled, or “jigged” as it is referred to in dip brazing. Due to the thin sheets involved in these experiments, spot welding was not a suitable jigging method. Instead, a method of wrapping the sample was developed. Chromel ® wire was wrapped around the samples in a manner similar to that in Figure 3.6. The Chromel ® wire did not react with the brazing salts, and worked at the temperatures required. This method, although crude, proved to be an excellent method for quick sample lay-up.



Figure 3.6 : Wrapping with Chromel ® wire

Aluminum requires thorough cleaning before it can be joined by any welding or brazing operation, due to its tenacious oxide layer. Table 3.1 details the pre-cleaning procedure used for this research. Sodium hydroxide at 10% w/v (VWR #3470-4) was used followed by nitric acid at <70% w/v (VWR #4815-6). After the sample was thoroughly cleaned and air dried it was then dipped into the salt bath.

Table 3.1 : Pre-cleaning procedure for laboratory samples

<i>1) Dip assembled sample(including Chromel ® wire) in a 10% sodium hydroxide solution at 70 deg. C for 20-40 seconds</i>
<i>2) Rinse sample in cold water to remove NaOH</i>
<i>3) Dip assembled sample (including Chromel® wire) in 70% nitric acid solution for 1 minute</i>
<i>4) Rinse sample in cold water</i>
<i>5) Rinse sample in hot water at 100 deg. C for up to 5 minutes.</i>
<i>6) Air dry sample. No moisture may be allowed to remain on sample.</i>

Since the Wenesco furnace being used was not specifically designed for dip brazing, it took some effort to determine the optimal properties required to produce quality fillet brazes with this equipment. Table 3.2 displays the experimental variables and the resulting sample quality. The optimal temperature range was found to be 573-575 °C for panels with hexagonally perforated cores and 575-578 °C for diamond

Table 3.2 : Observations of different dipping parameters

Temp. Range °C	Dip Time	Joint Quality	Observations
600	3 min	Poor	Melting of metal
580	2 min	Medium	Warping of facesheet
573-575	3 min	Good (for hexagonal core) Poor (for diamond core)	These values work for hexagonal but not diamond cores.
575-578	5-6 min	Good (for diamond core)	Diamond cores require longer dip time than hexagonal. (Thicker facesheet used to eliminate warping problem).

cores. The optimal dip time was also determined to be 3 minutes for hexagonal cores and 5-6 minutes for diamond cores. The values were used to create excellent quality laboratory brazed samples. The deviation in dip temperature and time between these laboratory samples and typical industrial parameters can be attributed to the small size of the laboratory furnace as well as the brazing salts used.

The samples were air cooled for 10-30 seconds subsequent to dipping. Flux removal is mandatory for all brazing operations. The molten salt flux is extremely corrosive to aluminum. Table 3.3 is the post cleaning procedure used in these experiments. It should be noted that aluminum loses its temper when heated to high temperatures. There was no post braze heat treatment performed on the laboratory samples.

Table 3.3 : Post cleaning procedure for laboratory produced samples

<i>1) Air cool sample for 10-30 seconds.</i>
<i>2) Rinse sample in hot water at 100 deg. C for up to 5 minutes. This removes most flux from sample.</i>
<i>3) Dip assembled sample (including Chromel® wire) in 70% nitric acid solution for 1 minute.</i>
<i>4) Rinse sample in cold water.</i>
<i>5) Use tin snips to remove Chromel ® wire.</i>
<i>6) Air dry sample. Once dry weigh.</i>

3.2 Procedure for procured samples

All mechanical tests were performed on samples procured from J. Kittredge and Sons, Inc. (Hudson MA). J. Kittredge had the aluminum dip brazing capabilities to fabricate the sandwich panels to much tighter tolerances and on a larger size scale than was possible in the lab. Figure 3.7 shows the size difference between laboratory samples and the procured panels. Added benefits of the procured samples included that they were heat treated to a temper of T6, while the laboratory produced panels were not heat treated.

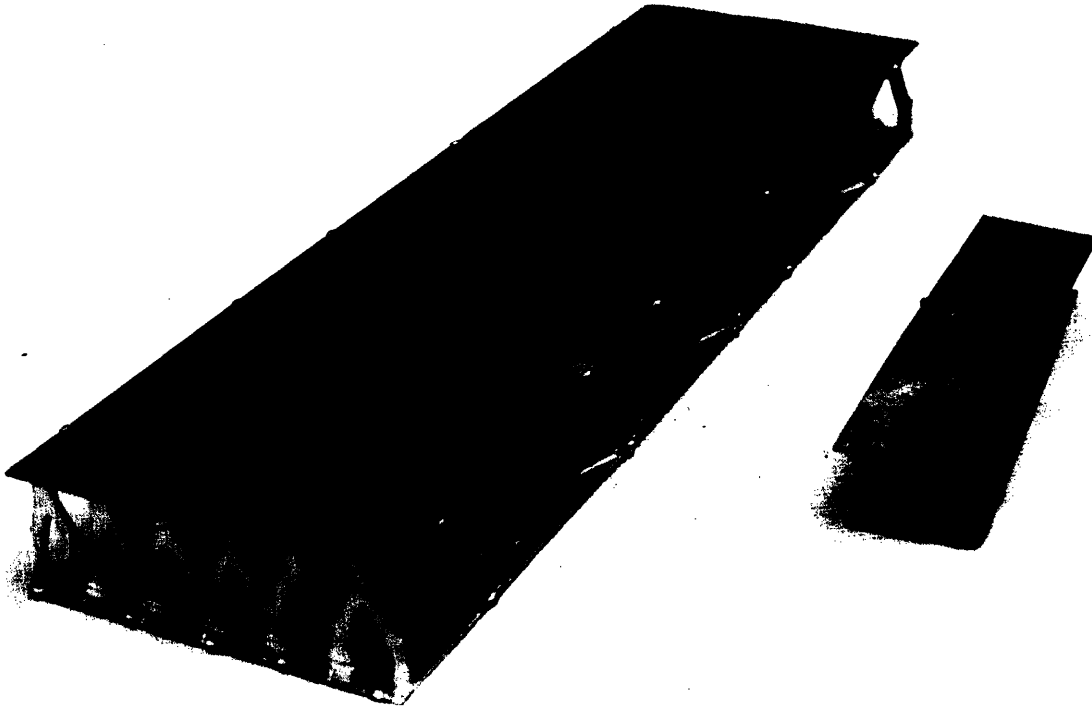


Figure 3.7 : Size difference between procured panels and laboratory panels

Foam filler was used for some of the experiments. The foam filler was either polymeric or metallic. The polymeric foam used was Great Stuff® (Dow Chemical Co.), which is an expandable, lightweight polyurethane foam used for filling large gaps. The metallic foam was of both the open and closed cell types. The open cell foam used was Duocel® (ERG Materials, Oakland CA). The Duocel Aluminum Foam contained 10 pores per linear inch (PPI), as well as a nominal density range of 8%. The alloy used to make Duocel was 6101-T6. The closed cell metallic aluminum foam was Alporas® (Shinko Wire Co., Japan). Figure 3.8 shows the difference between these two types of metal foam.

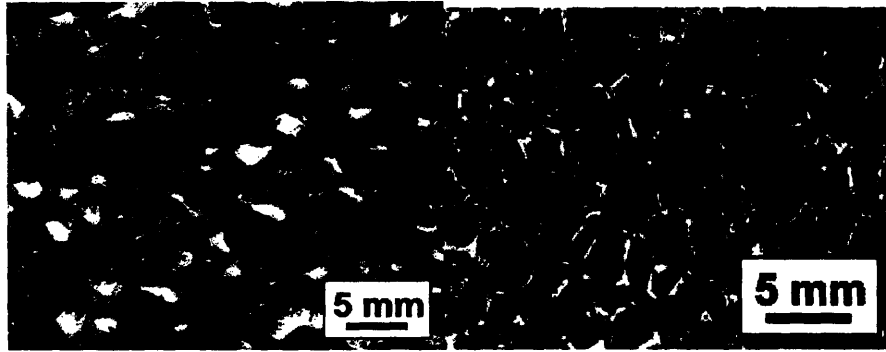


Figure 3.8 : Closed and open cell metallic foams. On the left is Alporas, Duocel is on right. [46]

In the case of the polymeric foam, foam must be applied as a second operation post brazing. The polymer cannot withstand the high temperatures at which brazing takes place. The Great Stuff® was applied to the core region of the sandwich panel and allowed to cure. A knife was used to cut off excess foam. The final hybrid sandwich panel is shown in Figure 3.9. Certain types of metallic foam can be brazed simultaneously with the cellular sandwich panel. In particular, the open cell Duocel® was successfully brazed with the square cell diamond core in the laboratory experiments. The Duocel® was polished to give smooth surfaces with a maximal contact area prior to brazing. Figure 3.10 shows the resulting brazed metal-metallic foam hybrid.

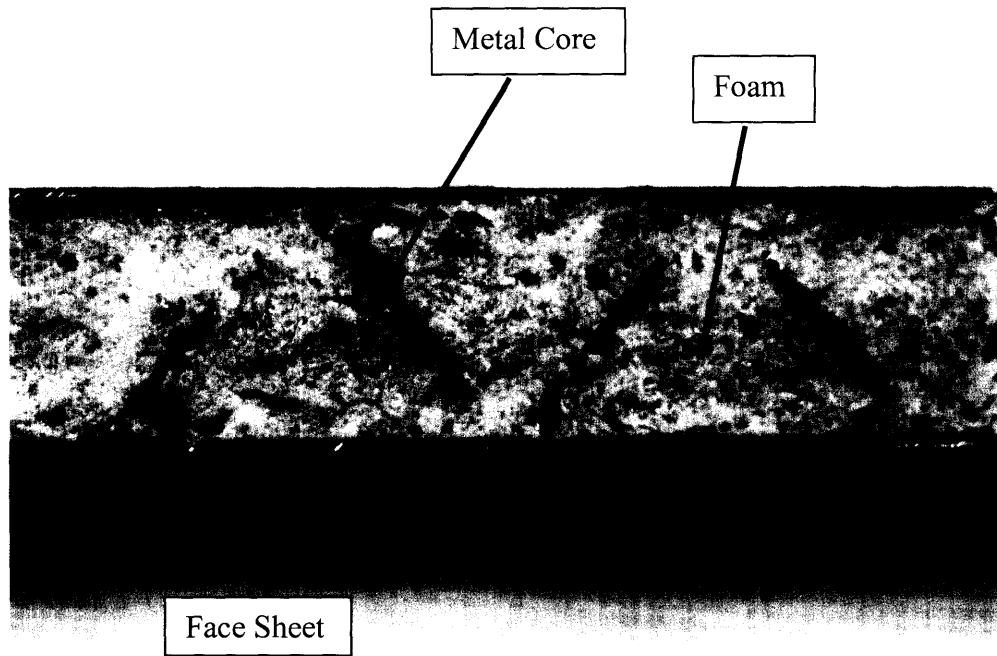


Figure 3.9 : Polymeric foam filled sandwich panel



Figure 3.10 : Metal-metallic foam hybrid sandwich panel produced in laboratory

The purchased samples did not have their metallic foam fillers brazed in a simultaneous dipping operation. It would be extremely difficult to dip braze Alporas[®] due to the added Calcium content in that foam [6]. Both types of metallic foam fillers were added as a secondary operation in the lab. Sections of filler were EDM cut, polished, and snugly inserted into the void space of the cellular sandwich panel. Close tolerances were obtained by EDM cutting the sample slightly larger than needed, and then polishing the metal foam until it could be forced into the void space with a mallet. Figure 3.11 shows both open and closed cell metallic foam samples. The outermost cells of the sandwich panels were not filled due to their limited supply and high cost. For all mechanical tests performed, having these outermost cells unfilled did not affect results. Only a limited number of mechanical tests of metal-metallic foam hybrids were performed.

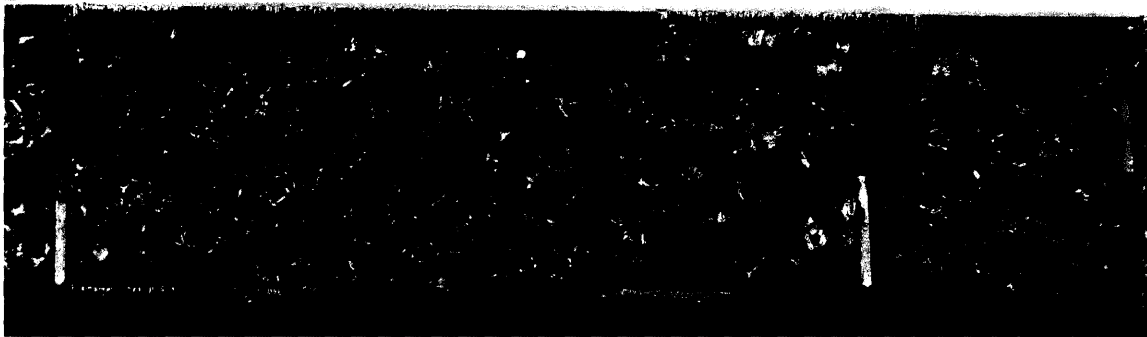
a)



b)



c)



**Figure 3.11 : a) Panel filled with Alporas ® b) Panel filled with Duocel ®
c) Close-up of metal foam filler snugness.**

Part of this research aimed at determining the defect tolerance of the different types of cellular sandwich panels. For this reason, defects were intentionally introduced into some of the samples. In principle, a defect is randomly occurring for a manufactured product. For these experiments however, the defects were all introduced in

a uniform manner. An entire row of the shaped cellular core was removed near the centerline of the sample. Figure 3.12 shows the resulting sample after defect introduction for a square and triangular shaped core.

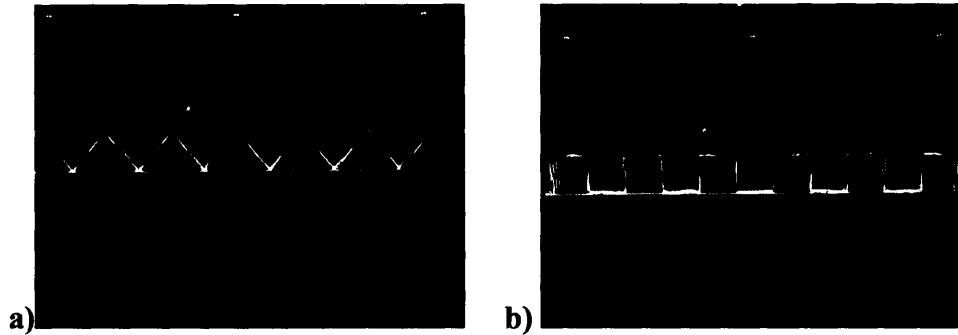


Figure 3.12 : a) Triangular core defect b) Square core defect

Defects were also introduced into polymeric and metallic cores, prior to the filling of the foam. Tin snips were used to remove the aluminum section from the sample core.

3.3 Microscopy

Microscopy was performed on both samples produced in the lab and purchased samples. Both scanning electron microscopy and light optical microscopy were carried out. The microscopy was aimed at determining if there were any significant disparities between the microstructure of the laboratory samples versus those of the industrially manufactured sample.

Fillet sections of both laboratory and industrial samples were cut. The sections were then mounted using Konductomet[®] black carbon conducting mount (Buehler No. 20-3375-016). The mount was placed in the Simplimet 3[®] (Buehler) for 4 minutes at 4200 psi and 150 °C (300 °F). After mount preparation a rough grind at 240 grit was made on the Metaserv 2000 Grinder/Polisher (Buehler). Sequential grinding at 400, 600,

800, and 1200 grit was then performed, with a 90 degree rotation of the mount between each grinding step. Samples were then polished using a 3 micron monocrystalline diamond suspension followed by a 1 micron diamond suspension. Polishing was done on 8 inch PSA backed Mastertex ® polishing pad, and both grinding and polishing speeds were 150-250 RPM.

3.3.1 Scanning Electron Microscopy

Scanning electron microscopy (SEM) was performed using the LEO 438VP (Zeiss SMT formerly Electron Microscopy Ltd., Thornwood, NY). Figure 3.13 shows a typical fillet region that was examined. The image shows the joint formed between the deformation shaped core piece of aluminum and the facesheet for one of the laboratory brazed samples. Light optical microscopy revealed the microstructure of this braze region.

SEM analysis was also used to determine the adhesion of the polymeric foam to the aluminum. Figure 3.14 is an SEM image of the polymer/metal interface. Porosity of the foam is evident from Figure 3.14.

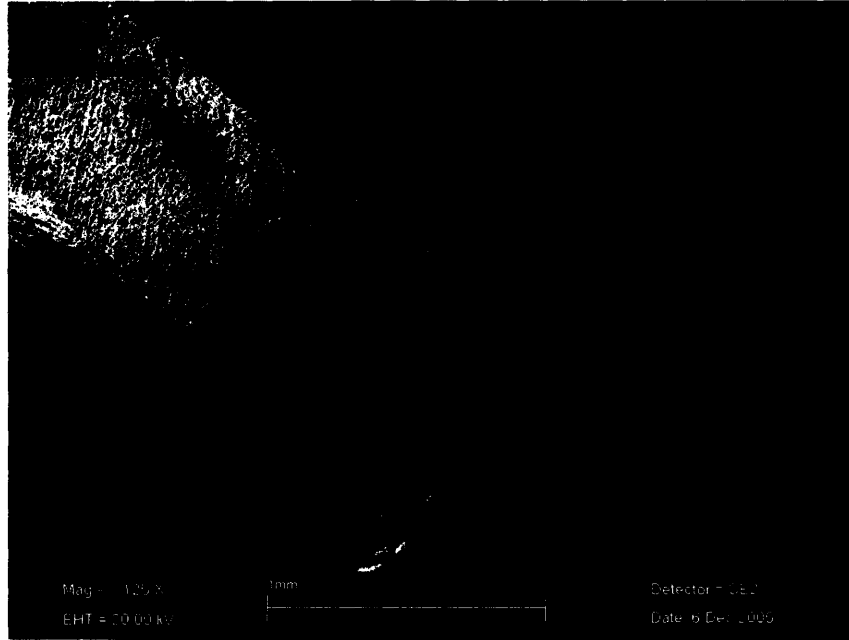


Figure 3.13 : SEM image of brazed joint from laboratory produced sample

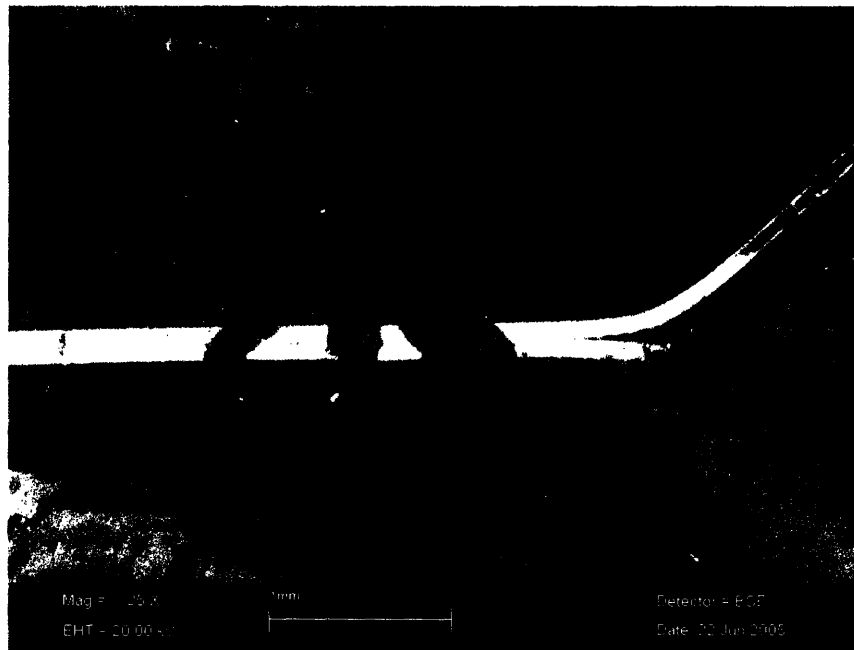


Figure 3.14 : Polymer/Metal interface

3.3.2 Light Optical Microscopy

Light optical microscopy was performed with the Olympus Vanox-T Optical Microscope (Micro-Tech Optical, Bloomfield, Conn.). The camera attachment to the scope was the Digital OPTEM Model DM-302. The light optical microscopy was used to analyze the microstructure of the joints formed via dip brazing. A comparison of the microstructures of laboratory produced joints and industrial joints is included in the results section.

3.4 Mechanical Testing

All mechanical tests were performed on an Instron ® universal testing machine (Model 4206., Norwood, MA). Compression tests were performed at a test rate of 0.1 inch/min. and were run up to a maximum compression extension of 0.2 inches. Four point bend tests were run at a test rate of 0.2 inch/min. The maximum flexure extension was set at 1.5 inches. Bluehill ® software was used to obtain all data.

3.5 Simulations

Simulations of the sandwich panel cores were created using the Solidworks ® CAD program. Figure 3.15 shows the CAD perforated hexagonal and diamond square cores. The computer drawings were made using the sheet metal toolbox. A base flange was made, which becomes the sheet. The desired perforation pattern is inserted as an

overlay on the base flange, and then the extrude cut option is chosen to remove the unwanted solid sheet material. The copy and mirror features can then be used to extend

(a)



(b)



Figure 3.15 : CAD drawings of shaped perforated cores

the perforated sheet to the desired length.

Once the perforated sheet is of desired length, the sketched bend function is used to bend the sheet into the desired cell shape. To insert foam material into the void spaces, make a block to overlay over the cellular shaped sheet. The “combine” feature can then be used in subtract mode. As long as the bodies are not combined, the foam block is then

inserted into the void spaces without removal of the perforated core. Figure 3.16 shows an example of a panel with foam insertion.



Figure 3.16 : CAD drawing of sandwich panel with foam filler

The final sandwich panel is then made using the assembly file. The facesheets must be aligned with the core and then the type of joint can be specified. Figure 3.17 is a CAD drawing of a hexagonal square assembly. Once these assemblies have been created they can then be imported into a finite element analysis (FEA) program. The FEA program used to perform a stress simulation of the diamond square cell for this thesis was COSMOS, which is an FEA program built into Solidworks®. Importing these models into more robust FEA programs was attempted, however errors occurred during importation.



Figure 3.17 : Assembly of hexagonal square cell sandwich panel

Chapter 4 : Experimental Results

4.1 Mechanical Testing Results

Appendix C contains tables with Load/Density ratios for all mechanical tests performed. A solid sandwich panel of aluminum alloy 6061, having a density of 2.7 g/cm^3 and dimensions $10'' \times 1.5'' \times 1''$, was determined to have a weight of 664g. Relative densities were determined by taking the absolute weight of the sandwich panel tested, including any weight gains or losses associated with foam and defects, and dividing by 664g. For the compression tests, peak compressive loads were determined. Local maxima in the linear elastic region were taken as the peak values for tests where metallic foam hybrid sandwich panels showed a densification region leading to large compressive load increases at high strains. Maximum compressive stresses were determined by dividing the peak compressive loads by 9 in^2 . Even though the cross section of the rectangular sandwich panels were 15 in^2 , the compressive fixtures only covered 9 in^2 , so the area of the samples which overhung the fixture did not take any load and were not included. The flexure stresses in the four point bend tests were calculated by using 15 in^2 as the cross section.

4.1.1 Compression results

Based upon the Load/Density ratios in Appendix C, it is seen that sandwich panels with a diamond square repeating core, with no foam and no defects have the best overall Load/Density ratio with a value just under 26,000. In general, the square repeating core performed better than the triangular repeating core for all experiments, as was expected since the square core cells were aligned perpendicular to the loading

direction. In terms of highest peak compressive load, sandwich panels with the diamond square repeating core containing Alporas® and no defects reached a load of 4107.3 lbf. The added weight associated with the closed cell metal foam lowered its Load/Density ratio to just below 24,000 however. Defects significantly lowered peak compressive loads, except when hybrids with metal foam filler were tested. For those tests the results were insensitive to whether defects were present or not.

Table 4.1 shows percent differences of Load/Density ratio from the baseline tests of no foam and no defects for the four varying repeating core cell types. A 29%

Table 4.1 : Effect of defects and polymeric foam for each core type

Core Type	Load/Density Percentage change			
	NF,ND	NF,D	Poly,ND	Poly,D
Diamond Square	1	0.71	0.93	0.76
Diamond Triangle	1	0.67	0.99	0.74
Hex Square	1	0.84	1.02	0.91
Hex Triangle	1	0.85	1.03	0.91

reduction in compressive strength resulted in diamond square sandwich panels due to defect introduction. This value is consistent with the results of Silva and Gibson. The effect was even greater in the diamond triangular panels, while both core types of the hexagonal perforated panels showed a greater defect tolerance. The addition of polymeric foam resulted in a higher Load/Density ratio for both the hexagonal square and triangular sandwich panels when no defects were initially present. The addition of polymeric foam resulted in a higher absolute peak compressive load for the diamond cores, as seen by Figure 4.1, however the added weight associated with the polymer more than offset this gain. As seen in Figure 4.1, after reaching peak compressive load, “softening,” represented by the downward slope of the curve existed due to buckling in

the square cell columns. This was typical in the panels with diamond perforated pattern. Appendix D contains time lapse photography of the mechanical tests, and both buckling and plastic hinge formation are clearly evident.

Specimen 1 to 3

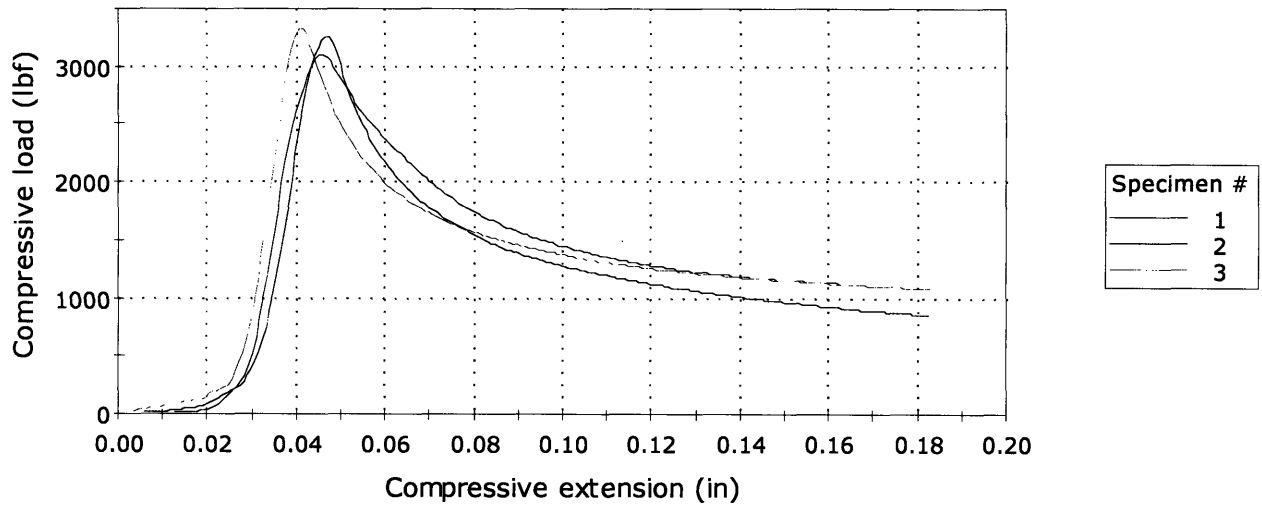


Figure 4.1 : Load-extension curve for three samples of a diamond square pattern with polymeric foam and no defects

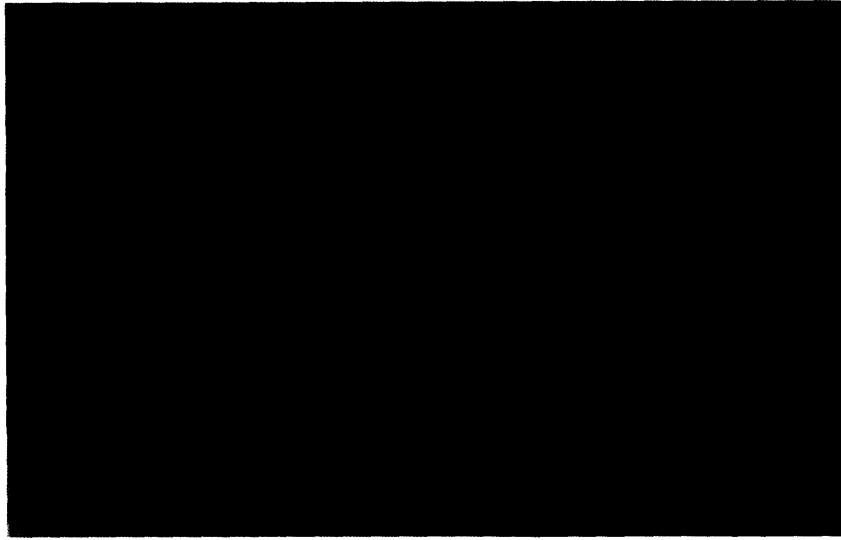
An extreme difference in peak compressive load is apparent between cores with a hexagonal perforated pattern and cores with a diamond perforated pattern. Table 4.2 shows this difference after normalizing for a slight weight difference between the respective patterns. In general the diamond patterns have a compressive strength about four times that of the hexagonal ones. This difference arises due to the different deformation mechanisms that sandwich panels of each pattern undergo. Sandwich

Table 4.2 : Load/Density Ratios for Hexagonal and Diamond perforations

Description	(Hexagonal/Diamond) Load/Density ratios	
	Square	Triangle
NF,ND	0.22	0.21
NF,D	0.26	0.27
Poly,ND	0.24	0.22
Poly,D	0.26	0.26

panels with a hexagonal pattern deform by in plane crushing while out of plane buckling occurs in the diamond pattern. Figure 4.2 illustrates the difference. Figure 4.3 shows the resulting load-extension curve for a panel with no foam, no defects, and a hexagonal square repeating cell. A plateau region followed by a softening region for the load-extension curve is evident once cell collapse begins.

a)



b)

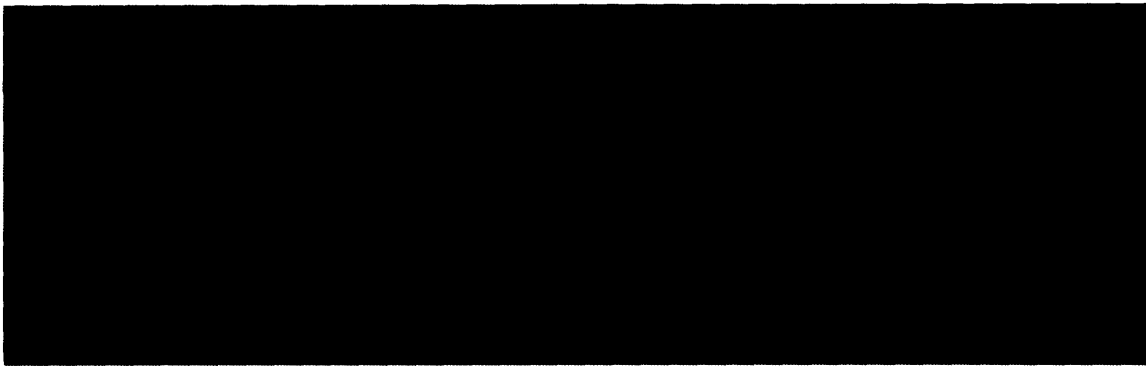


Figure 4.2 : Crushing occurs in (a), while buckling occurs in (b)

Specimen 1 to 2

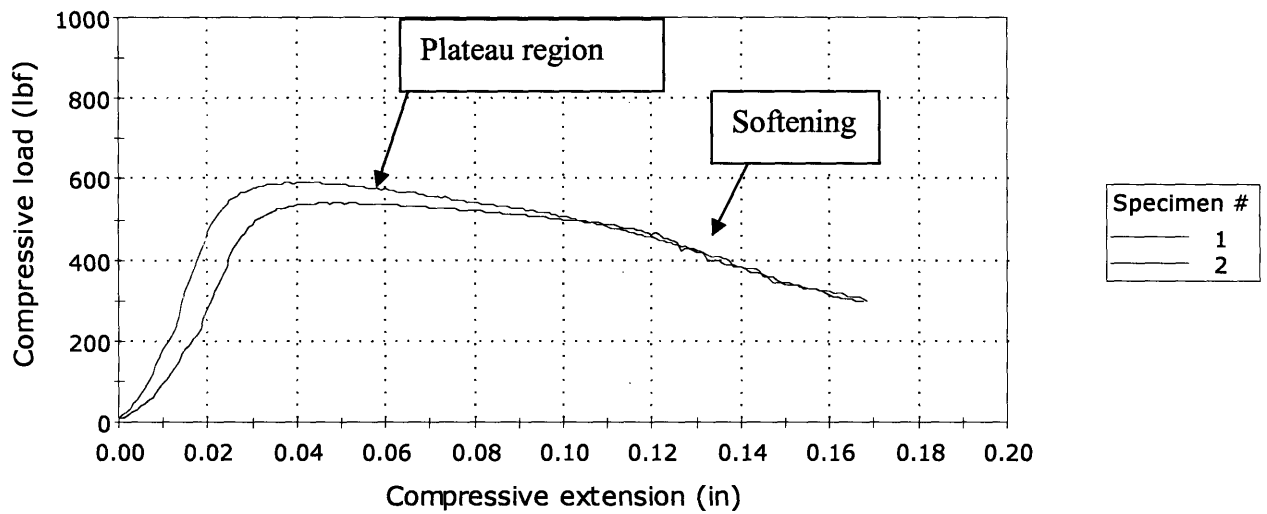


Figure 4.3 : Load-extension curve for two samples of hexagonal square core, no foam, no defects

The effect of foam filler varies significantly depending once again on whether the perforated pattern that was deformation shaped was of hexagonal or diamond shape.

Table 4.3 has normalized the effect of metallic foam filler versus the baseline case of no foam and no defects for each core type. When the core type is of diamond pattern, the

Table 4.3 : Effect of Metal Foam Filler on Load/Density Ratio

Core Type	Effect of Metal Foam Filler			
	NF,ND	ALP,ND	DUO,ND	ALP,D
Diamond Square	1	0.92	0.86	0.85
Diamond Triangle	1	0.75	N/A	0.55
Hex Square	1	2.21	2.20	2.51
Hex Triangle	1	3.18	N/A	3.10

Load/Density ratio decreases slightly for square cells and more significantly for triangular cells. Hexagonal patterns show a marked increase however. The presence of defects is also rather insignificant for the hexagonal patterns, while the effect of defects is more telling for diamond patterns. Figure 4.4 compares the load-extension curves for polymer filled diamond triangular cells with and without defects. Figure 4.5 compares

the load-extension curves for polymer filled hexagonal square cells with and without defects. The difference between these two figures is striking. Also evident from

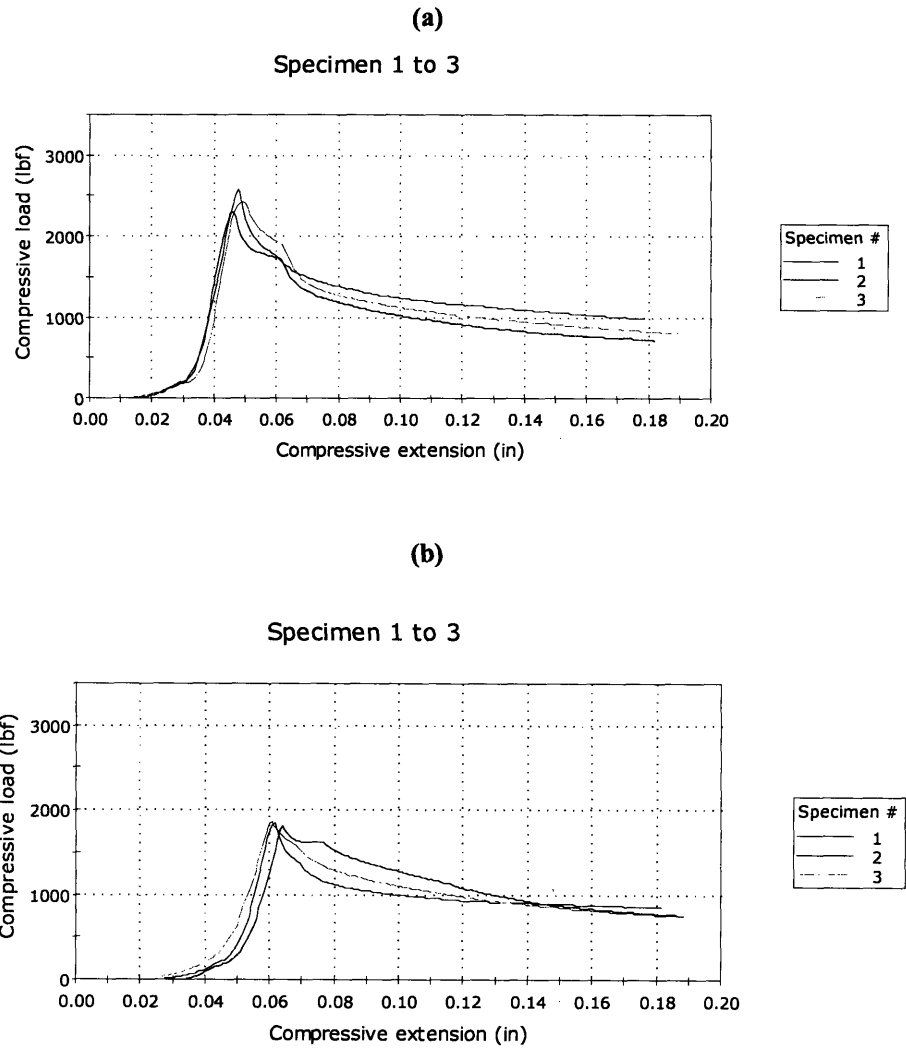


Figure 4.4 : Polymer filled diamond triangular panels (a) without defects and (b) with defects

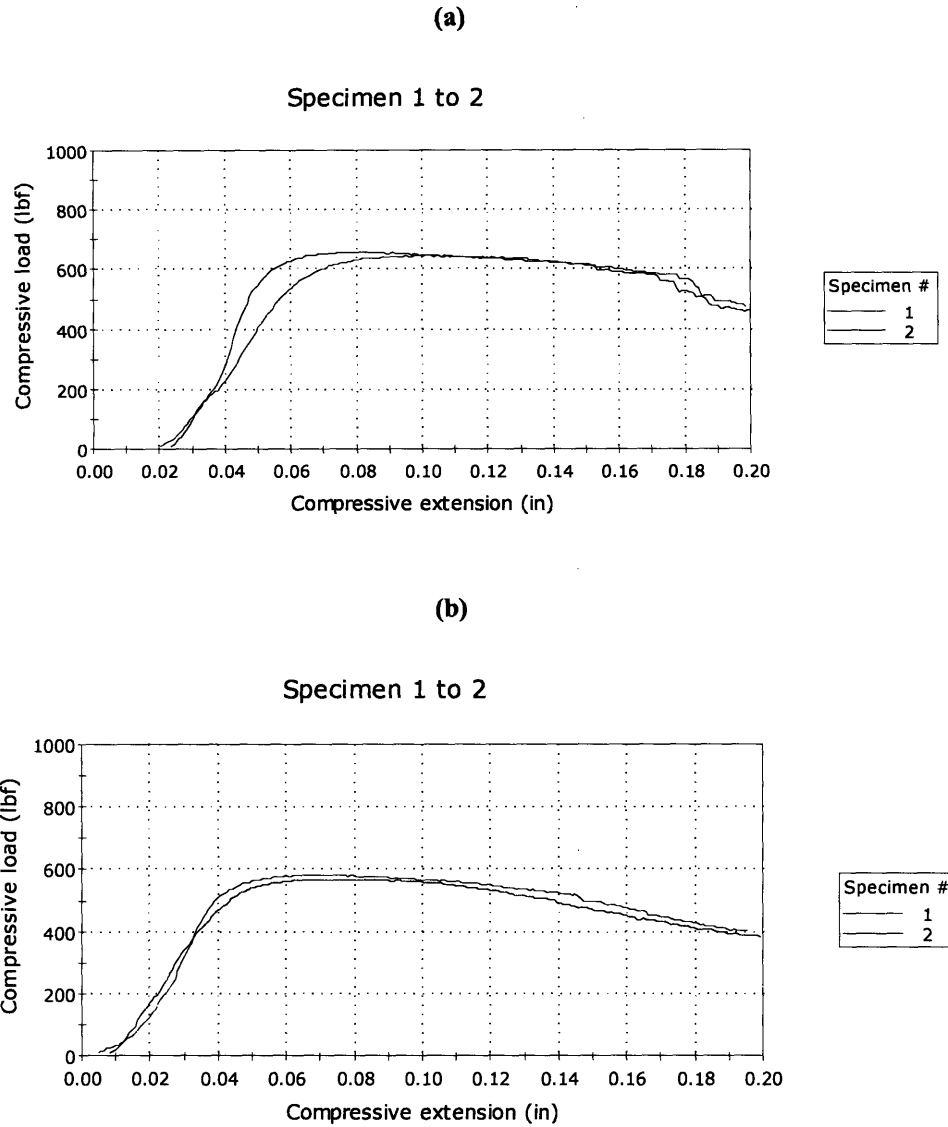


Figure 4.5 : Polymer filled hexagonal square panels (a) without defects and (b) with defects

Table 4.3 is that metal foam filler increased the Load/Density ratio of hexagonal triangular panels by over 300% regardless of defects. Figure 4.6 shows almost a linear relationship in the load-extension curve for these panels. This suggests that the dominant deformation mechanism for this cell orientation is dependant on the metallic foam filler and not the repeating cell shape. This region could be the linear elastic regime of the Alporas[®] foam, as no plateau has been reached at the 0.20 inch limit set for extension.

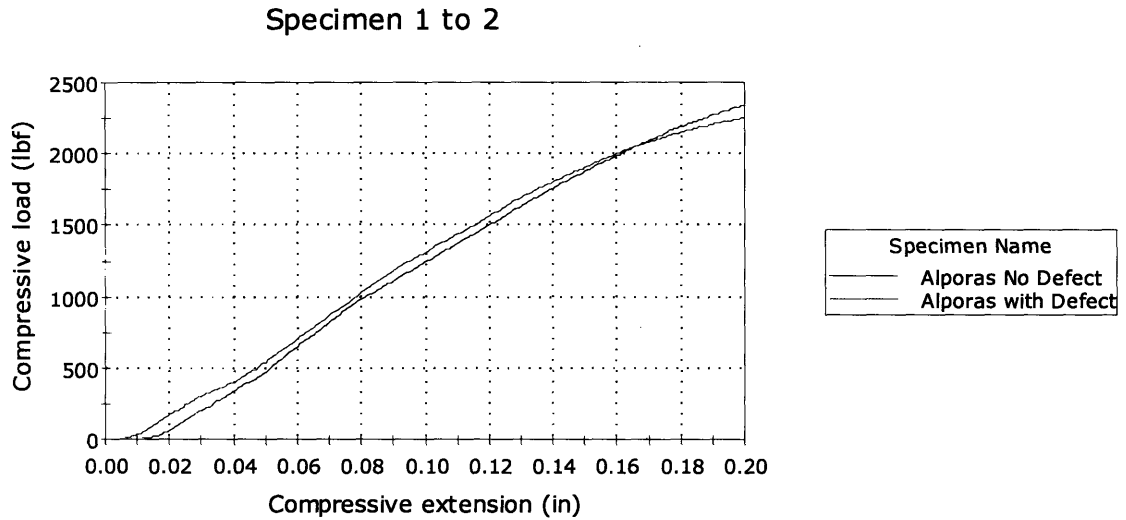


Figure 4.6 : Hexagonal Triangular sandwich panel cores, filled with Alporas. There is no significant difference due to the presence of defects for this cell architecture.

Table 4.4 shows the percentage compressive strength lost as a result of defects, expressed as the ratio of Defects/No Defects. This ratio is shown for three cases; when there was no foam filler, when polymeric foam filler was added, and when Alporas metallic foam was added. Also shown for each case is the difference in relative density due to the introduction of defects (i.e. removal of core material) for each core shape. This relative density difference is expressed by the term ΔRD . For the majority of the cases this value is negative, indicative of the defective sandwich panel having less weight. For some of the experiments however, an increase is seen. This is attributed to the fact that the filler used had a greater density than the honeycomb region removed.

Table 4.4 : Effect of Defects when No Foam, Polymeric Foam, and Alporas foam were used as filler

Core Type	Effect of Defects					
	NF		Poly		ALP	
	(D/ND)	Δ RD	(D/ND)	Δ RD	(D/ND)	Δ RD
Diamond Square	0.71	-0.005	0.82	-0.004	0.92	0.014
Diamond Triangle	0.67	-0.002	0.75	0.001	0.73	0.000
Hex Square	0.84	-0.008	0.89	-0.001	1.13	-0.003
Hex Triangle	0.85	-0.001	0.88	-0.001	0.98	-0.004

4.1.2 Four point bend results

An analysis similar to that for the compression tests was made for the four point bend tests. Table 4.5 shows the percentage change in the Load/Density ratio for each core type of sandwich panel. Values of 1.0 for the case of no foam and no defects for each

Table 4.5 : Percentage change in the Load/Density ratio for four point bend tests

Core Type	Load/Density Percentage change			
	NF,ND	NF,D	Poly,ND	Poly,D
Diamond Square	1	0.87	0.98	0.99
Diamond Triangle	1	0.86	0.81	0.89
Hex Square	1	0.82	1.11	1.16
Hex Triangle	1	0.90	1.08	1.01

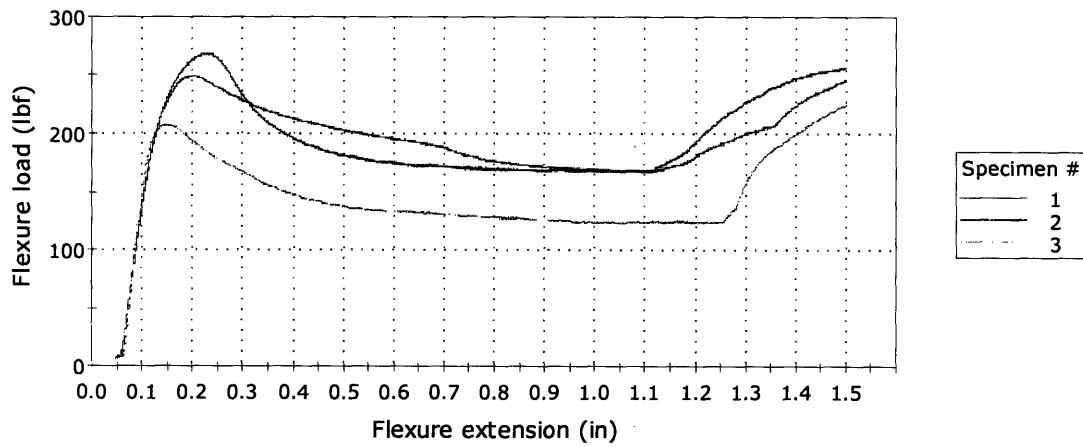
core type have established a baseline from which to compare the effect of defects and polymeric foam filler. From Table 4.5 it is apparent that the addition of polymeric foam results in a stiffer panel for the hexagonal square and hexagonal triangular cores. The increase in load more than compensates for the added weight associated with the use of foam. For the diamond square core the addition of polymer results in a panel with nearly the same Load/Density ratio, and the diamond triangle core shows the greatest decrease.

The results from Table 4.5 point out an important observation. The polymeric foam used for these experiments is *not* considered a structural material, but just the presence of foam material in the void spaces is shown to significantly increase the peak flexure load. The only exception to this statement is in the case of the diamond triangular core shape. A peak flexure load of 248 lbf for this shape occurred in the no defects, no foam case, while in the polymer foam, no defects case the peak flexure load actually dropped to 227.5 lbf. Bond failure between the foam and the facesheet most likely caused the

decrease. Figure 4.7 compares the flexure load-extension curves for these two cases. In both of these curves a linear-elastic, plateau, and densification region is apparent.

(a)

Specimen 1 to 3



(b)

Specimen 1 to 3

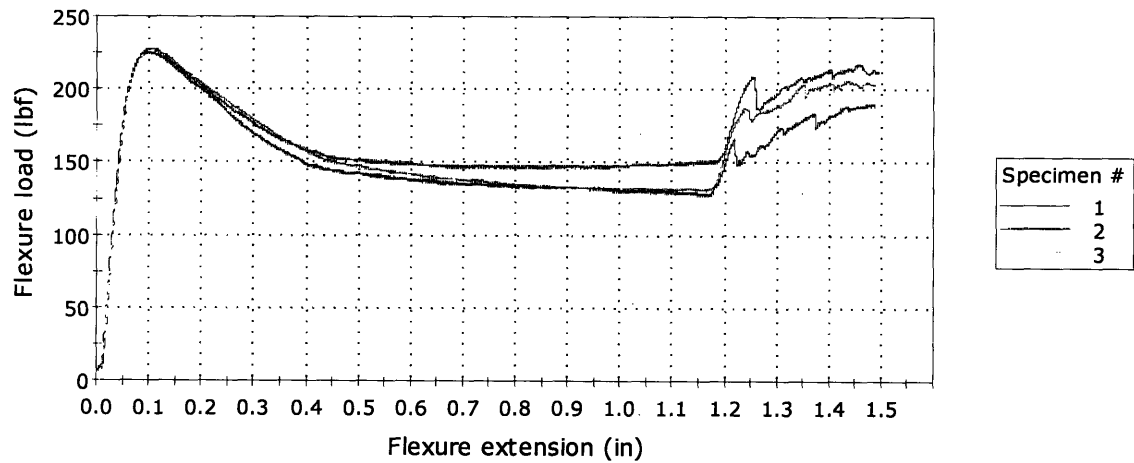


Figure 4.7 : Flexure load-extension curves for (a) no foam, no defects and (b) polymeric foam, no defects for diamond triangular core panels

Figure 4.8 shows the difference between a diamond square core with polymeric foam and a diamond triangular core with polymeric foam. The diamond

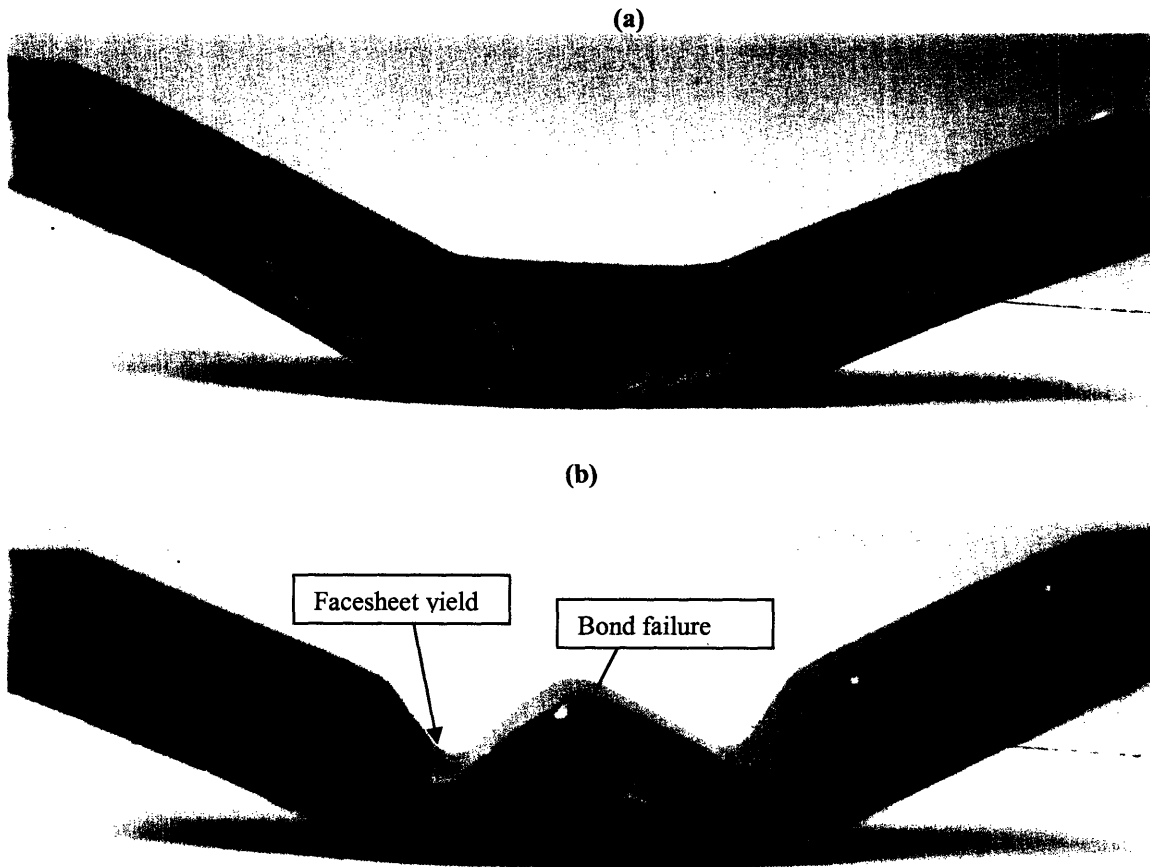


Figure 4.8 : Sandwich panels with polymeric foam filling, no defects and (a) diamond square core and (b) diamond triangular core

square core undergoes Mode A core shear. The panel shows a fairly symmetric response under loading, and plastic hinge formation under the rollers. The diamond triangular core however shows both face yielding and bond failure. The bond failure results in a large pore underneath the facesheet which most likely resulted in decreased peak flexure load.

The Load/Density ratio of hexagonal to diamond cores was much greater in the bending experiments than in the compression experiments. Table 4.6 shows the diamond

patterned cores had Load/Density ratios about 1.5 to 2 times greater than hexagonal patterned cores. This ratio is about half the amount it was for the compression tests and

Table 4.6 : Ratio of Hexagonal to Diamond patterned Load/Density values

Description	(Hexagonal/Diamond) Load/Density ratios	
	Square	Triangle
NF,ND	0.57	0.59
NF,D	0.54	0.61
Poly,ND	0.65	0.78
Poly,D	0.67	0.66

suggests that the choice of 2D honeycomb perforated sheet is less critical in bending than in compression. This is a result of the shear stresses involved in bending, which spoil the periodicity of the panels faster than the uniaxial compressive force does.

Metal foam filler resulted in panels with higher Load/Density ratios for all core types when compared with baseline no foam, no defect experiments. Table 4.7 lists these results. One striking observation from Table 4.7 is that in some cases metal foam filler

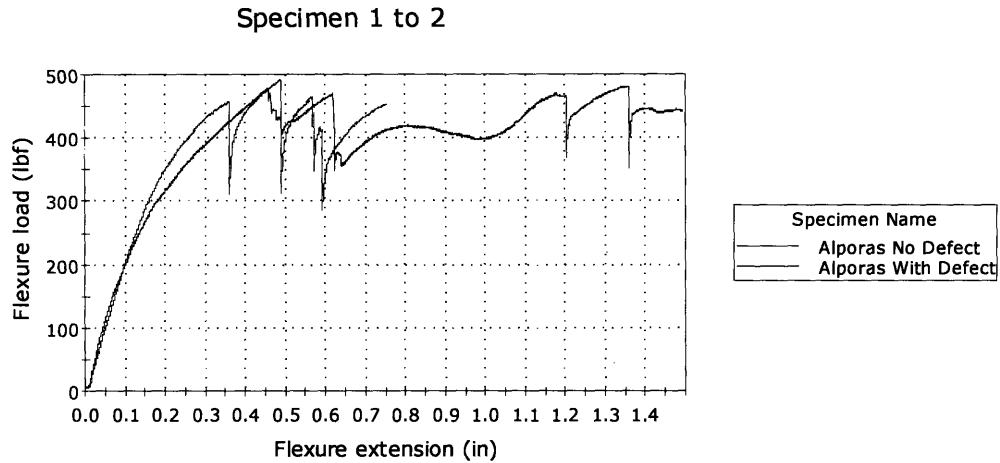
Table 4.7 : Metal foam filler effect on Load/Density ratios

Core Type	Effect of Metal Foam Filler		
	NF,ND	ALP,ND	ALP,D
Diamond Square	1	1.56	1.49
Diamond Triangle	1	2.00	2.55
Hex Square	1	3.41	5.11
Hex Triangle	1	3.05	2.76

resulted in higher peak flexure loads for defective cells than for non-defective cells.

Figure 4.9 shows the resulting flexure load-extension curves for diamond square panels and hexagonal triangular panels with Alporas ® foam filler. The shape of the curve is quite different from Figure 4.7. Sharp spikes and drops occur at multiple points on both curves. These drops result when a fracture occurs in one of the repeating cells. More fractured cells occur in the square cell core as would be expected due to the significant

(a)



(b)

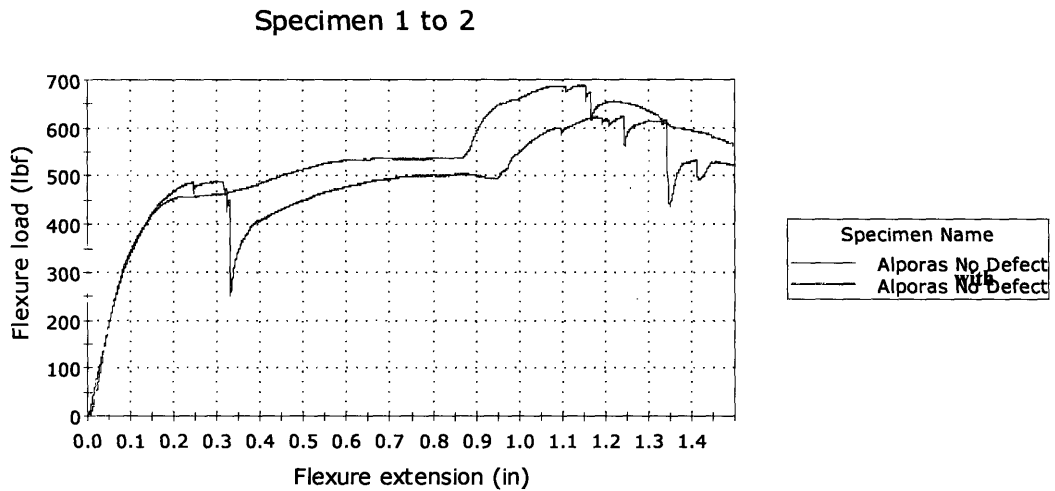


Figure 4.9 : Effect of metallic foam on load-extension curves. (a) diamond square core and (b) hexagonal triangular core

amount of shear involved. For four point bending, the periodicity of the cores puts the sandwich panels in a state of self stress. Defects in this periodicity may act as stress relief locations, allowing greater peak flexure loads to be obtained. Table 4.8 appears to

verify this observation, with (Defect/ No Defect) ratios of greater than unity for many of the foam filled core types.

Table 4.8 : Defect/No Defect ratios on Load/Density values for experiments

Core Type	Effect of Defects					
	NF		Poly		ALP	
	(D/ND)	Δ RD	(D/ND)	Δ RD	(D/ND)	Δ RD
Diamond Square	0.87	0.000	1.01	-0.002	0.96	-0.180
Diamond Triangle	0.86	-0.001	1.11	0.001	1.27	-0.176
Hex Square	0.82	-0.003	1.04	0.002	1.50	0.014
Hex Triangle	0.90	-0.001	0.94	-0.001	0.90	0.000

Appendix D contains time lapse photography for the four point bend tests. When defective cells with no foam filler were tested, a clear asymmetry in the deformation mechanism resulted. The asymmetry resulted in uneven load distribution and a greater shear force on one particular side of the sandwich panel. The use of foam filler mitigated this asymmetry, and higher flexure loads were obtained. When metal foam filler was used in hybrid panels, a significant increase in stiffness resulted, however fracture of metal core regions led to large instantaneous decreases in flexure loads.

4.2 Metallographic analysis

Figure 4.10 shows a comparison between the microstructure of a laboratory brazed joint and the microstructure of a joint from a procured sandwich panel.

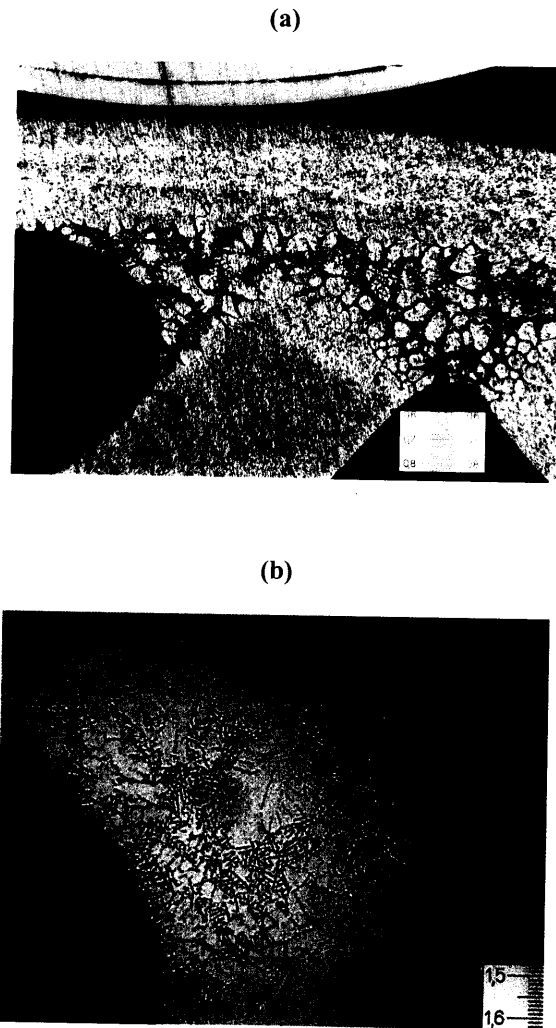


Figure 4.10 : Comparison of microstructures of (a) laboratory panel and (b) procured panel. All scales are in terms of mm

The second phase present in both microstructures is Mg_2Si , and results from diffusion of the clad brazing sheet. The distribution of Mg_2Si is much finer in the procured samples, indicative of better control in the dip brazing process. Figure 4.11 shows a small amount

of silicon interdiffusion into the brazed joint of the procured sample. This amount of diffusion is not expected to degrade the mechanical properties of the brazed joint.

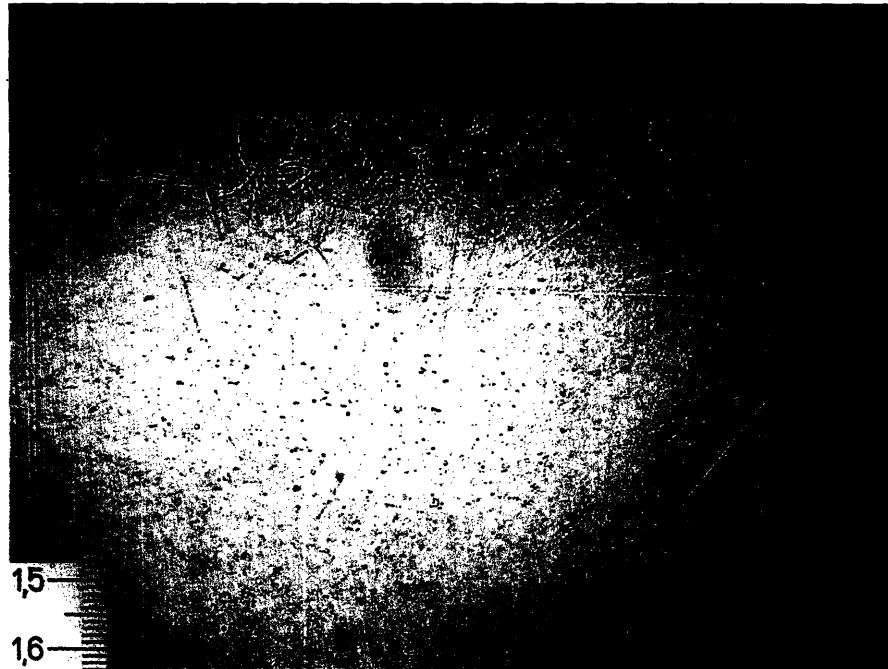


Figure 4.11 : Silicon interdiffusion into bulk aluminum brazed joint. Mag=50x. Scale in mm.

Magnification of this region to 200x shows the needle like second phase dispersed into the bulk aluminum. This is evident in Figure 4.12.

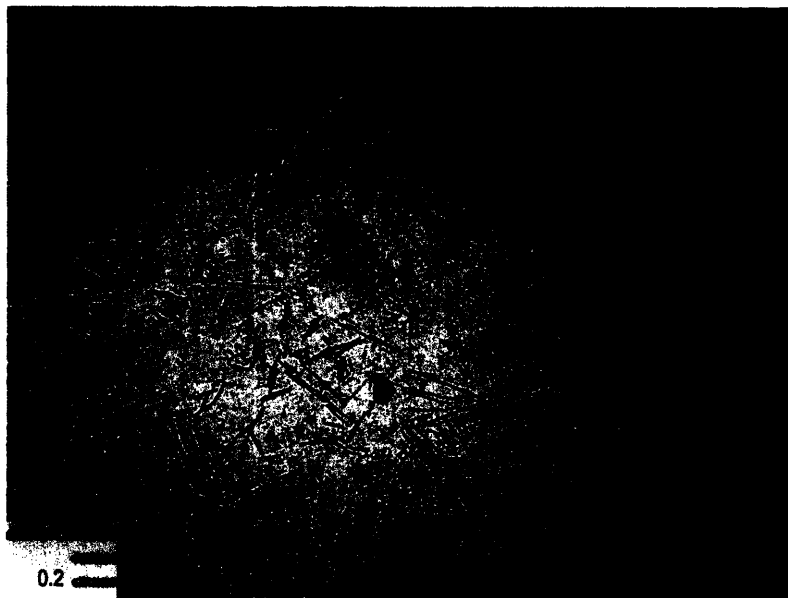


Figure 4.12 : Needle like Mg_2Si phase in the procured sample. Mag =200x . Scale in mm.

4.3 Simulation Results

Figure 4.13 shows the stress simulation result for the diamond square core sandwich panel. While the buckling mode of deformation in the core is consistent with experimental results, the stress in the core is approximately 1.25×10^4 Pa. Converting

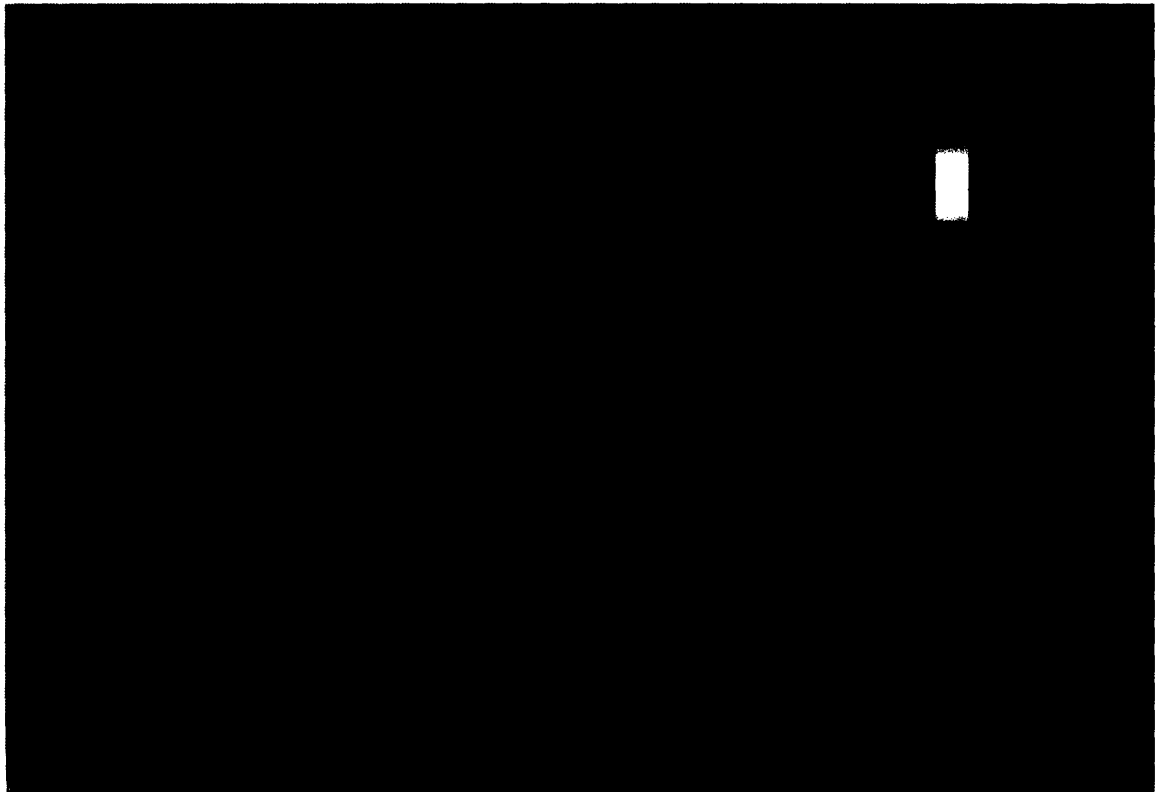


Figure 4.13 : Stress simulation results for diamond square sandwich panels

this value to psi gives a value of only 1.8 psi. This number is grossly less than what was observed in the experiments. There are two apparent causes for this result. The diamond core in this simulation does not extend fully to the edge of the sandwich panel, unlike the actual sandwich panels. Also, the facesheets show no stress in the simulation when in reality the facesheets carry the majority of the stresses in a uniaxial compression test. The facesheets had to be constrained in the COSMOS program, resulting in this inability to carry stress. This result signifies that buckling occurs when the diamond core

members alone reach a stress of 1.8psi. This is a more reasonable result although still less than what was observed experimentally. When tested without facesheets, square diamond cores reached an average peak compressive load of around 220 lbf. Dividing this value by 9 in², the area of the compressive fixture, gives a stress of about 15psi. The simulation is approximately one order of magnitude lower than experimentally observed. Refinement of the assembled CAD models and integration of these models into more robust FEA programs such as ABAQUS ® are expected to significantly improve future results.

Chapter 5 : Conclusions

This thesis has shown that cell shape, orientation of load, and presence of defects are critical parameters that must be addressed in the design process of sandwich panels. The choice of perforated honeycomb sheet combined with the choice of core cell shape significantly affected mechanical properties. Table 5.1 compares the absolute maximum and minimum compressive loads with baseline values for each of the sandwich panel core types. Table 5.2 does the same for the peak flexural loads of the four point bend results. For both tables the minimum values were obtained when no foam was added

Table 5.1 : Maximum and minimum peak compressive loads attained for each core type

	Core Type			
	Diamond Square	Diamond Triangle	Hex Square	Hex Triangle
Baseline (NF,ND)	3118.1	2192.9	567.1	398.4
Maximum	4107.3	2850	2205.2	2383
Minimum	2131.4	1440.6	440.4	335.8

Table 5.2 : Maximum and minimum peak flexural loads attained for each core type

	Core Type			
	Diamond Square	Diamond Triangle	Hex Square	Hex Triangle
Baseline (NF,ND)	206.9	248	97.3	124.9
Maximum	492.5	1056.4	770.4	688.9
Minimum	180.1	210.8	78	111.2

and the panels had defects. The maximum values were obtained when Alporas ® foam was added, however in some cases the panels had defects and in some cases they did not.

Sandwich panels with diamond shaped cores had compressive strengths about four times greater than hexagonal shaped cores, consistent with the theoretical findings of Wang and McDowell . In four point bending, the diamond cores were about twice as stiff as the hexagonal core types. These differences are attributed to the dominant modes of deformation in the panels. In compression, sandwich panels with a diamond honeycomb core deformed by out of plane buckling, while hexagonal core shapes deformed by in

plane crushing. In four point bending, shear stresses destroyed the periodicity of the sandwich structure faster than did the uniaxial compressive stress. It is shown that the mechanical properties of the sandwich panels are inherently related to the cell architecture.

Defect introduction resulted in lower Load/Density ratios for all core types in both compression and bending. In compression, panels with defective square and triangular diamond cores were approximately 30% weaker than non-defective cores, while defects in square and triangular hexagonal cores resulted in a 15% drop in strength for those panels. The panels with hexagonal cores were substantially lower in strength in the absence of defects than were panels with diamond cores. Filling defective panels with polymeric foam led to an increase of about 6% in the Load/Density ratio for all core types over defective panels with no foam filler. Addition of polymeric foam into non defective panels resulted in slightly less optimal panels with diamond cores but slightly better panels with hexagonal cores in compression. In four point bending, panels with defective square and triangular diamond cores were about 13% weaker than non-defective cores. Defective hexagonal square panels were 18% weaker and defective hexagonal triangular panels were 10% weaker than panels with no defects. The addition of polymeric foam into both defective and non defective panels resulted in higher Load/Density ratios in panels with hexagonal cores that when no foam and no defects were present. Panels with a defective diamond square core showed a 12% increase in flexural strength as a result of polymer foam filling. For defective diamond triangle cores this increase was only 3%. The addition of polymeric foam resulted in higher absolute peak compressive and

flexural strengths, however the weight increase associated with the foam did not always result in better panels.

Use of metallic foam also did not always result in more optimal panels than those without foam and defects. In compression, the addition of metallic foam resulted in an increase of about 1000 *lbf* over panels with a diamond square core, no foam, and no defects. However the diamond square core with no foam and no defects had the highest Load/Density ratio when normalized for weight. In contrast, panels with hexagonal square and hexagonal triangular cores exhibited a marked increase in their Load/Density ratios upon addition of metallic foam. A 200-300% increase in this ratio was observed regardless of whether defective or non-defective panels were examined. In four point bending, the addition of metallic foam resulted in significant increases in flexural strength for all core types. In some cases, defective panels filled with metallic foam achieved greater Load/Density ratios than non-defective panels filled with metallic foam.

The sandwich panels examined in this research have mechanical properties comparable with other sandwich core topologies examined in the literature. The use of perforated honeycomb sheet in the design of the sandwich panel core allowed for additional weight savings. The choice of dip brazing as the method of joining has been shown as an effective method to produce complexly shaped aluminum sandwich panels. An attempt at quantifying the effect of defects on sandwich structures resulted in values similar to previously published theoretical analyses. The study of multiple types of foam filler have shown that in most cases the addition of foam is justified and the strength or stiffness gained more than offsets the additional weight.

Future work involves improvement of the simulation models. The use of a more robust FEA program is expected to result in simulations that more accurately describe the interfacial effects and deformation mechanisms in the sandwich structure. Also, computational modeling will allow for tests to be made without having to procure individual samples. Expanding the experimental matrix to include panels with varying thicknesses in both the facesheet and core are also critical to fully characterizing these materials. Finally, evaluation of more core shapes and perforated sheet patterns will allow for an optimum design to be attained.

Appendix A : Background on the Importance of Welding and Joining

Often overlooked in everyday life is the importance welding and joining play in the products we use. You couldn't drive to work without the numerous welds needed to assemble your vehicle. Your place of work would cease to exist, as the majority of office buildings require extensive welding of structural steel in their foundations. While at work you would not be able to check your email, as the personal computer is a technological device that combines multiple joining techniques, such as soldering and adhesive bonding. So, while it may not seem that welding and joining play a vital role in an individual's daily life, the importance of welding becomes clearly apparent if one is responsible for manufacturing the product.

The discovery of the electric arc by Sir Humphry Davy in 1801 was a critical development in the growth of welding technology. Welding is the joining together of two pieces of metal by heating to a temperature capable of softening or melting the metal. Pressure may or may not be applied depending on the welding process, as well as the choice to use filler metal or not [47]. Figure A.1 shows a typical oxyacetylene welding process. Over 90 welding processes are currently developed, including oxyacetylene welding, TIG and MIG welding, spot welding, and electric beam welding to name a few[47]. Welding is a joining process used across many industries, however sometimes welding is an unsuitable process for a particular application and another joining process must be used.

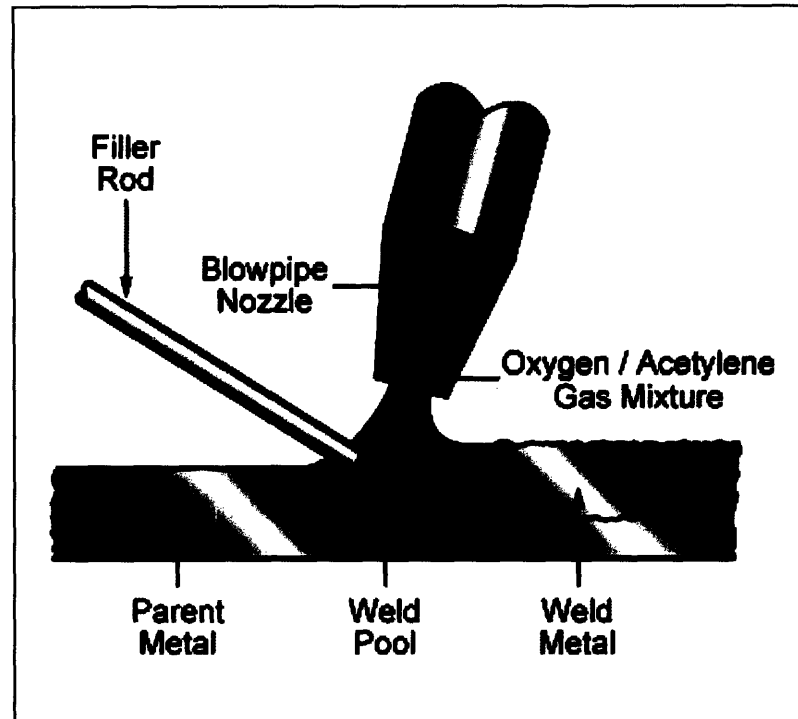
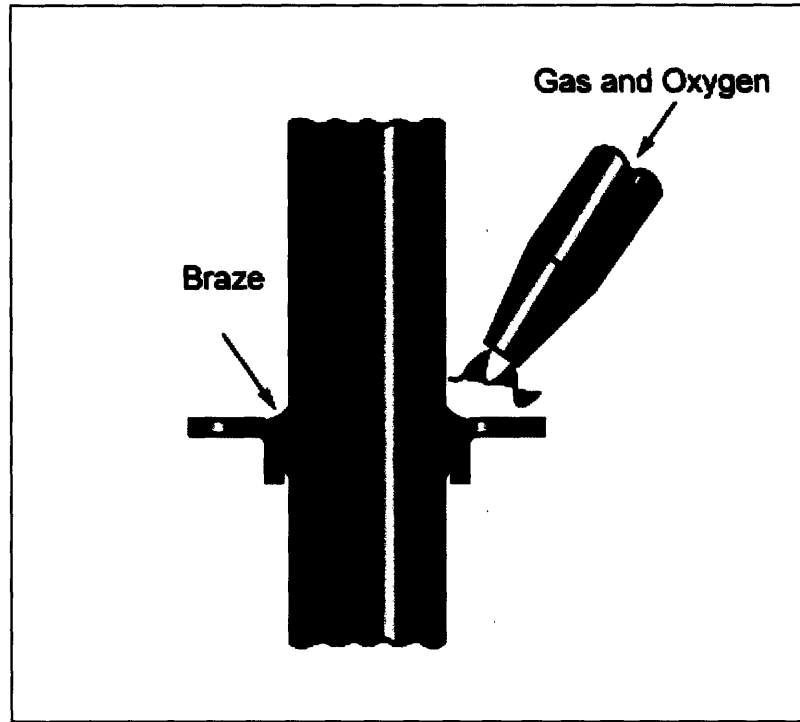


Figure A.1: Oxyacetylene welding process schematic [48]
(figure courtesy of Granta Design, Cambridge UK)

Brazing differs from welding in the temperature at which the process is performed. As opposed to soldering, which occurs below 450 °C, brazing is a joining process which takes place above 450 °C (840 °F) [8]. The term brazing encompasses a group of processes that produce coalescence of materials by the heating of a filler metal with a melting point above 450 °C but below the melting point of the base metal [40]. Figure A.2 depicts a typical brazing process. Brazing is often used when the operating temperatures of the materials being joined prohibit the use of a welding process.

There are important advantages to brazing as opposed to other joining techniques. Brazing produces products containing excellent stress distribution and heat transfer properties [40]. One of the most important advantages of brazing over other techniques

is brazing allows for the economical fabrication of complex and multi-component assemblies.



**Figure A.2 : Typical brazing process schematic [48]
(figure courtesy of Granta Design, Cambridge UK)**

Complicated assemblies, containing odd shapes and multiple joint thicknesses, would be extremely difficult to join by fusion welding. It is possible to join dissimilar materials, such as metals and ceramics, by brazing. Easily reproducible joints of precise tolerances can be made on complex-shaped samples only by brazing [40]. The multiple ways of applying heat lead to a variety of brazing processes, including torch, furnace, induction, vacuum, and dip brazing among others. Indeed, brazing is at times the only feasible method to join certain materials based on the material requirements.

There are limitations to brazing. Since a filler metal is often used, heterogeneous joints are made which may limit the overall strength of the product. Usually, since fillers are used that melt very close to the melting temperature of the base metal, a heat affected

zone (HAZ) is produced. The HAZ contains a strongly altered microstructure from the base metal, due to the kinetics involved in the mass transfer involved in filling the joint [41]. Table A.1 displays a comparison between welding, brazing, and soldering techniques. Other types of joining processes not involving the melting of filler metals include fastening and adhesive bonding.

Table A.1 Comparison of Welding, Brazing, and Soldering Processes (adapted from [4])

Item compared	Process		
	Welding	Brazing	Soldering
Filler-metal melting temp.	> 450 deg. C	> 450 deg. C	< 450 deg. C
Residual stresses	Significant around welding area	Minor	Minor
Tendency to warp	Typically warping of base metal occurs	Atypical	Atypical
Base metal	Melts	Does not melt	Does not melt

The choice of joining process is critical and must be made in the early stages of product design. The costs of joining can exceed 50 percent of the total product cost in certain complex assemblies, thus requiring specification of the joining process in early product design [8]. Improper selection of joining technique can lead to future material failure. In addition, improper joint preparation and pre-cleaning can lead to joint defects when the proper technique has been chosen. Understanding the material properties of the items being joined, as well as understanding the limitations imposed on the choice of joining process because of these properties can prevent improper selection. Ultimately, producing a quality joint at lowest cost is the desired outcome.

Appendix B : Background on Aluminum Alloys

Aluminum alloys are designated by a four digit number. For this thesis 6000 series aluminum alloys were used to manufacture all samples that were mechanically tested. The 6000 series aluminum alloys are known for their good formability as well as their ability to be heat treated [49]. Table B.1 displays the characteristics of different series of alloys.

Table B.1 : Aluminum Alloy Designations

Aluminum Series	Alloying elements	Ability to heat treat	General characteristics
1xxx	Aluminum (at least 99% pure)	No	1)Very high corrosion resistance 2)High electrical conductivity 3)High thermal conductivity 4)Good formability 5)Low strength
2xxx	Aluminum-Copper	Yes	1)High strength to weight ratio 2)Low corrosion resistance
3xxx	Aluminum-Manganese	No	1)Good formability 2)Moderate strength
4xxx	Aluminum-Silicon	No	1)Lower than usual melting point
5xxx	Aluminum-Magnesium	No	1)Good corrosion resistance 2)Easy to weld 3)Moderate to high strength
6xxx	Aluminum-Magnesium-Silicon	Yes	1)Moderate to high strength 2)Good formability and machinability 3)Good weldability 4)Good corrosion resistance
7xxx	Aluminum-Zinc	Yes	1) Moderate to very high strength 2)Prone to fatigue

The ability to heat treat is an important factor in alloy choice, because it determines the mechanism for hardening. Heat-treatable alloys can be hardened and have their properties improved by thermal treatments, such as solution heat treatment and artificial aging [30]. Non heat-treatable alloys increase their hardness through cold working processes such as rolling. For non heat-treatable alloys the maximum temperature to which the alloy can be heated without serious loss of mechanical

properties is 300-400 °F [30]. The dip brazing process occurs at a temperature higher than this, and thus requires a post-brazing heat treatment to restore mechanical properties.

The temper chosen for an aluminum alloy is another important design choice. The temper is a major determinant in an alloy's ultimate strength, hardness, and ductility [50]. Table B.2 details particular tempers while Table B.3 breaks down particular types of heat treated tempers (adapted from [29]). The choice of temper

Table B.2 : Tempers of Aluminum Alloys

Temper	Description of temper
-O	Annealed. This is the softest temper of wrought alloys.
-F	As fabricated. (Forgings and castings prior to heat treatment)
-H	Strain-hardened. (Strengths increased by cold working).
-T	Solution heat treated
-W	Unstable condition following solution heat treatment.

Table B.3 : Common solution heat treated tempers

Temper	Description of temper
T3	Solution heat treated, cold worked, and then naturally aged to a stable condition
T4	Solution heat treated and then naturally aged to a stable condition
T5	Artificial aging after an elevated temperature, rapid-cool fabrication process (such as casting).
T6	Solution heat treated and then artificially aged.
T8	Solution heat treated, cold worked, and then artificially aged.
T9	Solution heat treated, artificially aged, and then cold worked.

appears after the four digit series number.

Appendix C : Data from Mechanical Tests

COMPRESSION TEST RESULTS						
		(mean)	664	divide by 664	(mean)	
Description	Core Type	Weight (g)		Relative Density	Peak Compressive Load (lbf)	
Poly, ND	Diamond Square	89.10		0.134	3234.3	
Poly, ND	Diamond Triangle	79.46		0.120	2439.2	
Poly, ND	Hex Square	75.11		0.113	651.3	
Poly, ND	Hex Triangle	70.09		0.106	478.4	
NF, ND	Diamond Square	79.64		0.120	3118.1	
NF, ND	Diamond Triangle	70.40		0.106	2192.9	
NF, ND	Hex Square	66.57		0.100	567.1	
NF, ND	Hex Triangle	60.40		0.091	398.4	
NF, D	Diamond Square	76.64		0.115	2131.4	
NF, D	Diamond Triangle	68.80		0.104	1440.6	
NF, D	Hex Square	61.31		0.092	440.4	
NF, D	Hex Triangle	59.74		0.090	335.8	
Poly, D	Diamond Square	86.70		0.131	2571.8	
Poly, D	Diamond Triangle	79.92		0.120	1840.7	
Poly, D	Hex Square	74.36		0.112	576.6	
Poly, D	Hex Triangle	69.44		0.105	418.6	
ALP, ND	Diamond Square	113.65		0.171	4107.3	
DUO,ND	Diamond Square	115.85		0.174	3920.7	
ALP, D	Diamond Square	122.65		0.185	4069	
ALP, ND	Diamond Triangle	122.09		0.184	2850	* Local max
ALP, D	Diamond Triangle	122.34		0.184	2090	* Local max
ALP, ND	Hex Square	105.00		0.158	1977	
DUO,ND	Hex Square	100.20		0.151	1583.3	
ALP, D	Hex Square	103.30		0.156	2205.2	
ALP, ND	Hex Triangle	113.70		0.171	2383	
ALP, D	Hex Triangle	111.30		0.168	2277.3	

Definitions:
 NF = No foam added
 Poly = Polyurethane foam added
 ALP = Alporas metallic foam added
 DUO = Duocel metallic foam added
 ND = No Defects
 D = Defects

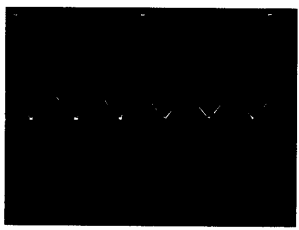

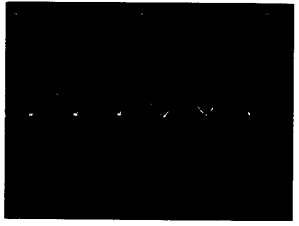
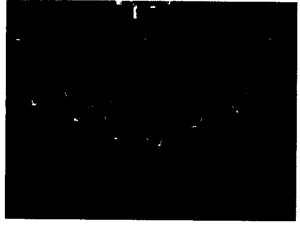



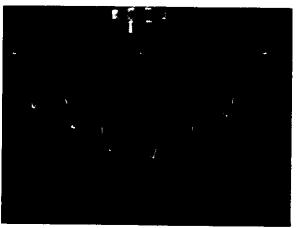

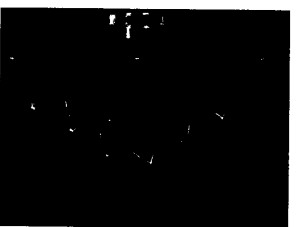

COMPRESSION TEST RESULTS Pg.2			
		divide Peak by 9in ²	9
Description	Core Type	Max. Compr. Stress (psi)	Load/ Density Ratio
Poly, ND	Diamond Square	359.4	24103.0
Poly, ND	Diamond Triangle	271.0	20382.9
Poly, ND	Hex Square	72.4	5757.7
Poly, ND	Hex Triangle	53.2	4532.1
NF, ND	Diamond Square	346.5	25997.2
NF, ND	Diamond Triangle	243.7	20683.0
NF, ND	Hex Square	63.0	5656.5
NF, ND	Hex Triangle	44.3	4379.8
NF, D	Diamond Square	236.8	18466.2
NF, D	Diamond Triangle	160.1	13903.5
NF, D	Hex Square	48.9	4769.6
NF, D	Hex Triangle	37.3	3732.4
Poly, D	Diamond Square	285.8	19696.4
Poly, D	Diamond Triangle	204.5	15293.1
Poly, D	Hex Square	64.1	5148.8
Poly, D	Hex Triangle	46.5	4002.7
		0.0	
ALP, ND	Diamond Square	456.4	23996.9
DUO,ND	Diamond Square	435.6	22471.7
ALP, D	Diamond Square	452.1	22028.7
ALP, ND	Diamond Triangle	316.7	15500.0
ALP, D	Diamond Triangle	232.2	11343.5
ALP, ND	Hex Square	219.7	12502.2
DUO,ND	Hex Square	175.9	10492.1
ALP, D	Hex Square	245.0	14174.8
ALP, ND	Hex Triangle	264.8	13916.6
ALP, D	Hex Triangle	253.0	13586.0

Four Point Bend Results						
		(mean)	664	divide by 664	(mean)	
Description	Core Type	Weight (g)		Relative Density	Peak Flexure Load (lbf)	
Poly, ND	Diamond Square	89.13		0.134	232.7	
Poly, ND	Diamond Triangle	79.34		0.119	227.5	
Poly, ND	Hex Square	71.77		0.108	121.3	
Poly, ND	Hex Triangle	69.59		0.105	155.7	
NF, ND	Diamond Square	78.04		0.118	206.9	
NF, ND	Diamond Triangle	69.91		0.105	248	
NF, ND	Hex Square	64.17		0.097	97.3	
NF, ND	Hex Triangle	60.16		0.091	124.9	
NF, D	Diamond Square	78.03		0.118	180.1	
NF, D	Diamond Triangle	69.15		0.104	210.8	* Local Max
NF, D	Hex Square	62.44		0.094	78	* Local Max
NF, D	Hex Triangle	59.80		0.090	111.2	
Poly, D	Diamond Square	87.55		0.132	230.8	
Poly, D	Diamond Triangle	80.14		0.121	254.4	
Poly, D	Hex Square	73.11		0.110	128.6	
Poly, D	Hex Triangle	68.86		0.104	144.8	
ALP, ND	Diamond Square	119.40		0.180	492.5	*Abs. max
ALP, D	Diamond Square	121.30		0.183	480.7	*Abs. max
ALP, ND	Diamond Triangle	119.00		0.179	842.8	* Abs max
ALP, D	Diamond Triangle	117.00		0.176	1056.4	* Abs max
ALP, ND	Hex Square	110.40		0.166	570.3	
ALP, D	Hex Square	99.40		0.150	770.4	
ALP, ND	Hex Triangle	108.65		0.164	688.9	
ALP, D	Hex Triangle	108.55		0.163	622.1	

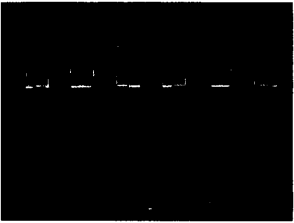
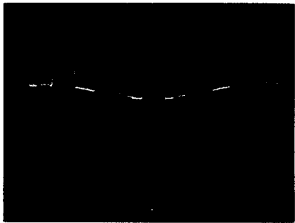
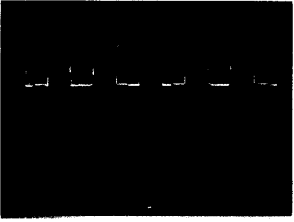
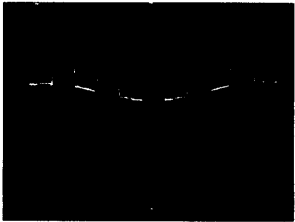
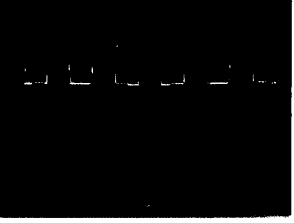
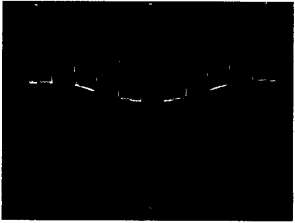
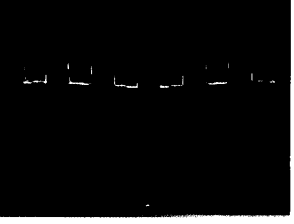
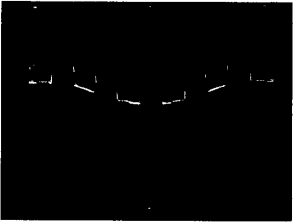
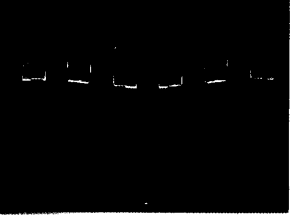
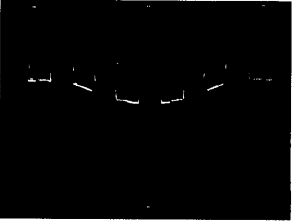

Four Point Bend Results Pg. 2			
		divide Peak by 15in^2	15
Description	Core Type	Max. Flex. Stress (psi)	Load/ Density Ratio
Poly, ND	Diamond Square	15.5	1733.6
Poly, ND	Diamond Triangle	15.2	1904.0
Poly, ND	Hex Square	8.1	1122.2
Poly, ND	Hex Triangle	10.4	1485.6
NF, ND	Diamond Square	13.8	1760.4
NF, ND	Diamond Triangle	16.5	2355.5
NF, ND	Hex Square	6.5	1006.8
NF, ND	Hex Triangle	8.3	1378.6
NF, D	Diamond Square	12.0	1532.6
NF, D	Diamond Triangle	14.1	2024.2
NF, D	Hex Square	5.2	829.5
NF, D	Hex Triangle	7.4	1234.7
Poly, D	Diamond Square	15.4	1750.4
Poly, D	Diamond Triangle	17.0	2107.8
Poly, D	Hex Square	8.6	1168.0
Poly, D	Hex Triangle	9.7	1396.3
		0.0	
ALP, ND	Diamond Square	32.8	2738.9
ALP, D	Diamond Square	32.0	2631.4
ALP, ND	Diamond Triangle	56.2	4702.7
ALP, D	Diamond Triangle	70.4	5995.3
ALP, ND	Hex Square	38.0	3430.1
ALP, D	Hex Square	51.4	5146.3
ALP, ND	Hex Triangle	45.9	4210.1
ALP, D	Hex Triangle	41.5	3805.4

Appendix D : Time Lapse Photography of Mechanical Tests

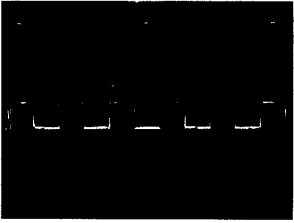

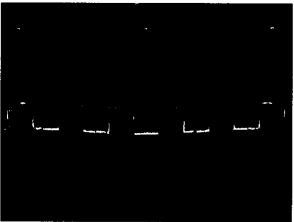
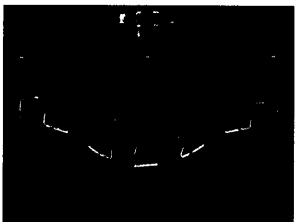
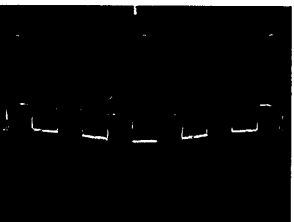
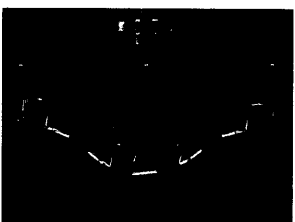
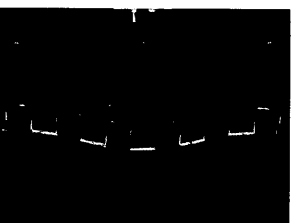
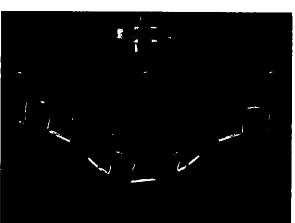
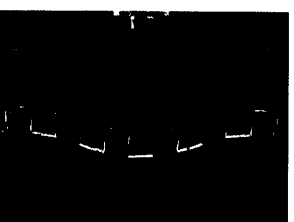


4 Point Bend Diamond Triangle with Defect

1) 	7) 
2) 	8) 
3) 	9) 
4) 	10) 
5) 	11) 
6) 	

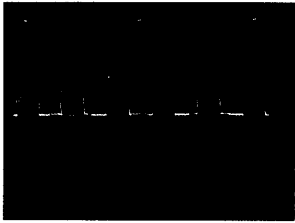

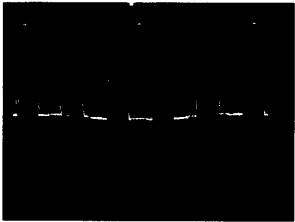

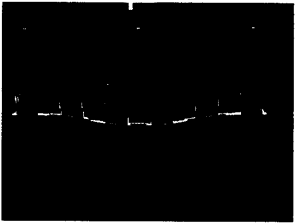
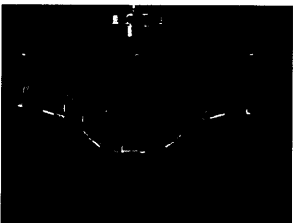
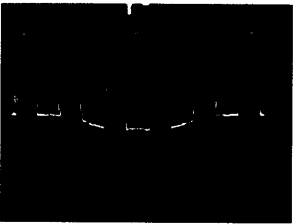
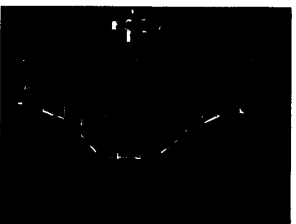
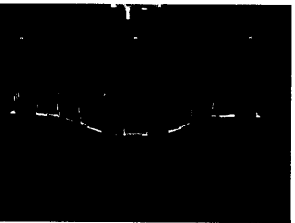

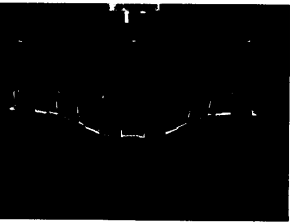
4 Point Bend Diamond Square

1) 	7) 
2) 	8) 
3) 	9) 
4) 	10) 
5) 	11) 
6) 	

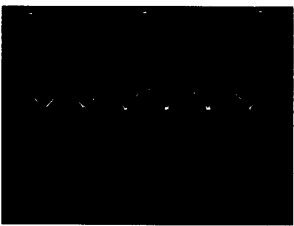

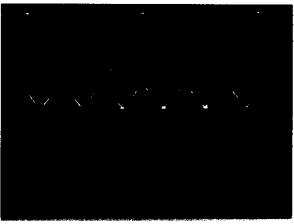
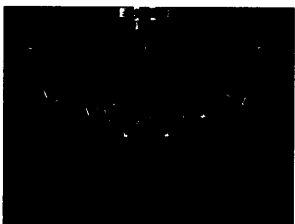
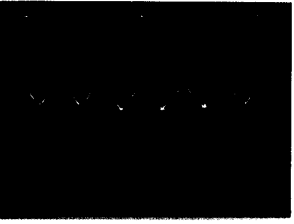
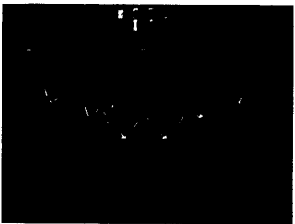
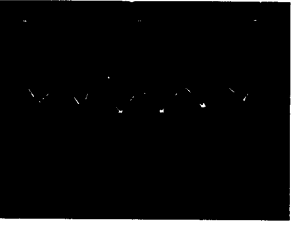
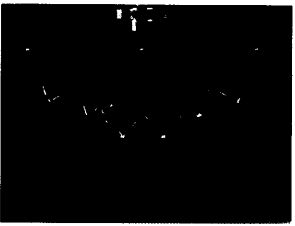



4 Point Bend Diamond Square with Defect

1) 	7) 
2) 	8) 
3) 	9) 
4) 	10) 
5) 	11) 
6) 	

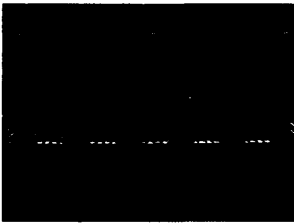
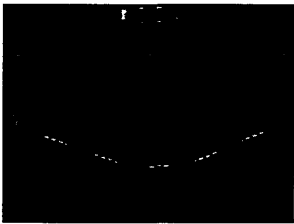
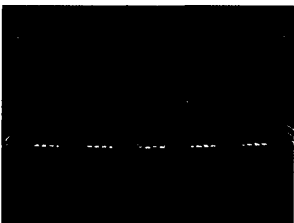
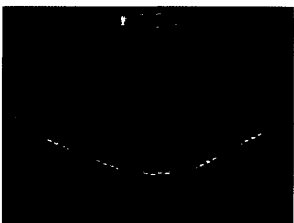

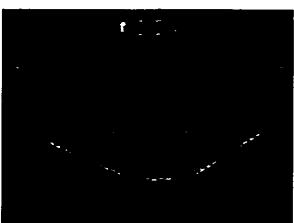
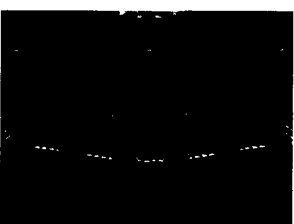
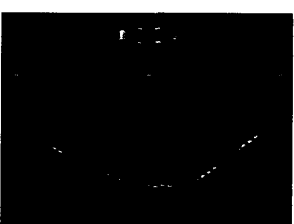


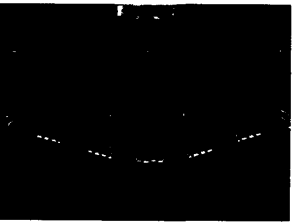
4 Point Bend Diamond Square 2

1) 	7) 
2) 	8) 
3) 	9) 
4) 	10) 
5) 	11) 
6) 	

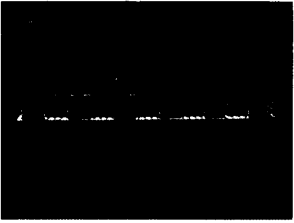

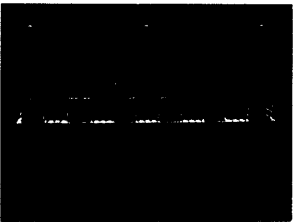
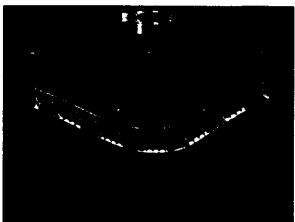
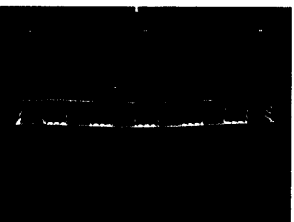
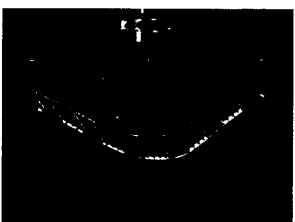
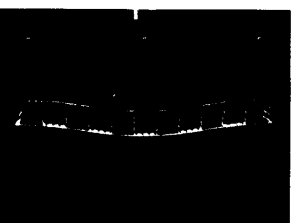

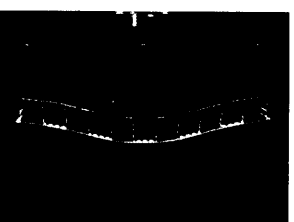
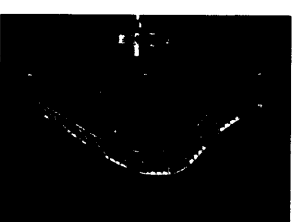

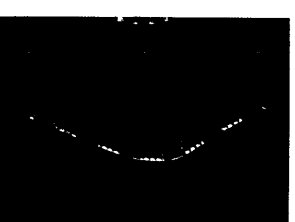
4 Point Bend Diamond Triangle

1) 	7) 
2) 	8) 
3) 	9) 
4) 	10) 
5) 	11) 
6) 	

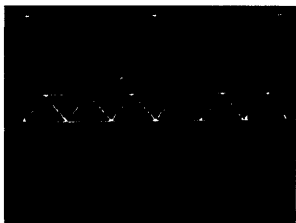

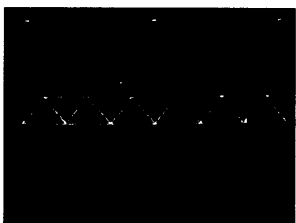
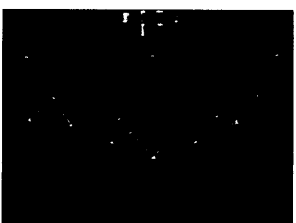
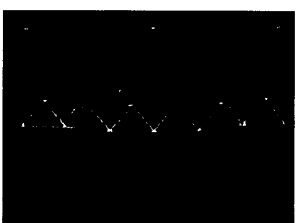





4 Point Bend Hexagonal Square with Defect

1) 	7) 
2) 	8) 
3) 	9) 
4) 	10) 
5) 	11) 
6) 	

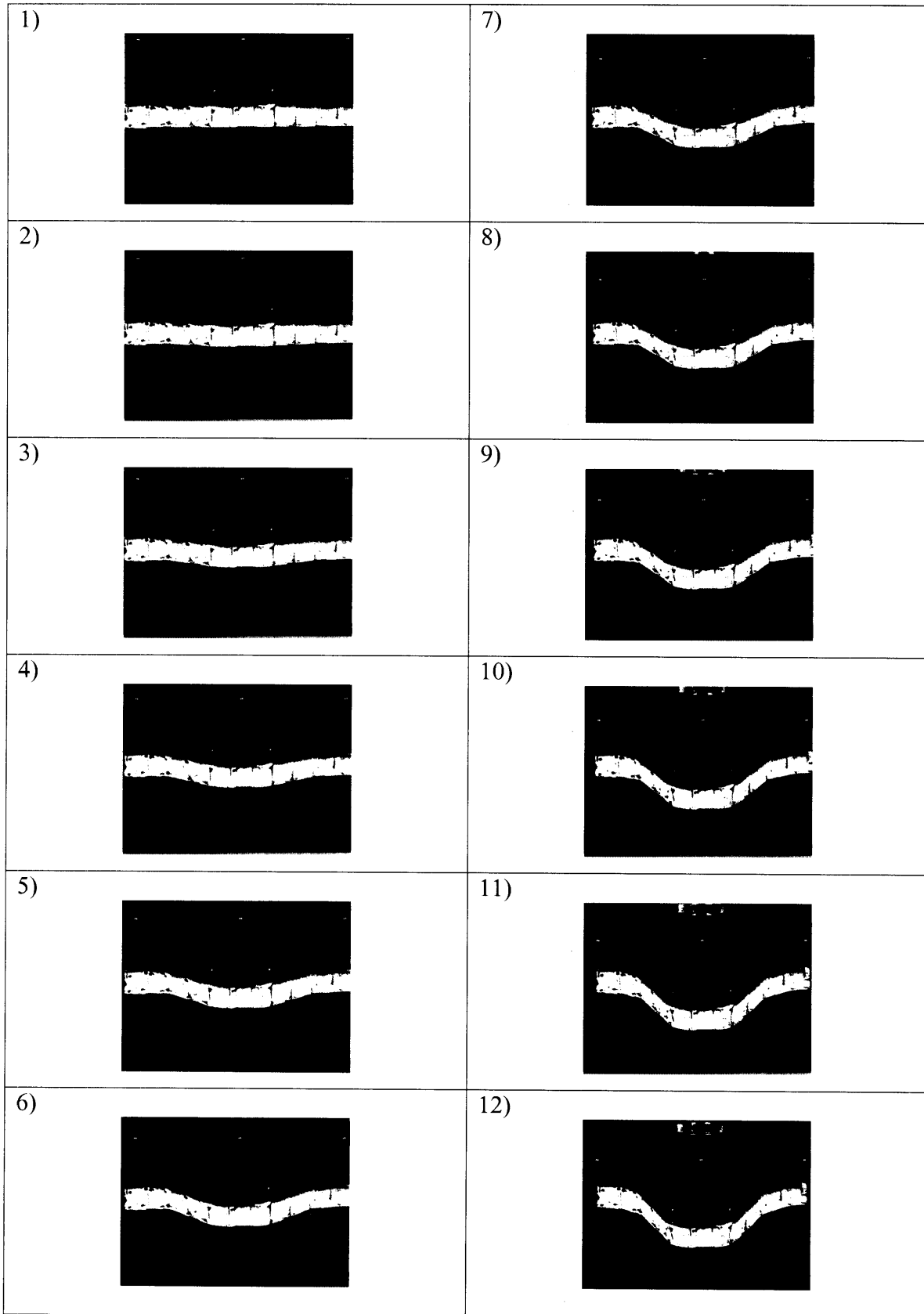
4 Point Bend Hexagonal Square

1)		7)	
2)		8)	
3)		9)	
4)		10)	
5)		11)	
6)		12)	

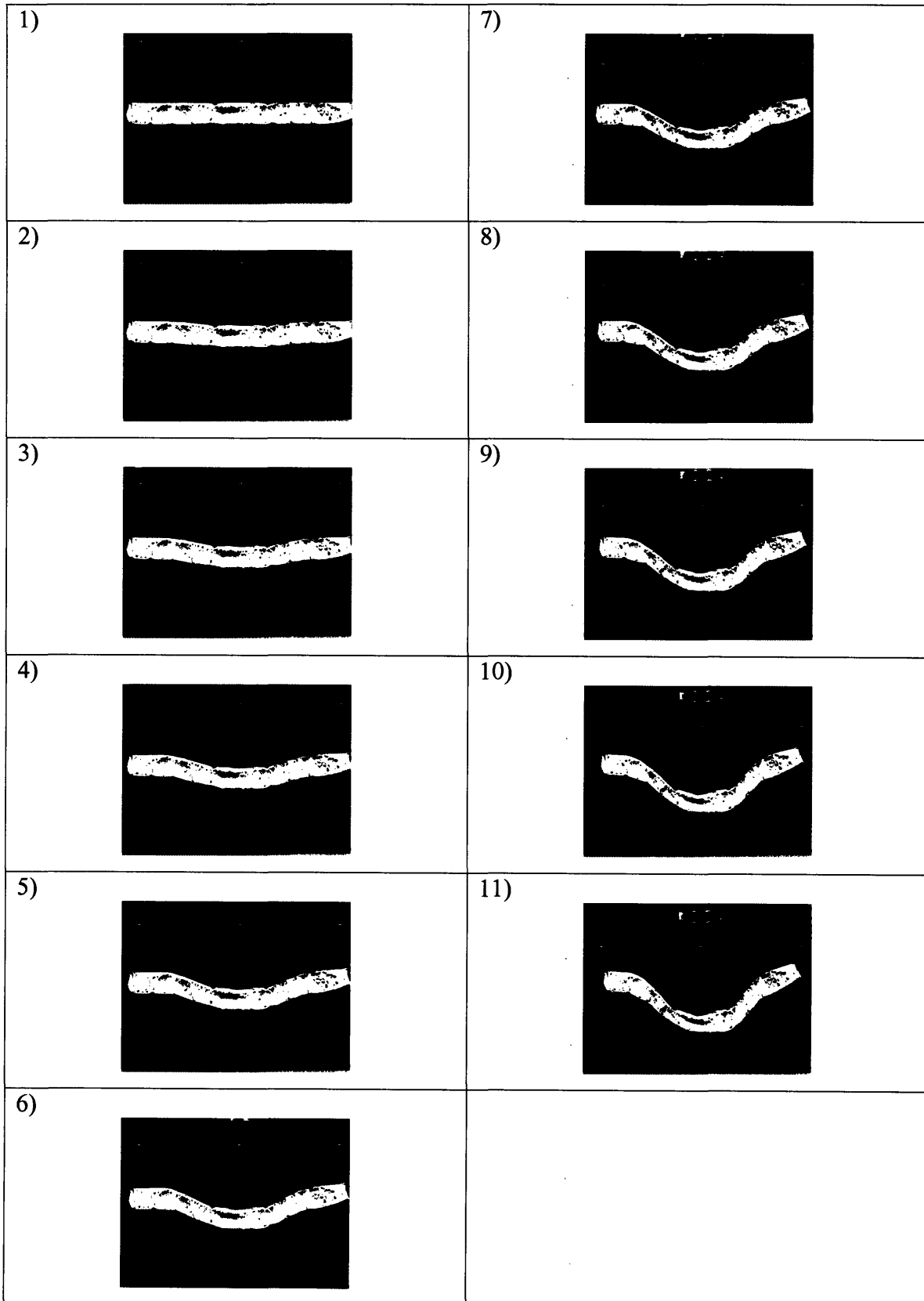
4 Point Bend Hexagonal Triangle

1) 	7) 
2) 	8) 
3) 	9) 
4) 	10) 
5) 	
6) 	

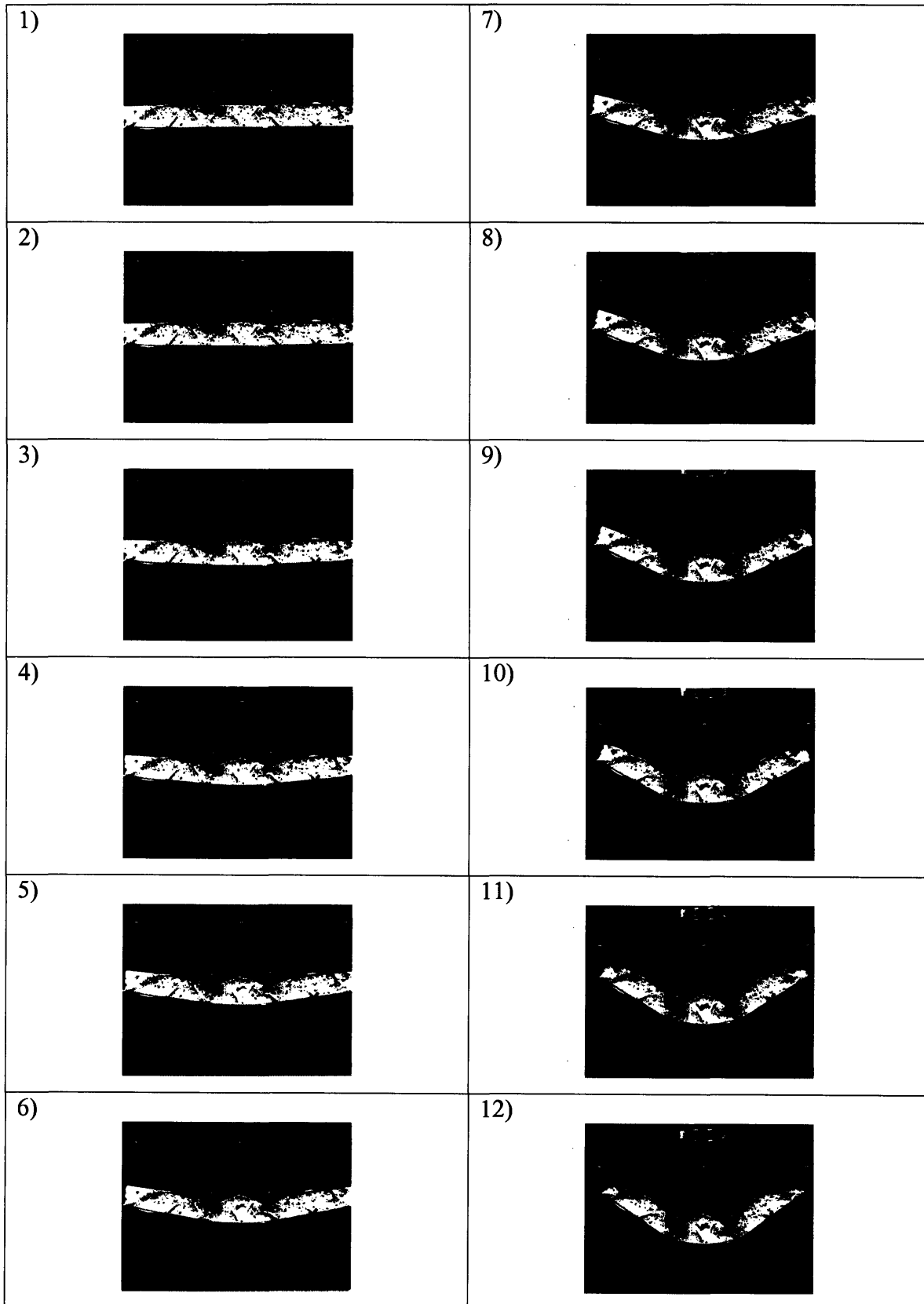
4 Point Bend Diamond Square with Polymeric Foam





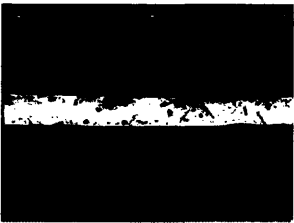

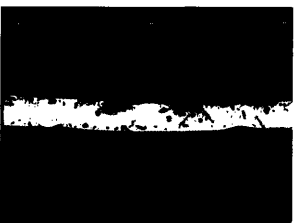

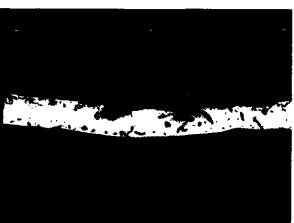
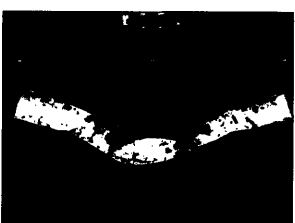



4 Point Bend Diamond Square with Polymeric Foam 2



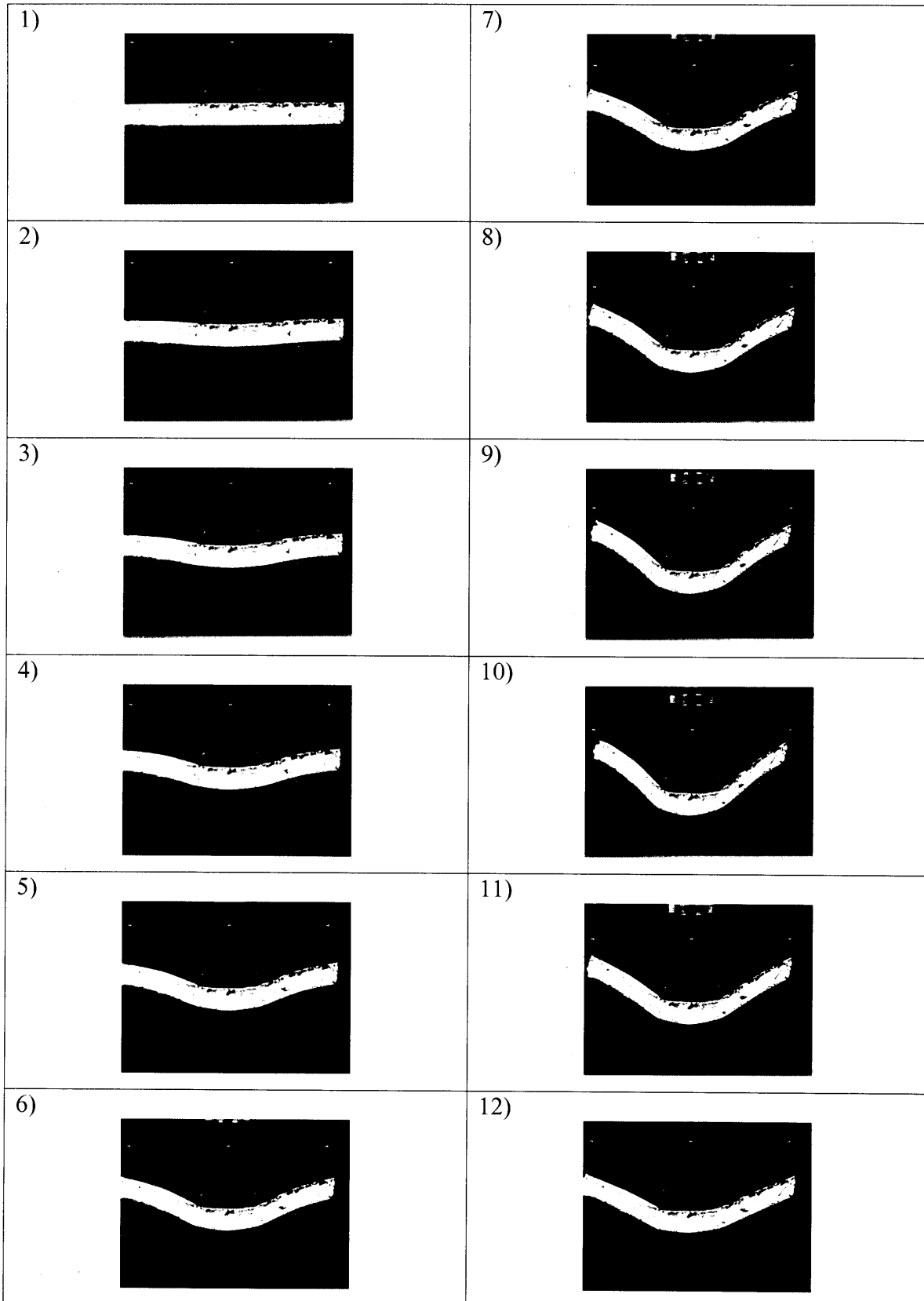
4 Point Bend Diamond Triangle with Polymeric Foam



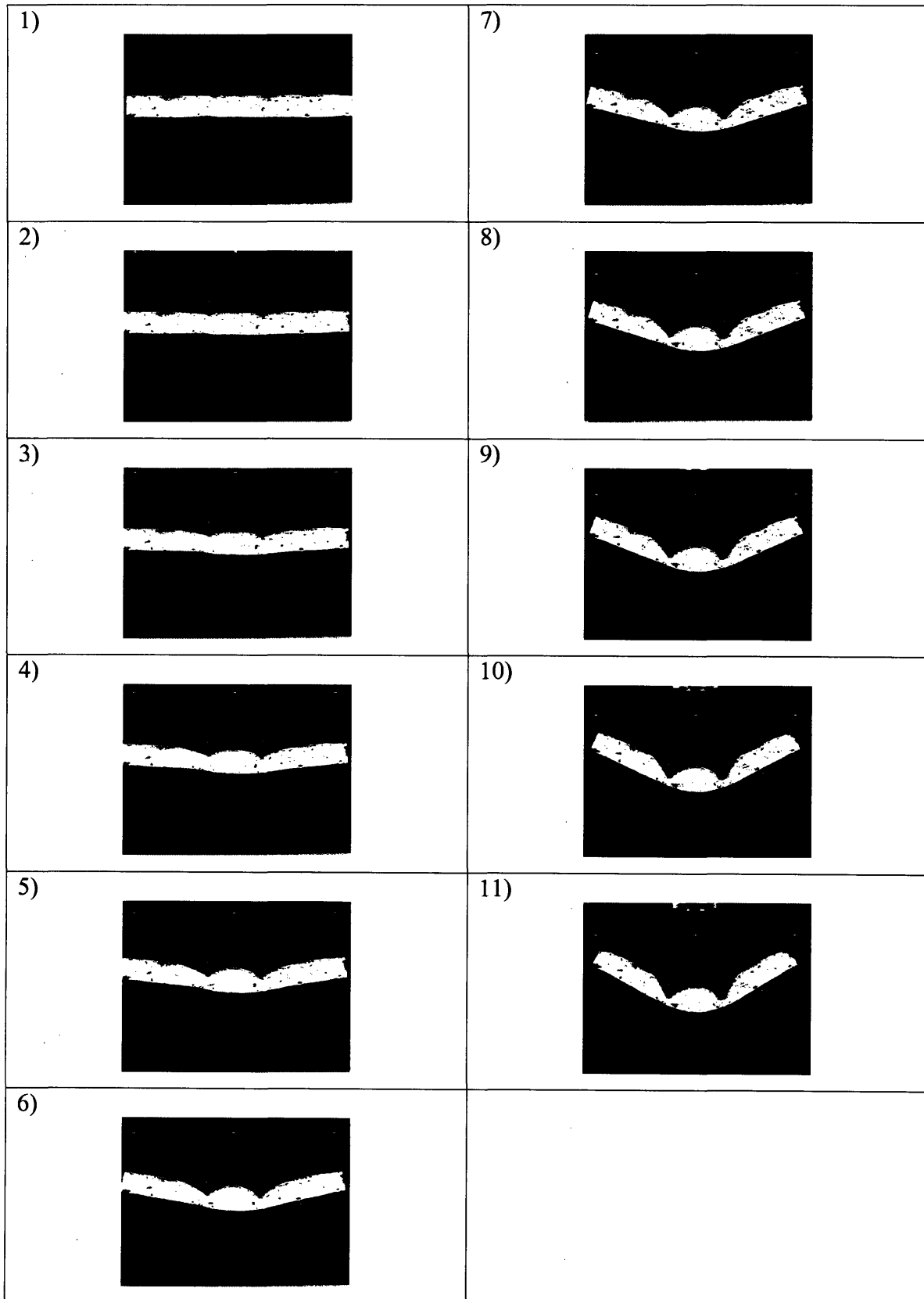
4 Point Bend Diamond Triangle with Defect with Polymeric Foam

1) 	7) 
2) 	8) 
3) 	9) 
4) 	10) 
5) 	11) 
6) 	


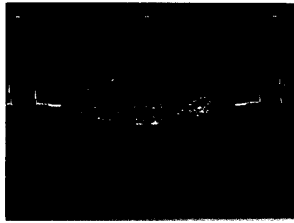





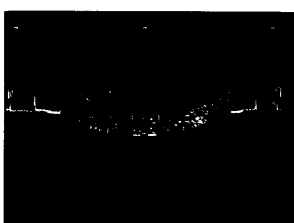


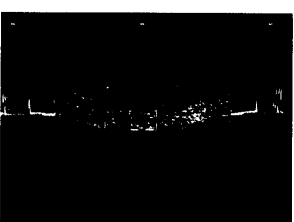
4 Point Bend Hexagonal Square with Polymeric Foam



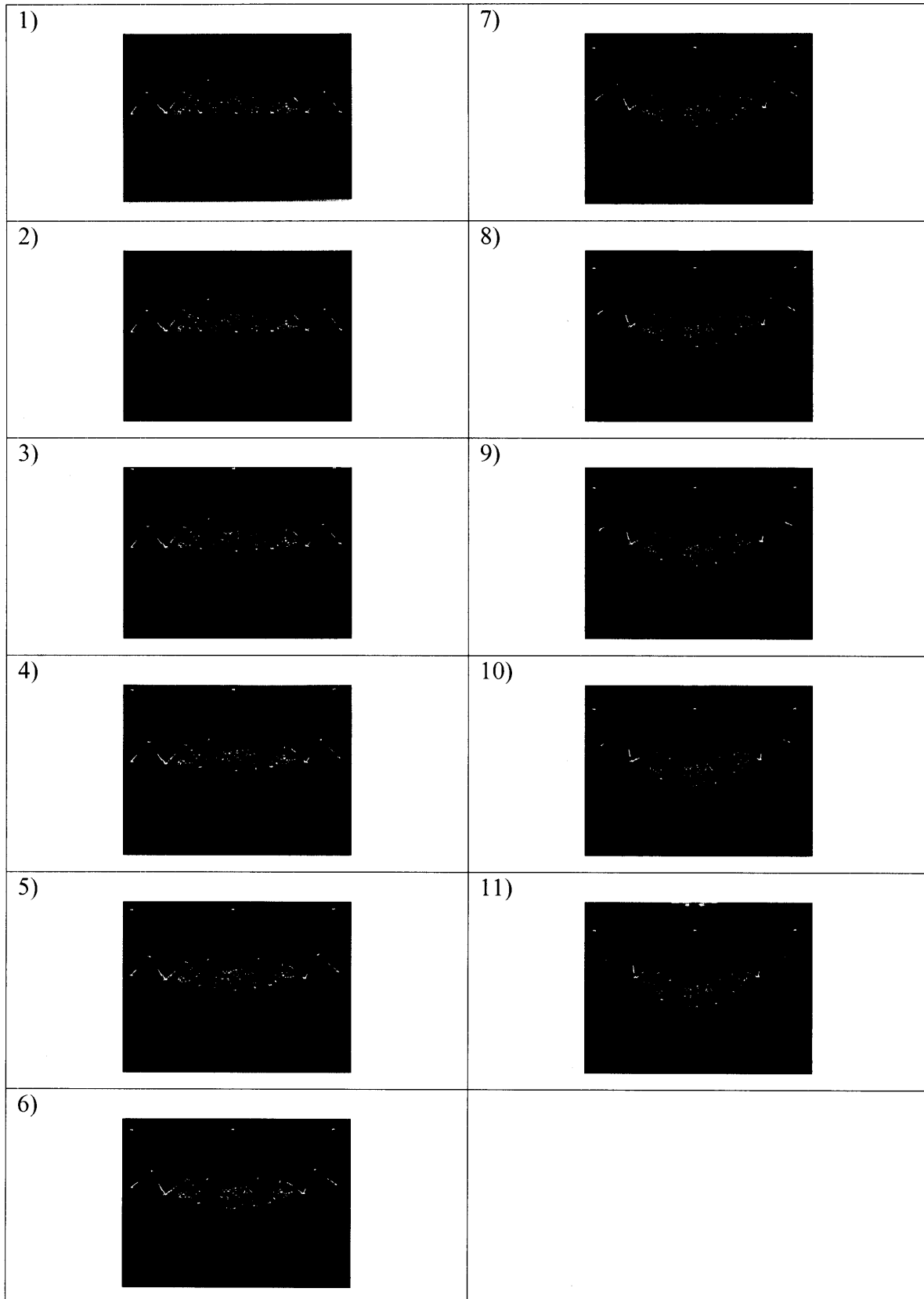
4 Point Hexagonal Triangle with Polymeric Foam













4 Point Diamond Square with Alporas Metal Foam

1) 	7) 
2) 	8) 
3) 	9) 
4) 	10) 
5) 	11) 
6) 	

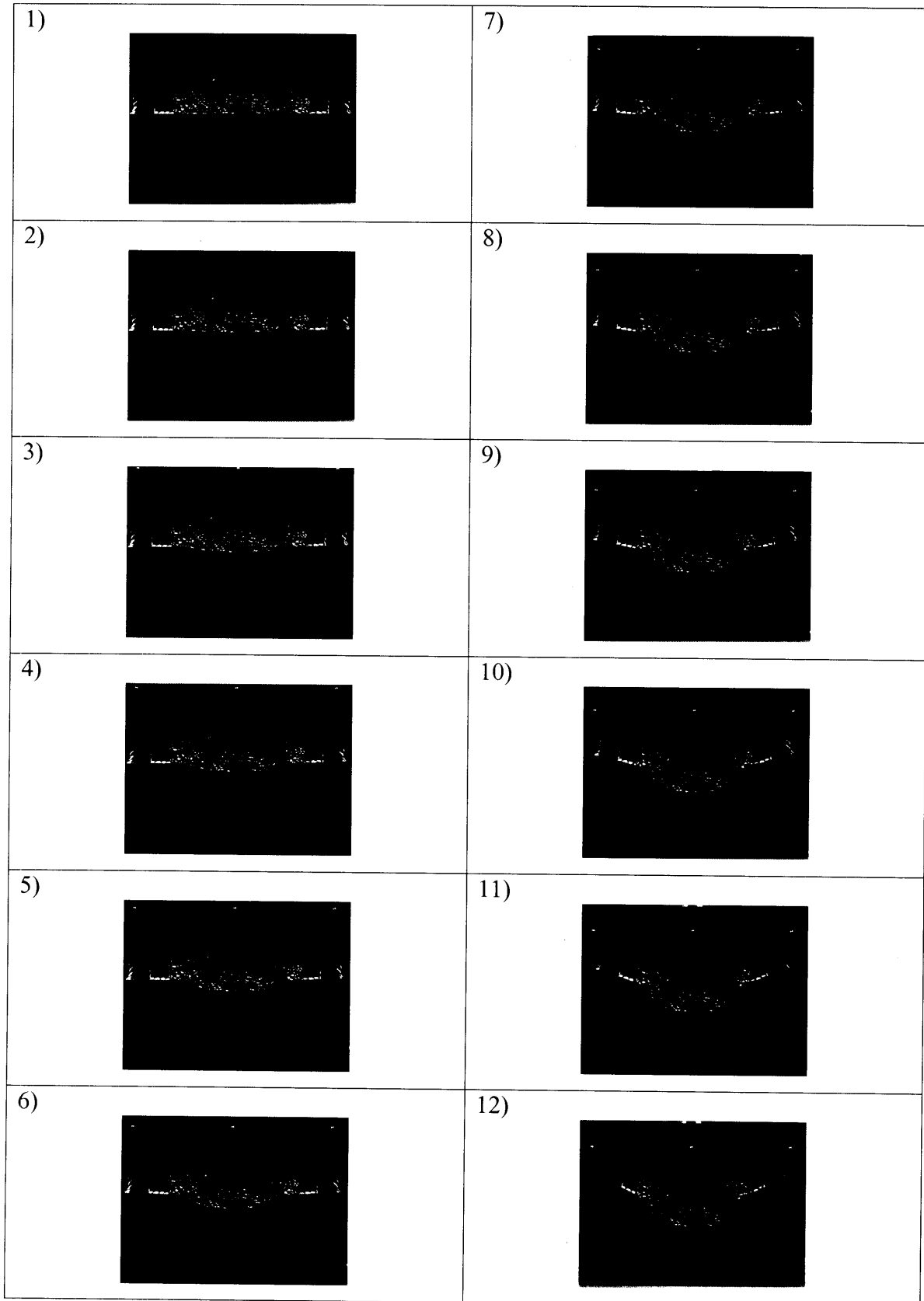
4 Point Bend Diamond Triangle with Defect with Alporas Metal Foam











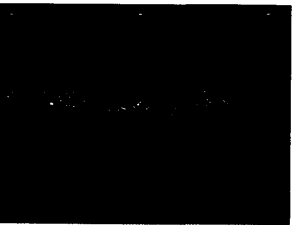
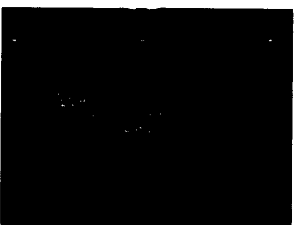

4 Point Bend Diamond Triangle with Alporas Metal Foam

1) 	7) 
2) 	8) 
3) 	9) 
4) 	10) 
5) 	
6) 	

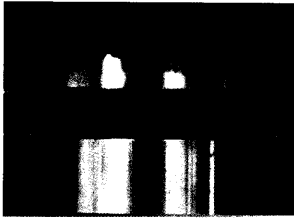
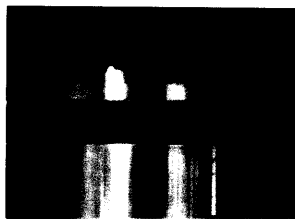
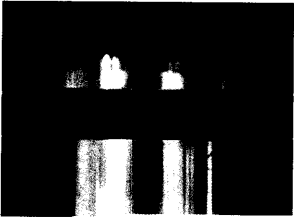

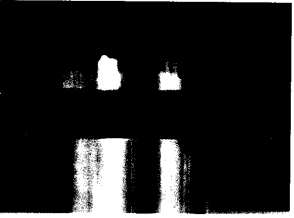

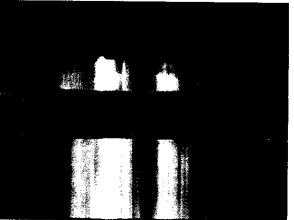
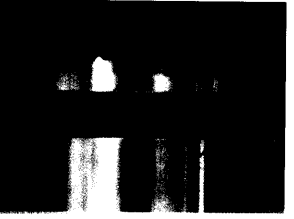

4 Point Bend Hexagonal Square with Defect with Alporas Metal Foam



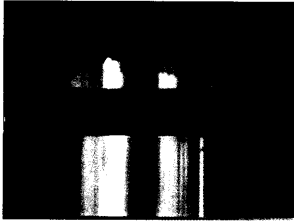
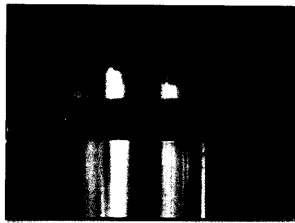
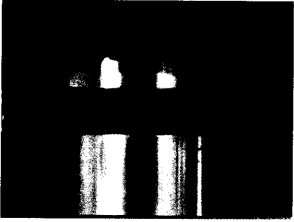
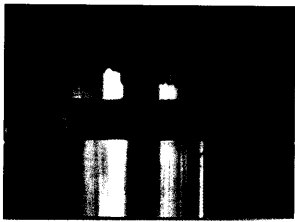
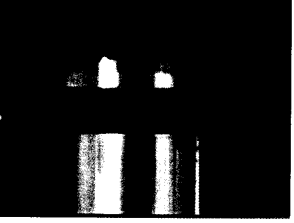
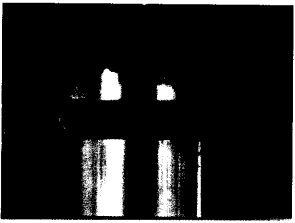
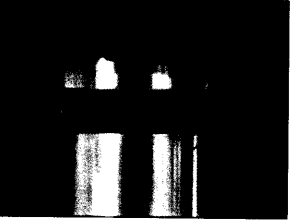
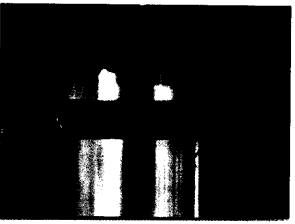
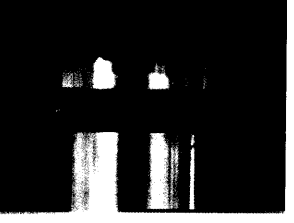
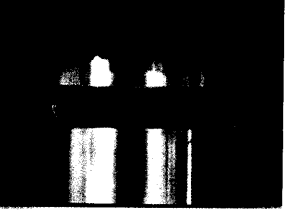
4 Point Bend Hexagonal Triangle with Defect with Alporas Metal Foam

1) 	7) 
2) 	8) 
3) 	9) 
4) 	10) 
5) 	11) 
6) 	

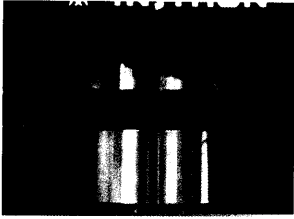
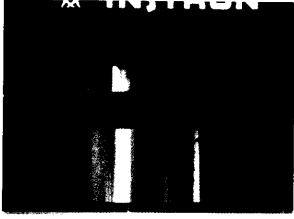
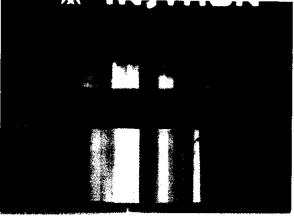
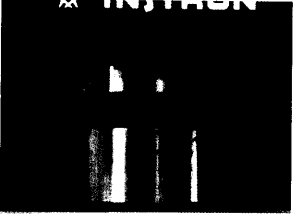
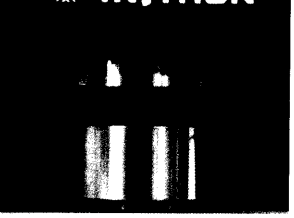
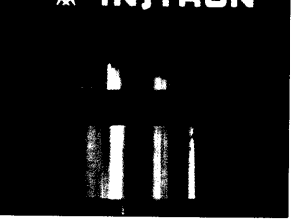
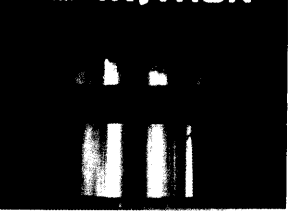
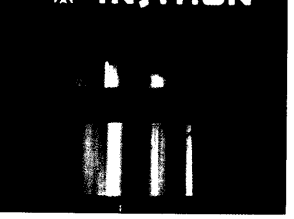
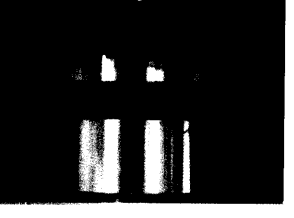
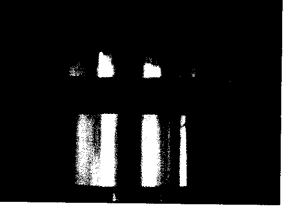
Compression Diamond Square with Defect

1) 	7) 
2) 	8) 
3) 	9) 
4) 	
5) 	
6) 	

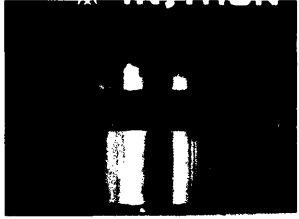

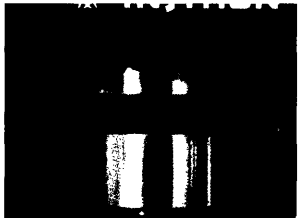

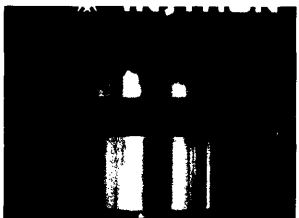



Compression Diamond Square with Defect 2

1) 	7) 
2) 	8) 
3) 	9) 
4) 	10) 
5) 	
6) 	

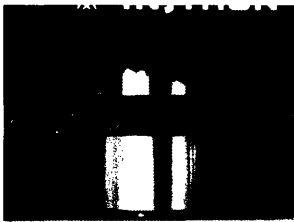
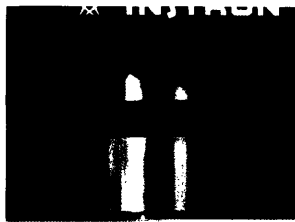
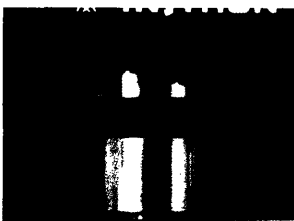

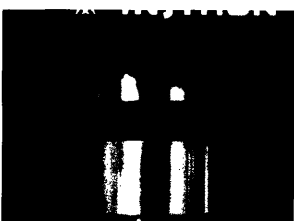
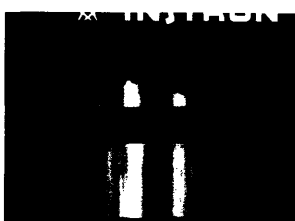
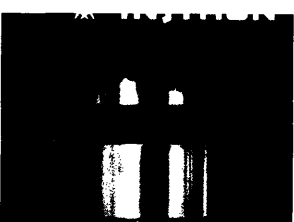
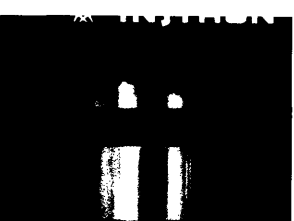
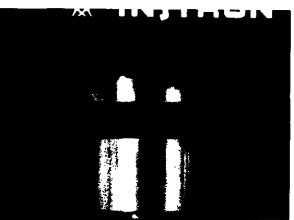
Compression Diamond Square

1) 	7) 
2) 	8) 
3) 	9) 
4) 	10) 
5) 	
6) 	

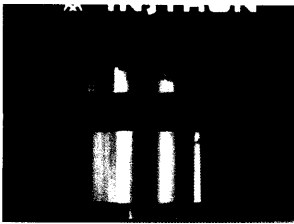
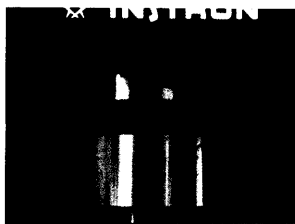
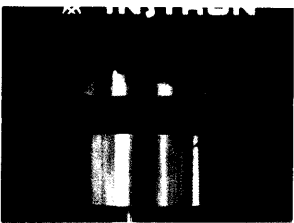
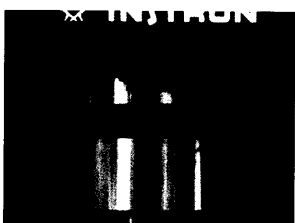
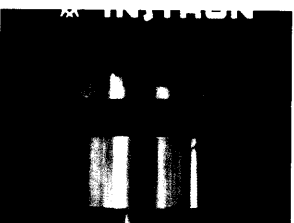




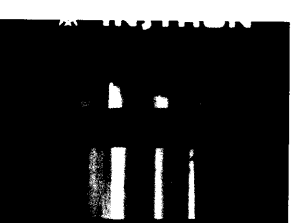

Compression Diamond Triangle with Defect

1) 	7) 
2) 	8) 
3) 	
4) 	
5) 	
6) 	

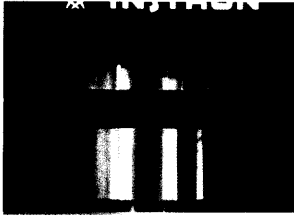

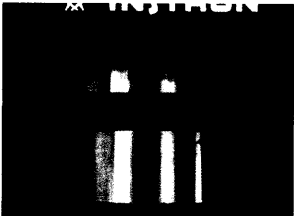
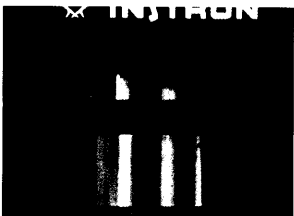
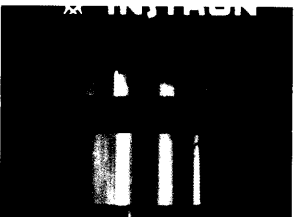

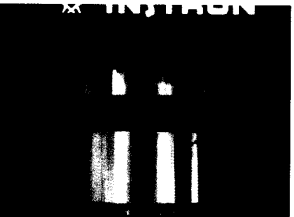
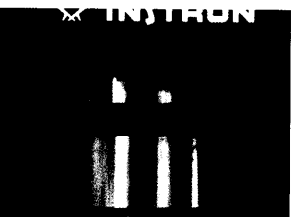

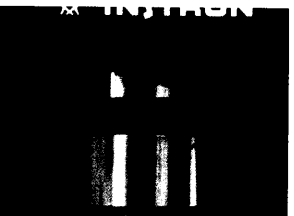

Compression Diamond Triangle with Defect 2

1) 	7) 
2) 	8) 
3) 	9) 
4) 	
5) 	
6) 	

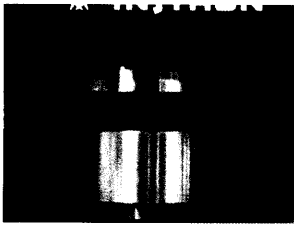
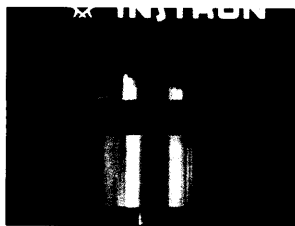
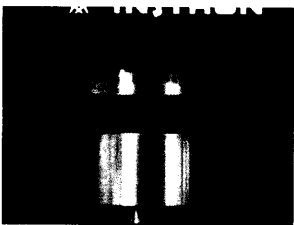


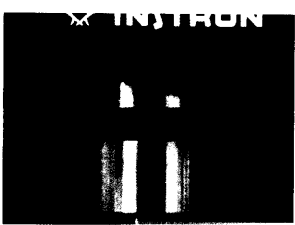
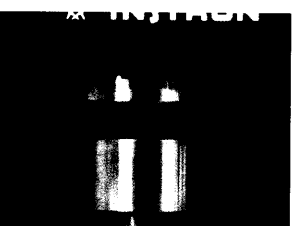

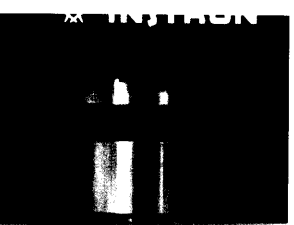
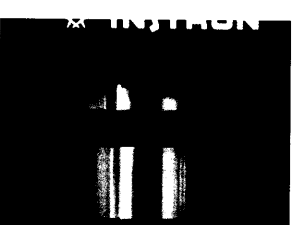
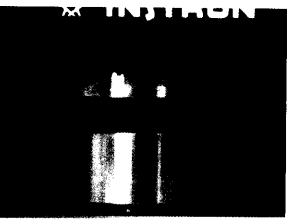
Compression Diamond Triangle

1) 	7) 
2) 	8) 
3) 	9) 
4) 	10) 
5) 	11) 
6) 	

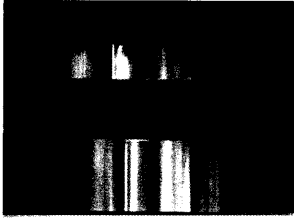
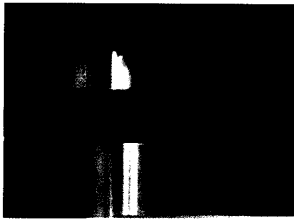
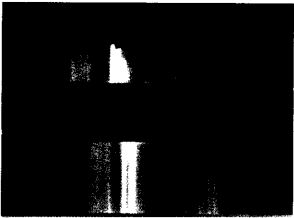
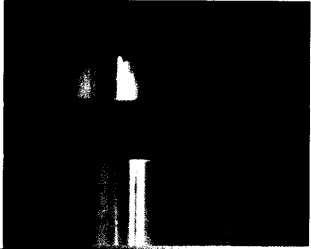
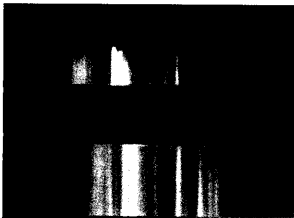
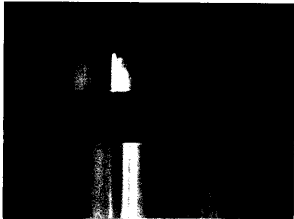
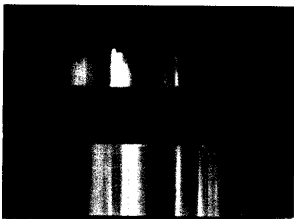
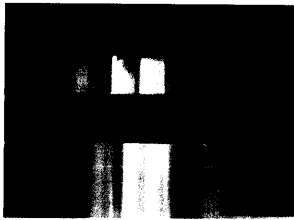
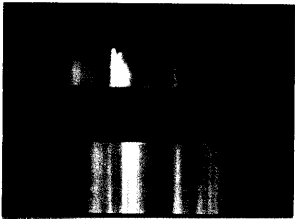
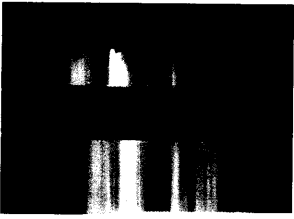
Compression Diamond Triangle 2

1) 	7) 
2) 	8) 
3) 	9) 
4) 	10) 
5) 	11) 
6) 	

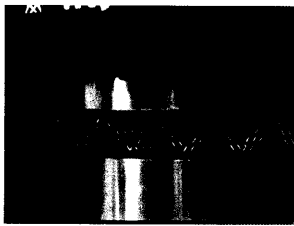
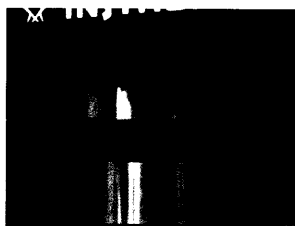
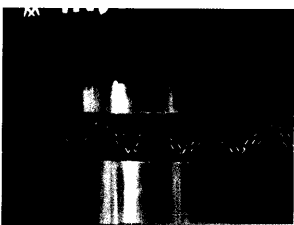
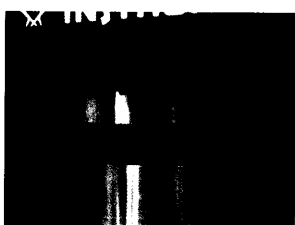


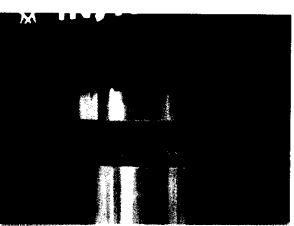
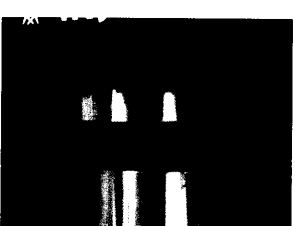

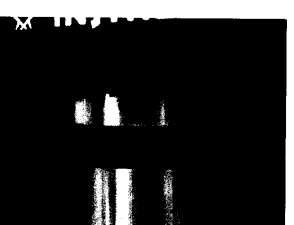
Compression Hexagonal Square

1) 	7) 
2) 	8) 
3) 	9) 
4) 	10) 
5) 	11) 
6) 	

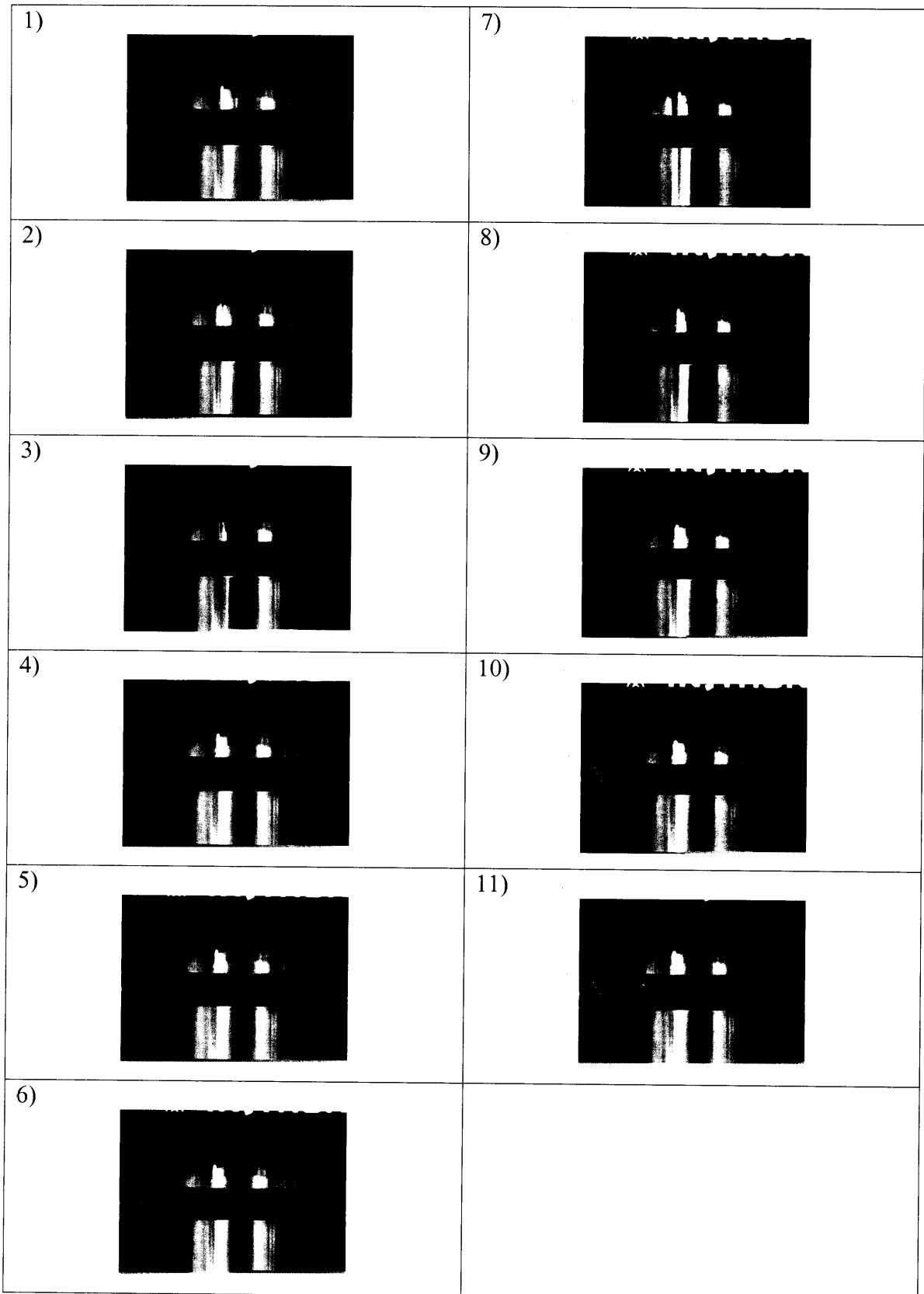
Compression Hexagonal Square 2

1) 	7) 
2) 	8) 
3) 	9) 
4) 	10) 
5) 	
6) 	

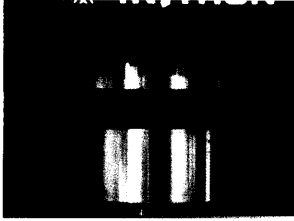
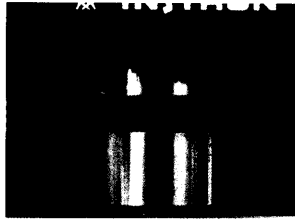
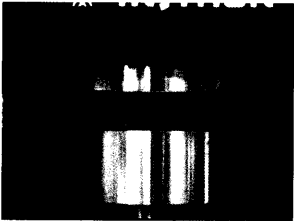
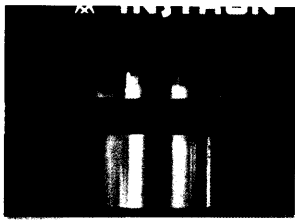
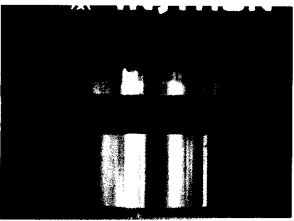
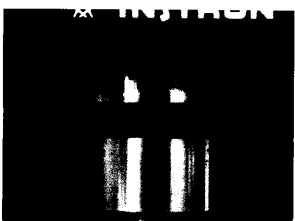
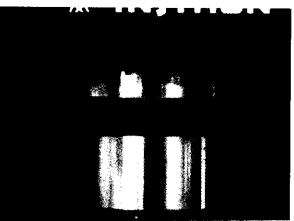



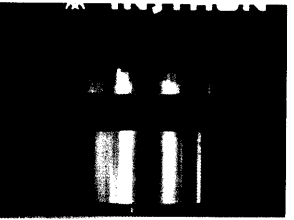
Compression Hexagonal Triangle

1) 	7) 
2) 	8) 
3) 	9) 
4) 	10) 
5) 	
6) 	

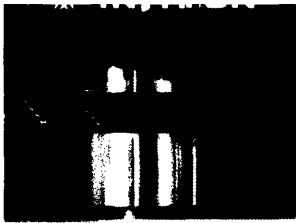
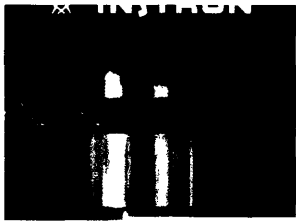
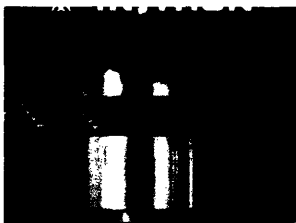






Compression Hexagonal Triangle 2





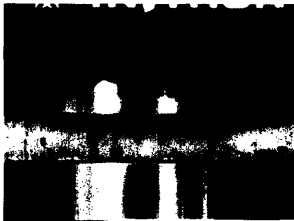






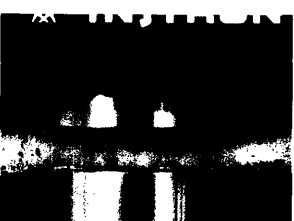
Compression Hexagonal Square with Defect

1) 	7) 
2) 	8) 
3) 	9) 
4) 	10) 
5) 	11) 
6) 	

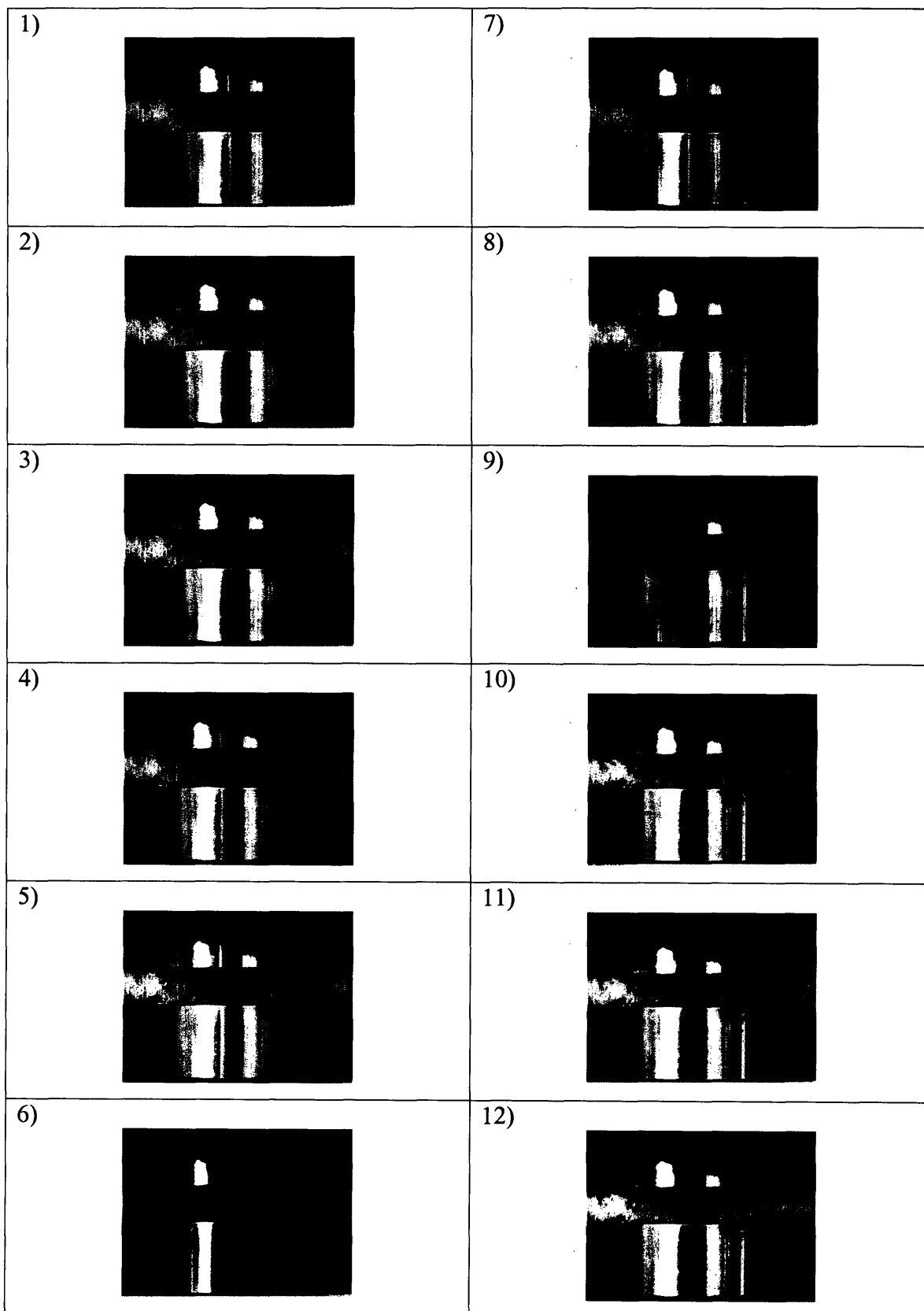
Compression Hexagonal Triangle with Defect

1) 	7) 
2) 	8) 
3) 	9) 
4) 	
5) 	
6) 	

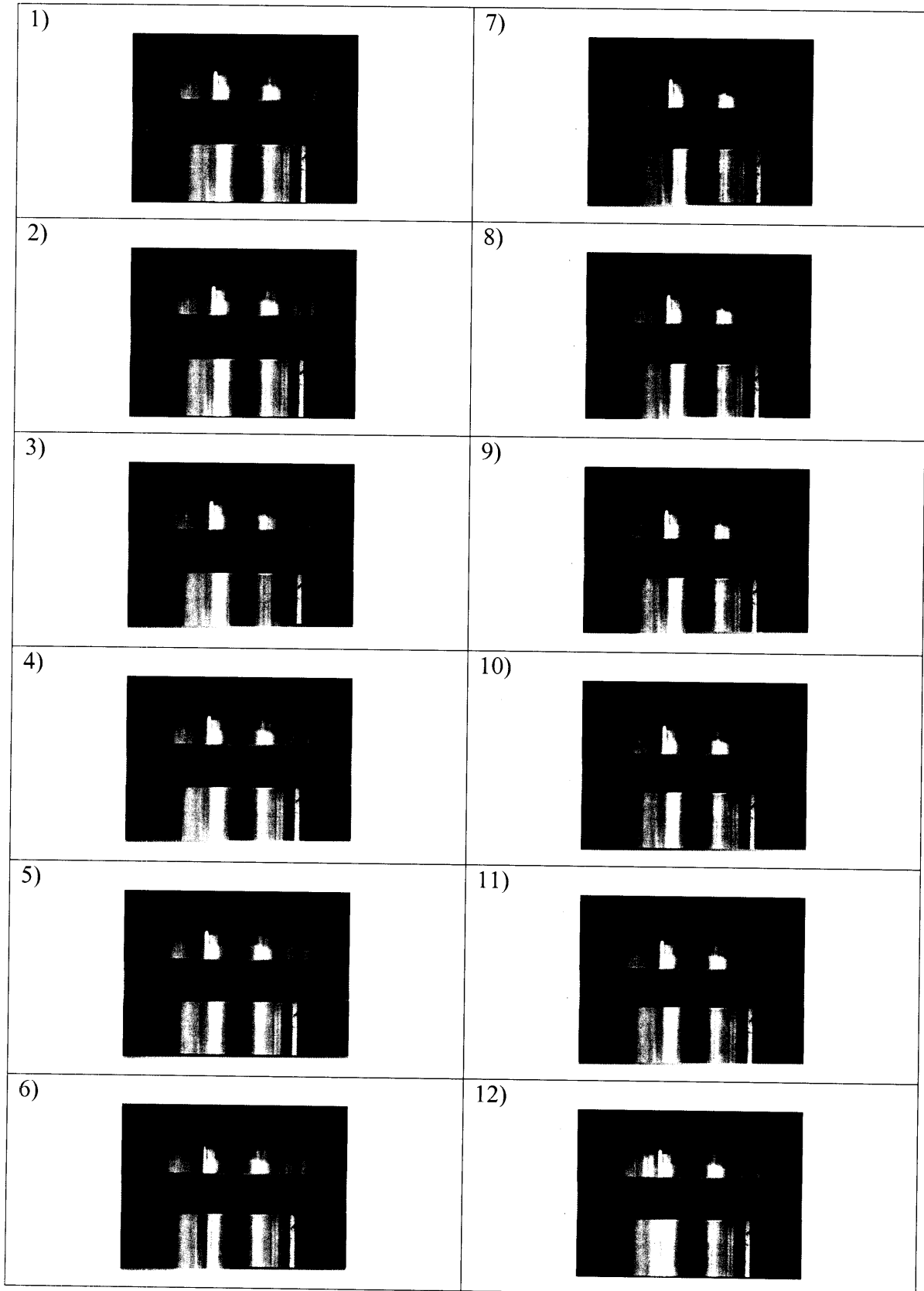
Compression Diamond Square with Defect with Polymeric Foam

1) 	7) 
2) 	8) 
3) 	9) 
4) 	10) 
5) 	
6) 	

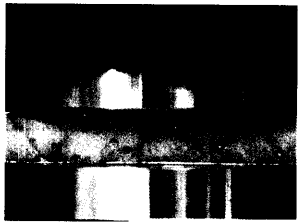
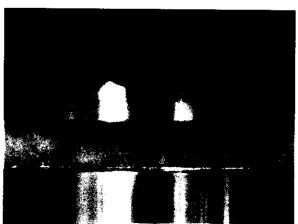
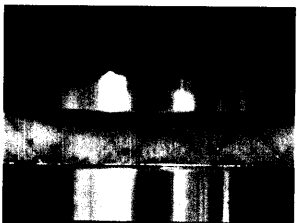

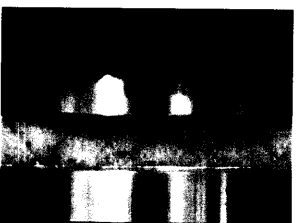


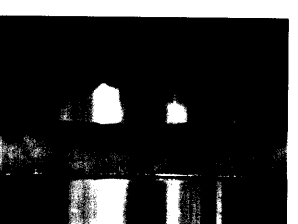

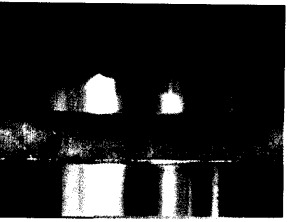
Compression Diamond Square with Polymeric Foam



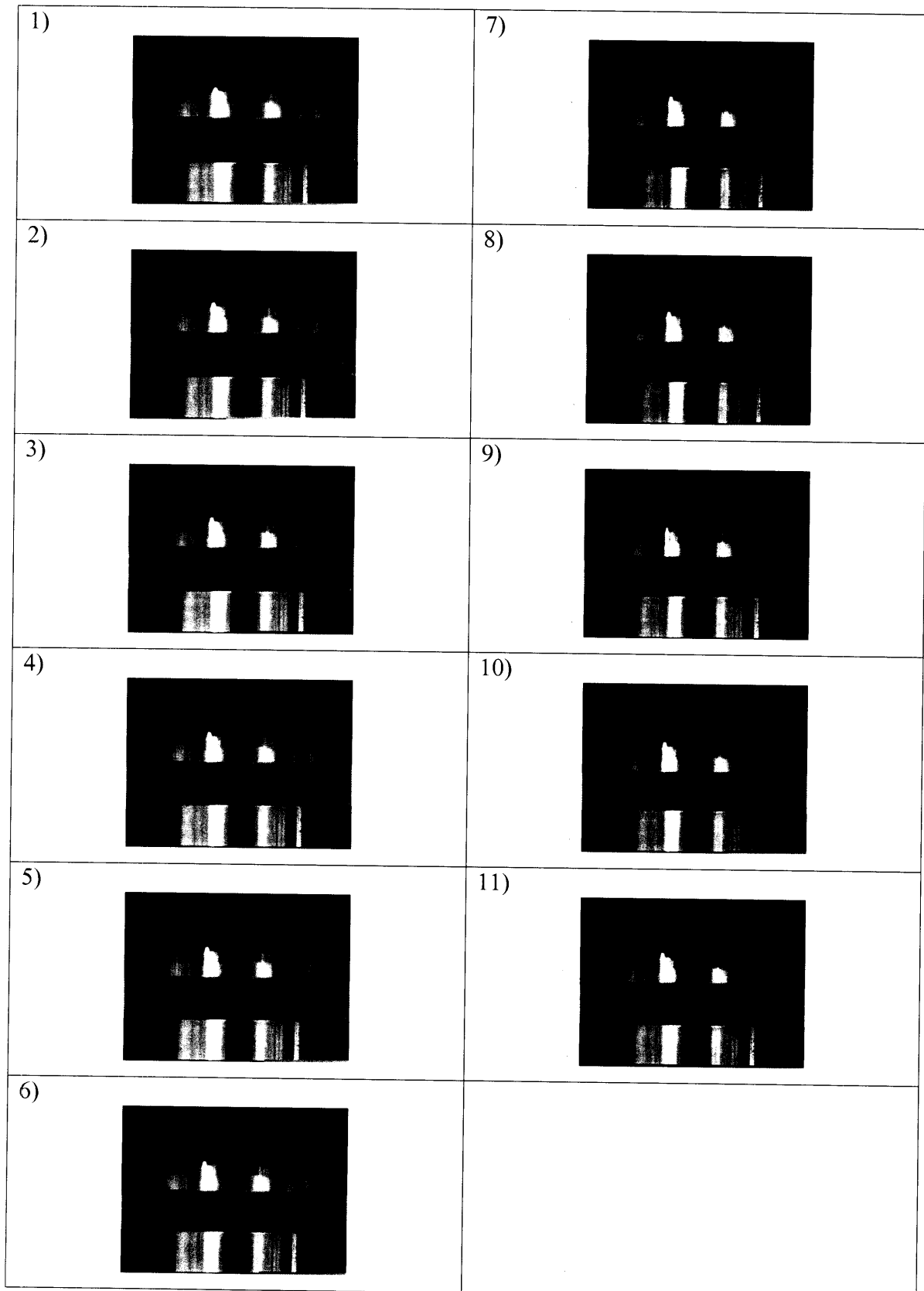
Compression Diamond Triangle with Defect with Polymeric Foam



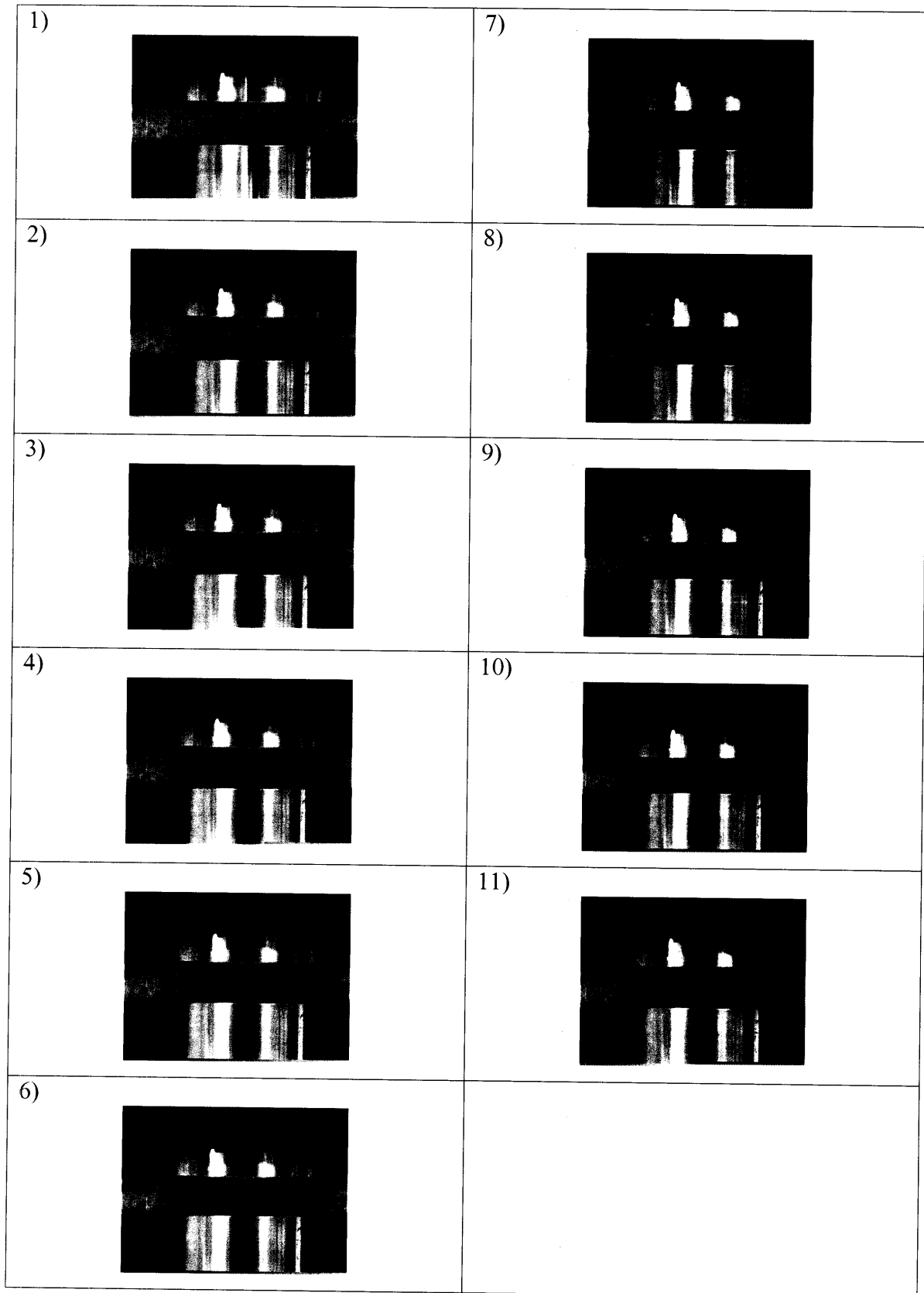
Compression Diamond Triangle with Polymeric Foam

1) 	7) 
2) 	8) 
3) 	9) 
4) 	10) 
5) 	
6) 	

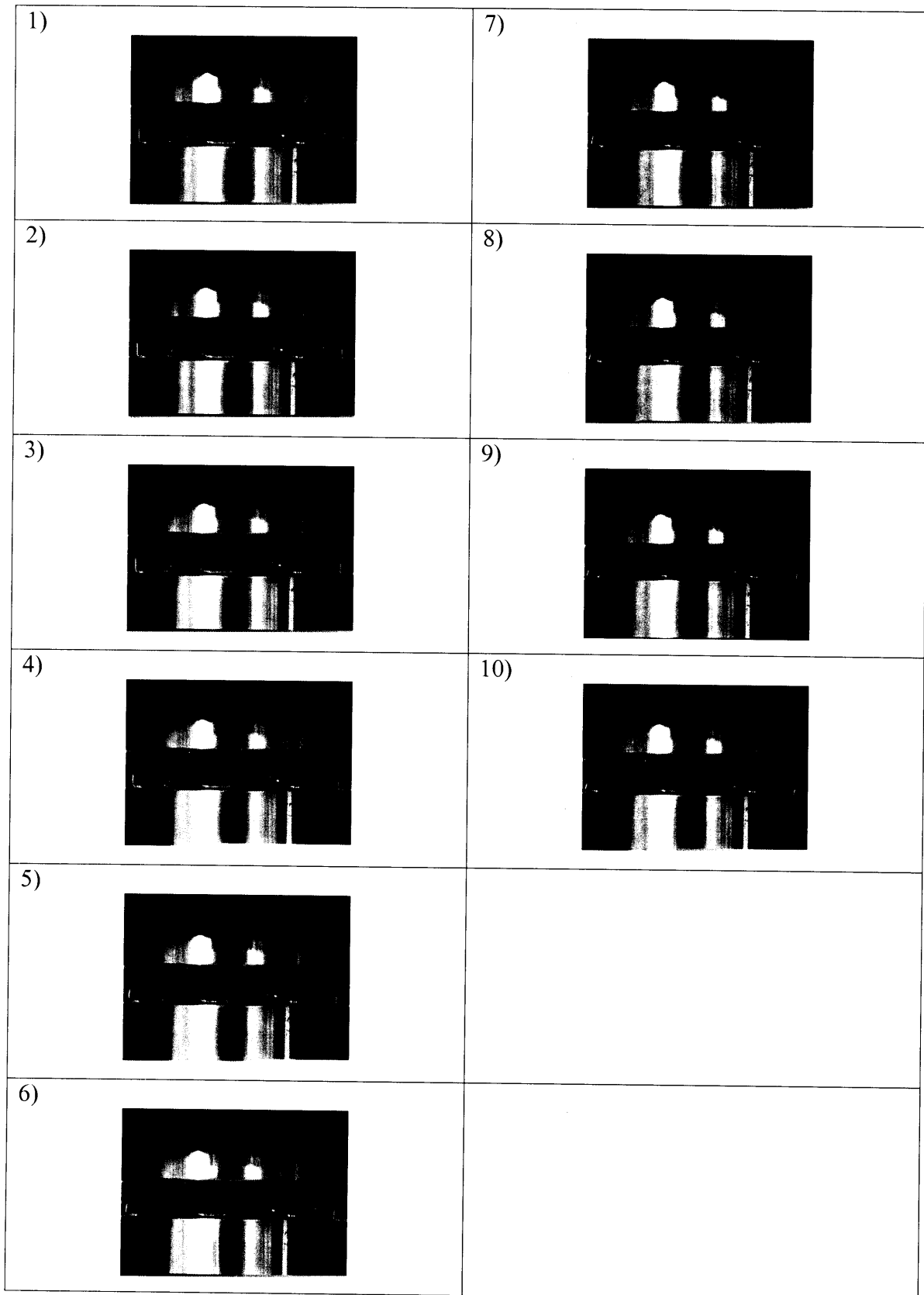
Compression Diamond Triangle with Polymeric Foam 2



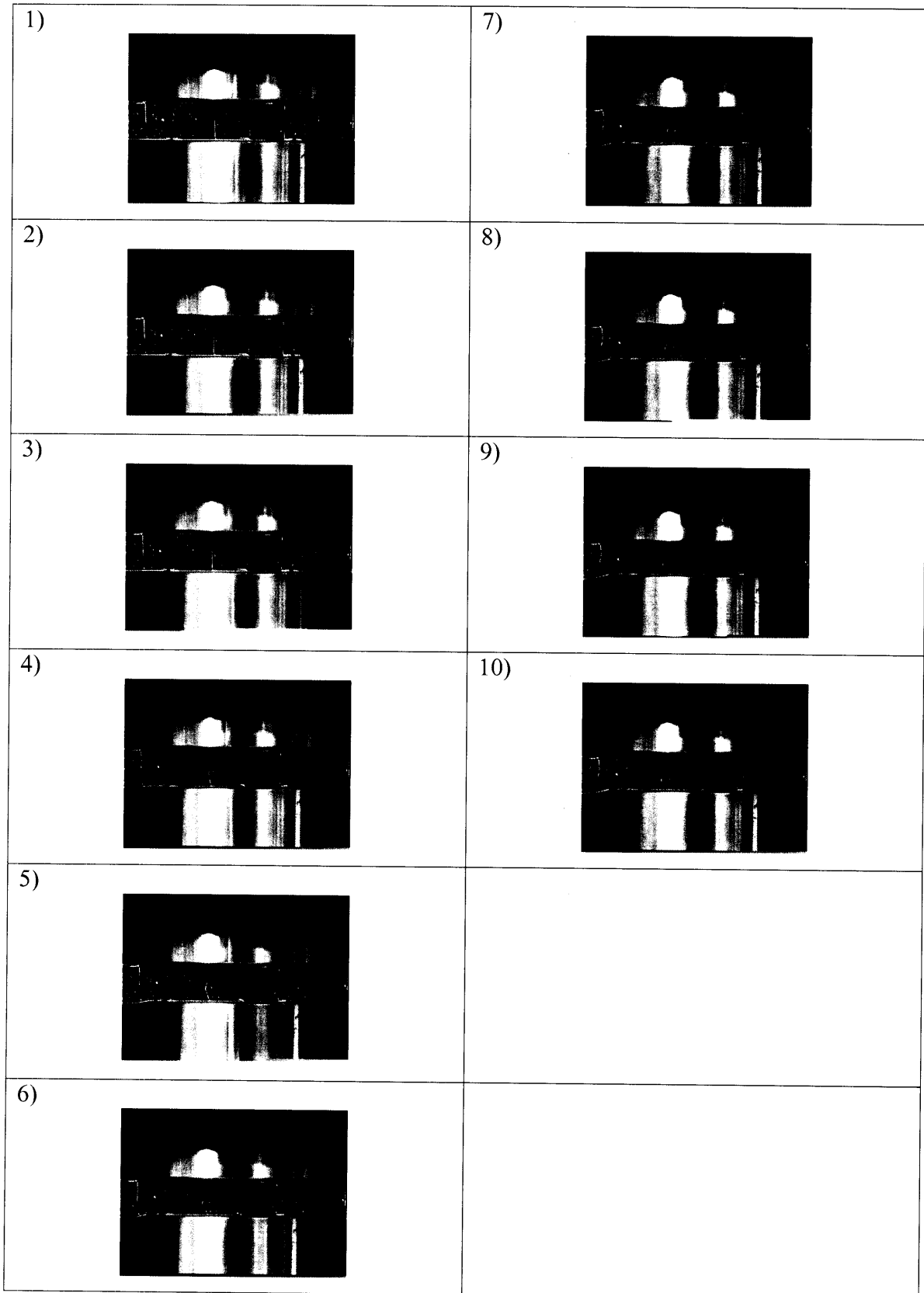
Compression Hexagonal Triangle with Polymeric Foam



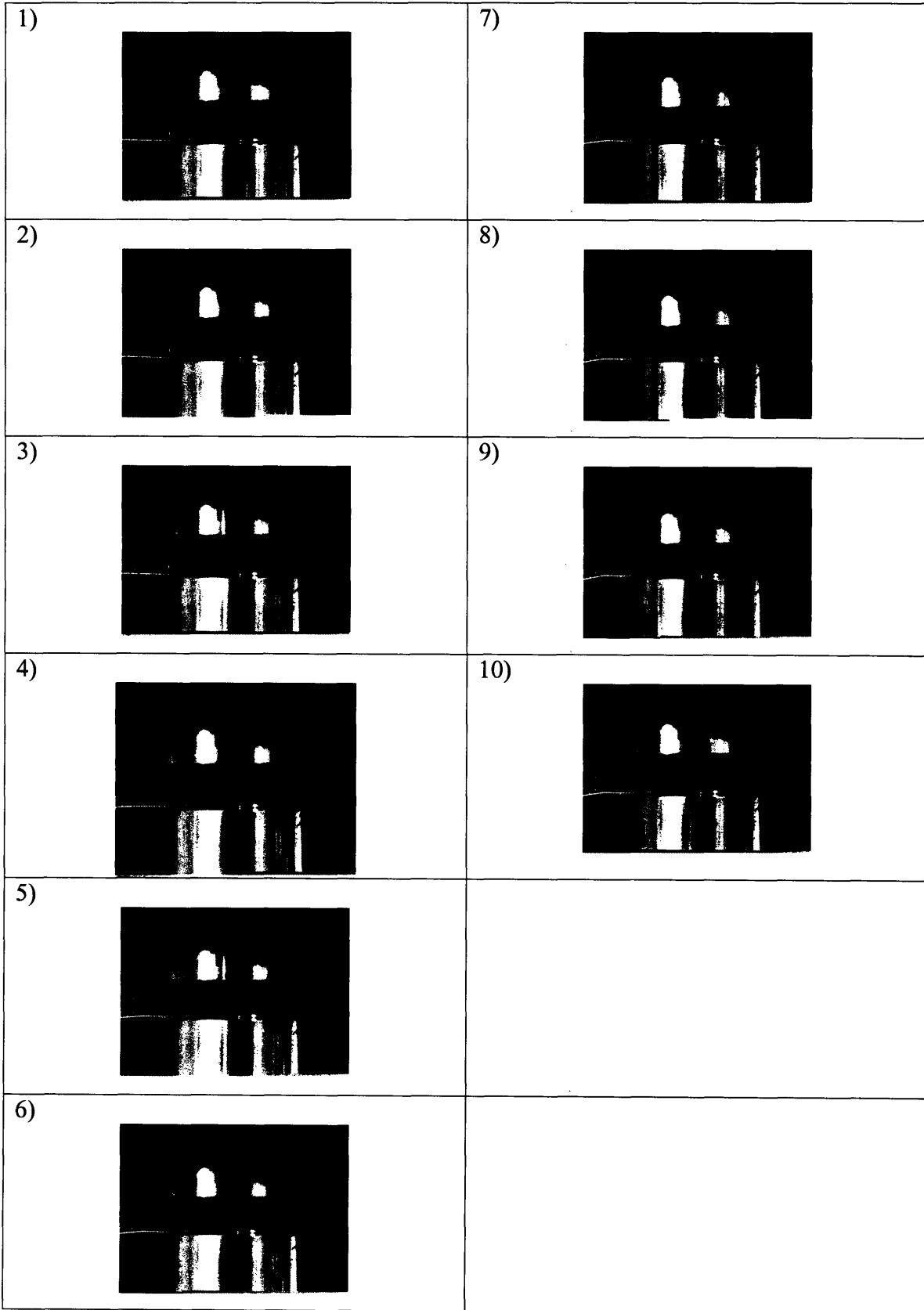
Compression Diamond Square with Defect with Alporas Metallic Foam





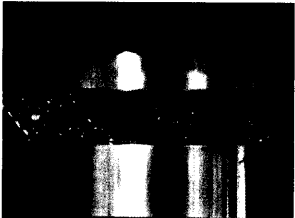
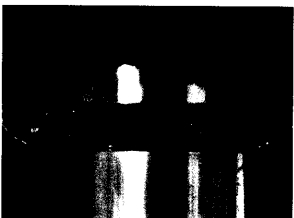

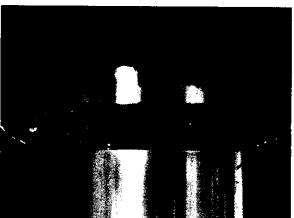
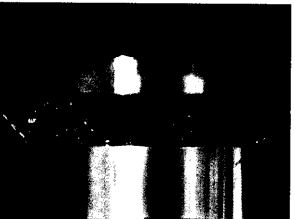

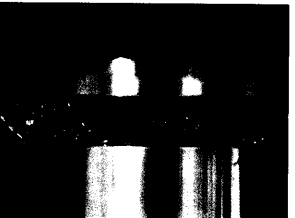
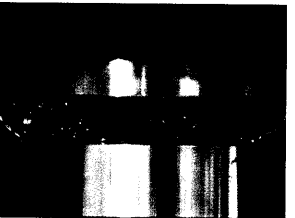
Compression Diamond Square with Alporas Metallic Foam



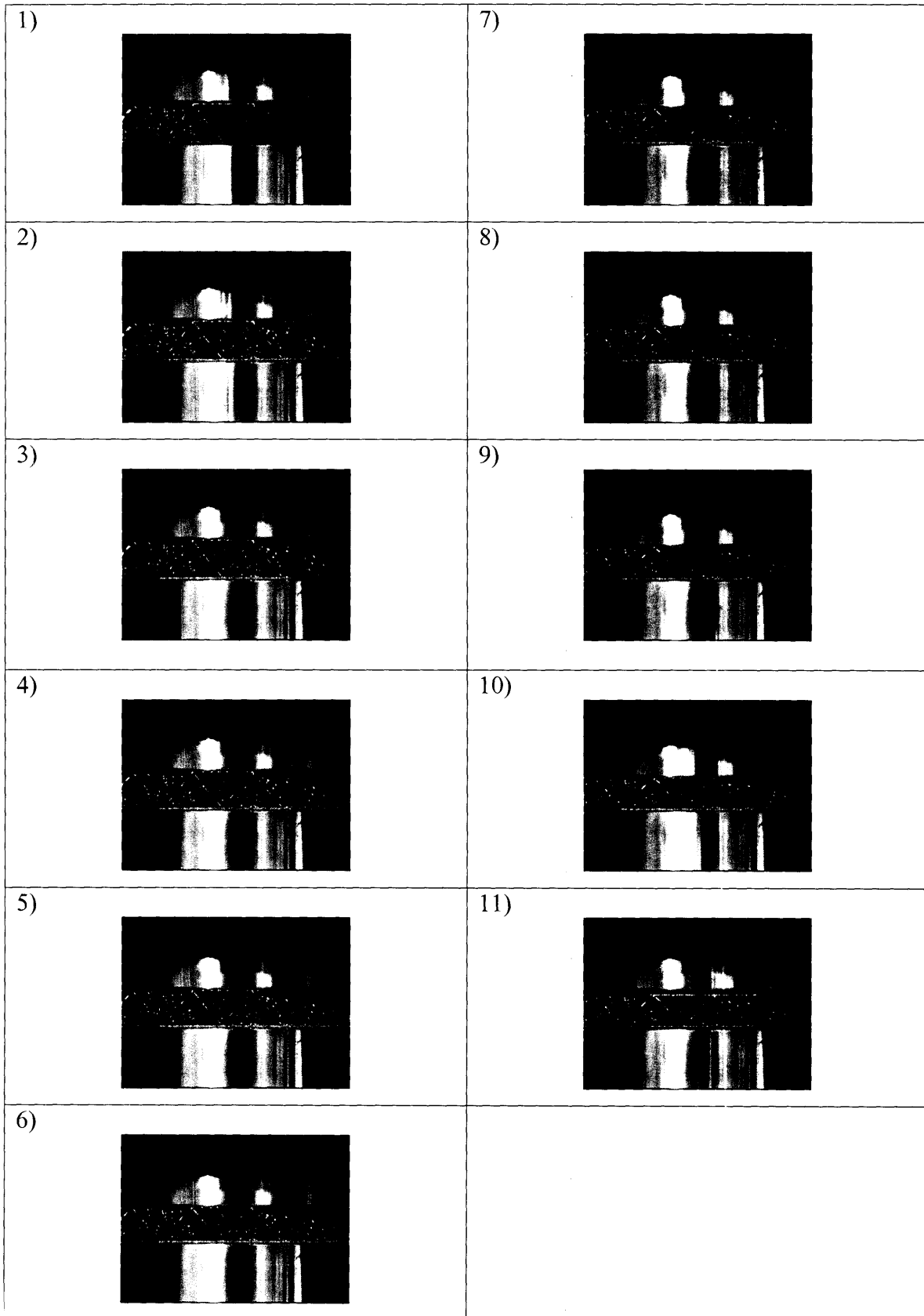
Compression Hexagonal Square with Alporas Metallic Foam



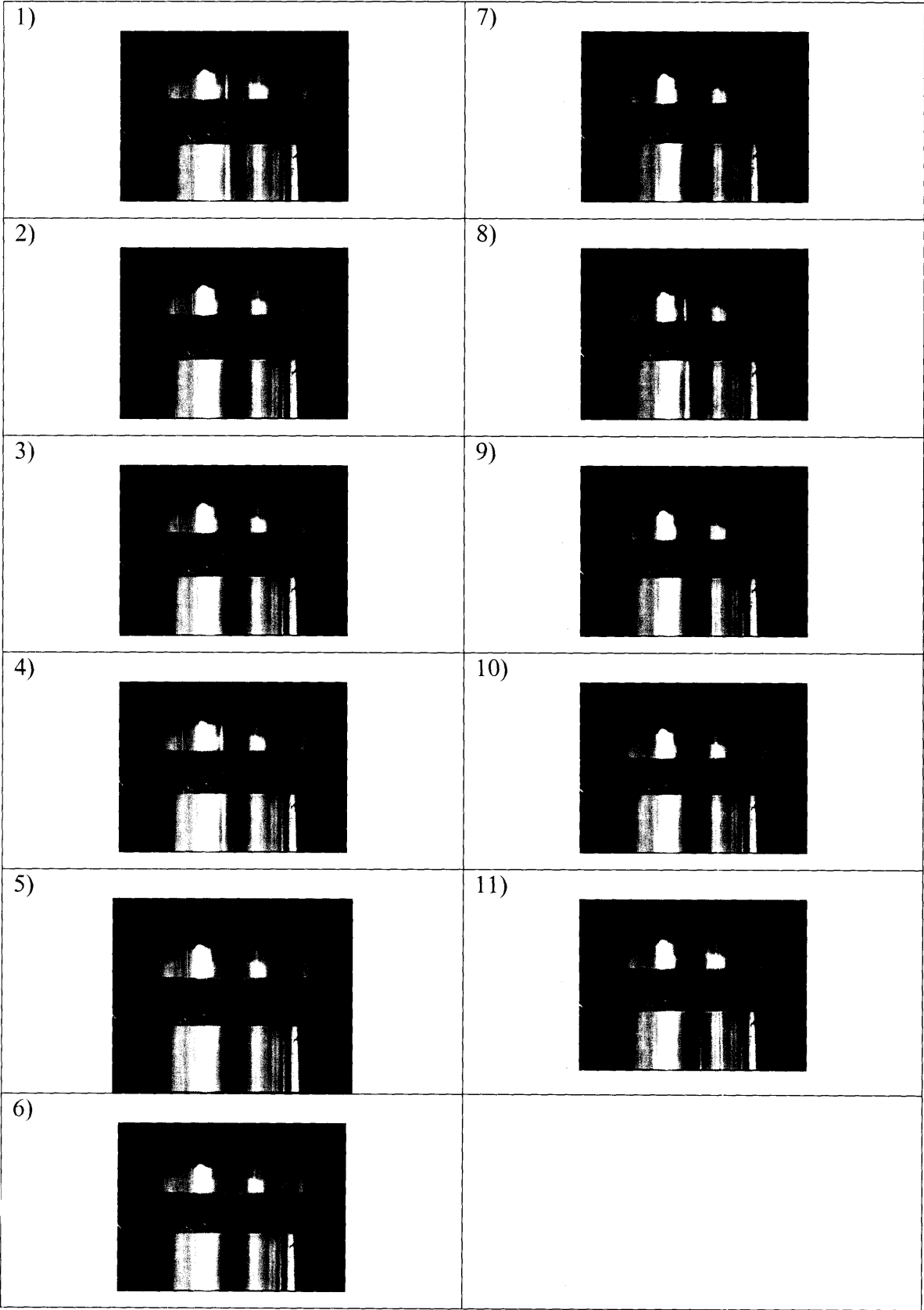
Compression Hexagonal Triangle with Defect with Alporas Foam

1) 	7) 
2) 	8) 
3) 	9) 
4) 	10) 
5) 	
6) 	

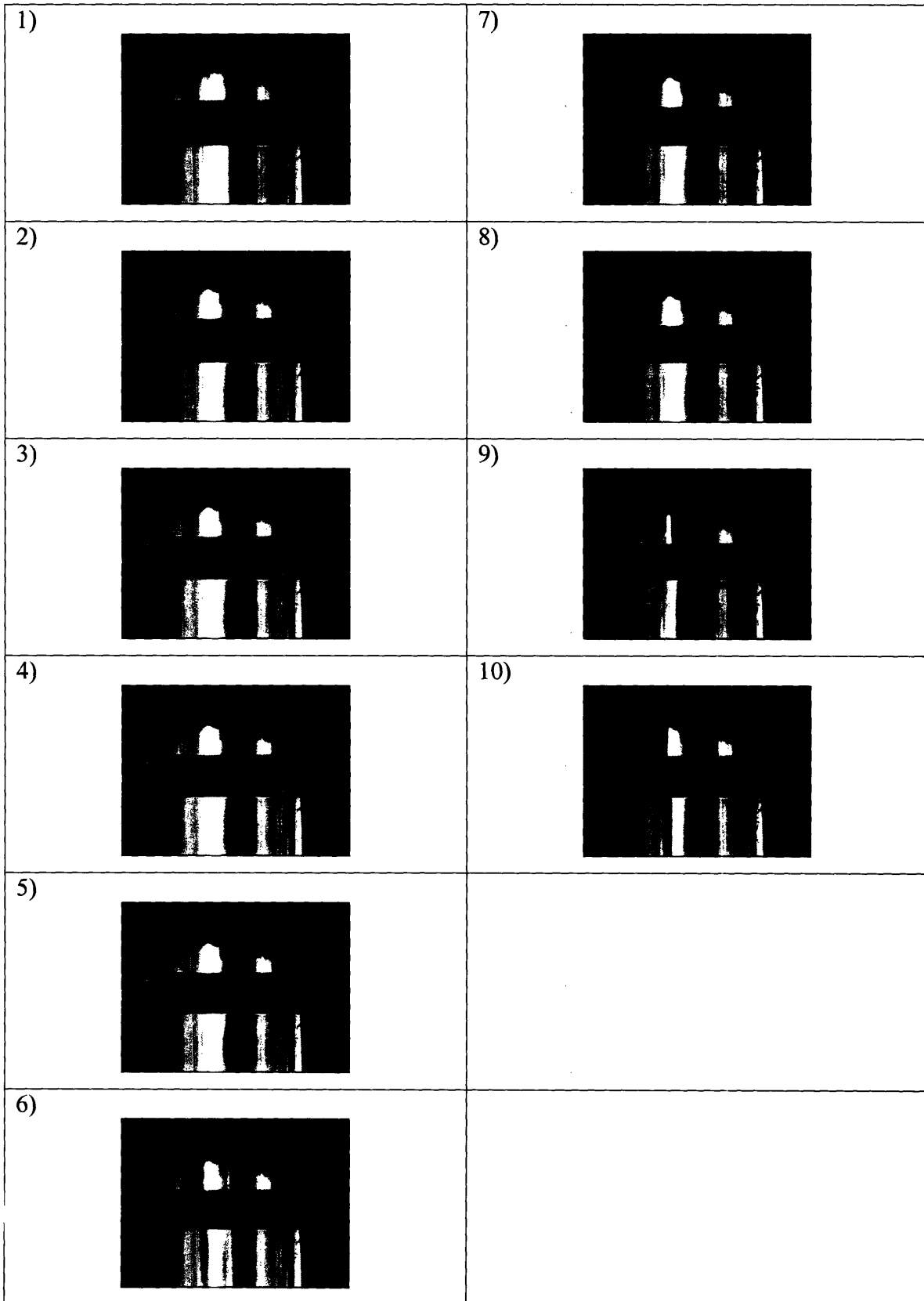
Compression Hexagonal Triangle with Alporas Metallic Foam




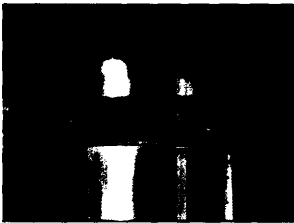
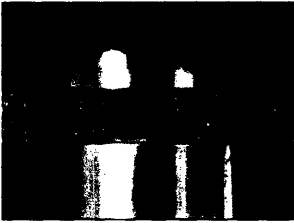
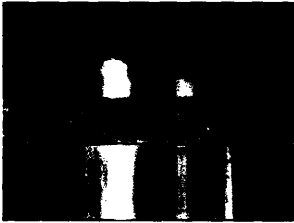
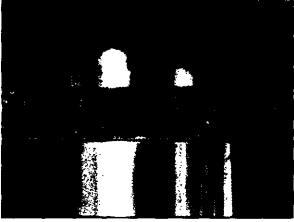
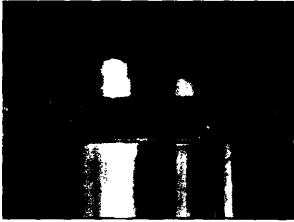
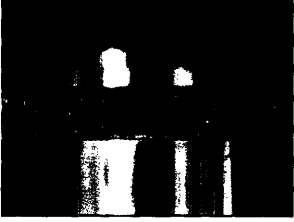
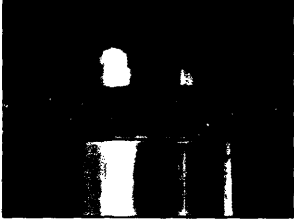
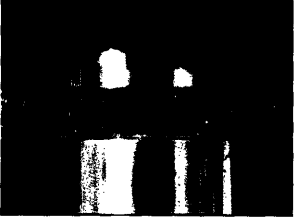
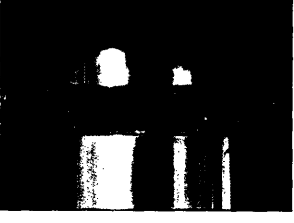
Compression Diamond Triangle with Defect with Aporas Metallic Foam



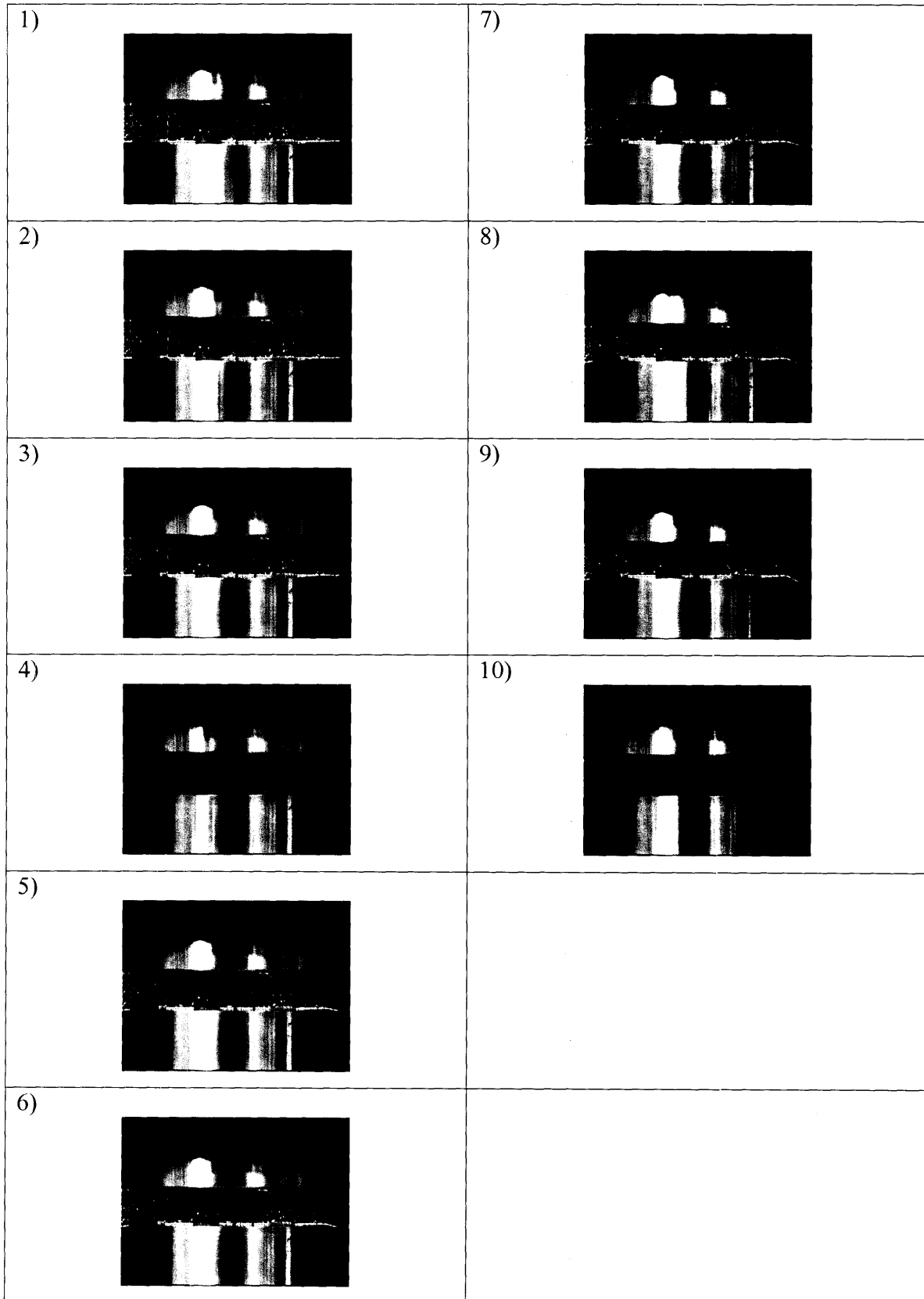
Compression Diamond Triangle with Aporas Metallic Foam



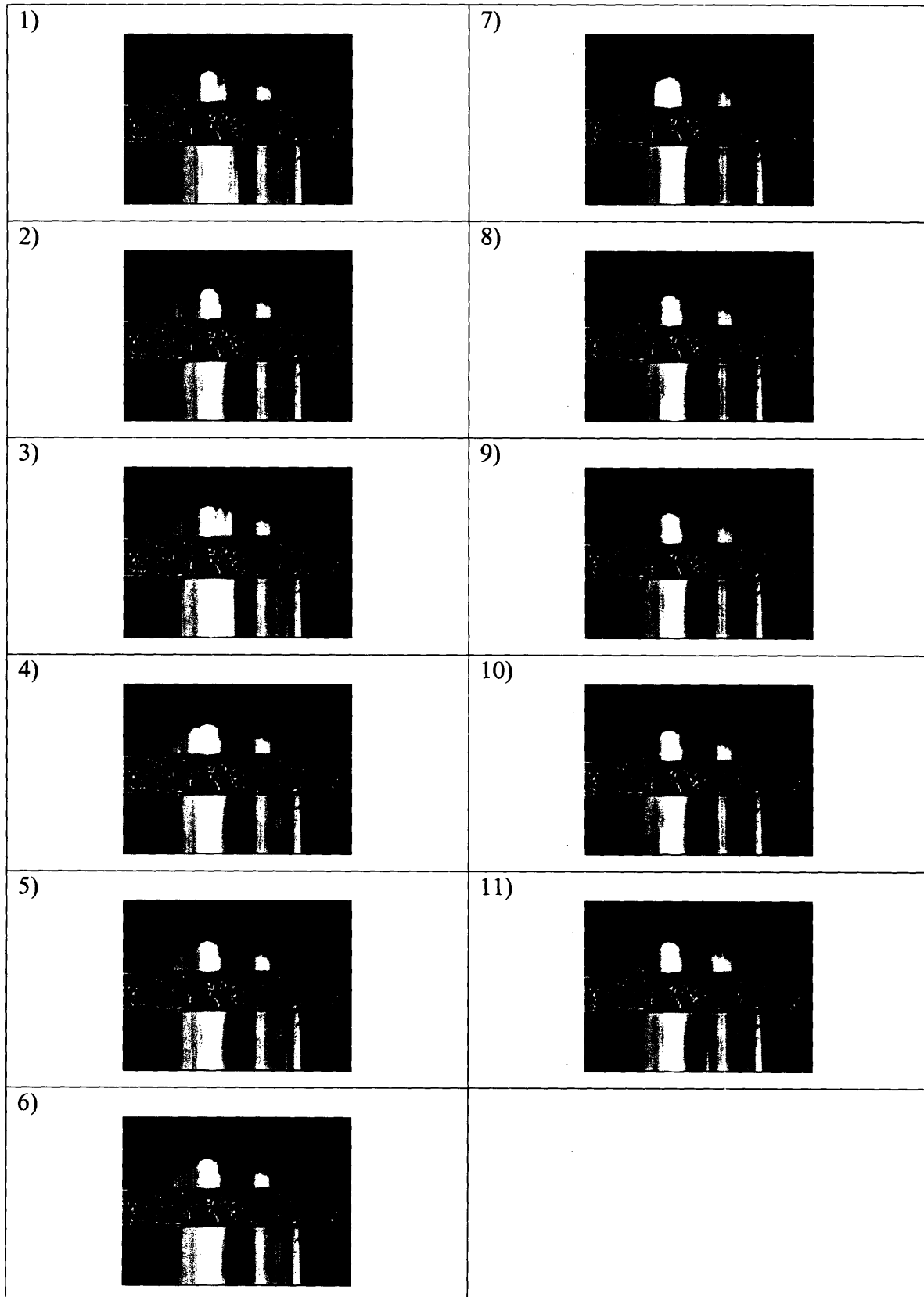
Compression Hexagonal Square with Defect with Alporas Metallic Foam

1) 	7) 
2) 	8) 
3) 	9) 
4) 	10) 
5) 	
6) 	

Compression Diamond Square with Duocel Metallic Foam



Compression Hexagonal Square with Duocel Metallic Foam



This page intentionally left blank

References

1. L.J. Gibson, M.F.A., *Cellular Solids : Structure and Properties*. 2 ed. 1997, Cambridge, UK: Cambridge University Press.
2. www.mccullagh.org/.../honeycomb-texture.jpg.
3. www.recemat.com/media/recemat.jpg.
4. Ashby, M.F., *Hybrids to fill holes in material property space*, in *Philosophical Magazine*. 2005. p. 3235-3257.
5. H.P. Degischer and B. Kriszt, e., *Handbook of Cellular Metals; Production Processing, Applications*. 2002: Wiley-VCH.
6. M.F. Ashby, A.G.E., N.A. Fleck, L.J. Gibson, J.W. Hutchinson and H.N.G. Wadley, *Metal Foams: A Design Guide*. 2000: Butterworth-Heinemann.
7. A.G. Evans, J.W.H.a.M.F.A., *Multifunctionality of Cellular Metal Systems*. *Progress in Materials Science*, 1999. 43: p. 171-221.
8. Eagar, T.W., *Chapter 16*, in *Processes of Joining Materials*. p. 16.1-47.
9. Bitzer, T., *Honeycomb Technology*. 1997: Chapman & Hall.
10. Mike Ashby, D.J., *Engineering Materials: An Introduction to their Properties and Applications*. Vol. 34. 1980, Cambridge: Pergamon Press.
11. Wadley, H.N.G., *Multifunctional periodic cellular metals*. *Phil. Trans. R. Soc. A*, 2006. 364: p. 31-68.
12. A.J.Wang, a.D.L.M., *In-Plane Stiffness and Yield Strength of Periodic Metal Honeycombs*. *Journal of Engineering Materials and Technology*, 2004. 126: p. 137-156.
13. Gibson, M.J.S.a.L.J., *The Effects of Non-Periodic Microstructure and Defects on the Compressive Strength of Two-dimensional Cellular Solids*. *Int. J. Mech. Sci.*, 1996. 39(5): p. 549-563.
14. Winkler, P.J., ed. *Materials for Transportation Technology*. EUROMAT. Vol. 1, Wiley-VCH.
15. Roush, W., *Aluminum foam*, in *Technology Review*. 2006. p. 19.
16. Banhart, J., *Metallic foams: challenges and opportunities*. MIT-Verlag Bremen, 2000: p. 13-20.
17. V.S. Deshpande, M.F.A.a.N.A.F., *Foam Topology Bending versus Stretching Dominated Architectures*. *Acta mater.*, 2001. 49: p. 1035-1040.
18. Senkov, O.N., ed. *Metallic Materials with high Structural Efficiency*. 2004, Kluwer Academic: Netherlands. 419-424.
19. Gibson, A.E.S.a.L.J., *Effects of Solid Distribution on the Stiffness and Strength of Metallic Foams*. *Acta mater*, 1997. 46(6): p. 2139-2150.
20. G.W. Kooistra, V.S.D., and H.N.G. Wadley, *Compressive behavior of age hardenable tetrahedral lattice truss structures made from aluminum*. *Acta Materialia*, 2004. 52: p. 4229-4237.
21. Wadley, D.T.Q.a.H.N.G., *Pyramidal lattice truss structures with hollow trusses*. *Materials Science and Engineering*, 2005. A(397): p. 132-137.
22. D.J. Sypeck, H.N.G.W., *Cellular Metal Truss Core Sandwich Structures*. *Advanced Engineering Materials*, 2002. 4(10): p. 759-764.

23. N. Wicks, J.W.H., *Optimal truss plates*. International J. Solids Struct., 2001. 38: p. 5165-5183.
24. S. Chiras, D.R.M., A.G. Evans, N. Wicks, J.W. Hutchinson, K. Dharmasena, H.N.G. Wadley, and S. Fichter, *Structural performance of near-optimized truss core panels*. Int. J. Solids and Struct, 2002: p. 4093-4115.
25. D.T. Queheillalt, a.H.N.G.W., *Cellular metal lattices with hollow trusses*. Acta Materialia, 2005. 53: p. 303-313.
26. J.C. Wallach, L.J.G., *Defect sensitivity of a 3D truss material*. Scripta mater., 2001. 45: p. 639-644.
27. A.-M. Harte, N.A.F.a.M.F.A., *The fatigue strength of sandwich beams with an aluminum alloy foam core*. International Journal of Fatigue, 2001. 23: p. 499-507.
28. A.G. Evans, J.W.H., N.A. Fleck, M.F. Ashby and H.N.G. Wadley, *The topological design of multifunctional cellular metals*. Progress in Materials Science, 2001. 46: p. 309-327.
29. *Alcoa Aluminum Handbook*. 1967: Aluminum Company of America.
30. *Forming Alcoa Aluminum*. 1962: Aluminum Company of America.
31. *Brazing Alcoa Aluminum* 1959: Aluminum Company of America.
32. *Aluminum's Use in transport : The Facts*, in *Aluminum Now*. Mar 2006. p. 23.
33. Eagar, T.W., *Materials Research to Meet 21st Century Defense Needs: Appendix C - "Integration of Materials Systems and Structures Development"*, National Academies Press.
34. Galanis, K., *Hull Construction with Composite Materials for Ships over 100m in length*, in *Ocean Engineering*. 2002, MIT: Cambridge.
35. *Guide for Aluminum Hull Welding D3.7:2004*. 2004, AWS.
36. Kasten, M. *Strength of Aluminum vs Strength of Steel*. 2005 [cited; Available from: www.kastenmarine.com/alumvssteel.htm].
37. Mondolfo, L.F., *Aluminum Alloys : Structure & Properties*: Butterworths.
38. Babcock, W., *The Role of Materials in Ship Design and Operation*. The AMPTIAC Quarterly. 7(3): p. 31-36.
39. *One Nimble Cat*, in *Aluminum Now*. Sep 2005. p. 8.
40. Schwartz., M., *Brazing*. Second ed. 2003: ASM International.
41. *Brazing Handbook*. 4 ed. 1991, Miami: American Welding Society.
42. *Aluminum Dip Brazing*. 2006 [cited 2/27/06]; Available from: www.mechtronics.com/f_brz.htm.
43. Vinton, B., *Aluminum dip brazing makes strong joints, strong business*. Heat Treating, 1988: p. 31-33.
44. *Wire, Cloth, Mesh, and Perforated Sheets*. [cited 10/27/2005]; Available from: www.mcmaster.com.
45. [cited; Available from: <http://www.wenescocom/hitempfurn.htm#furnacetop>].
46. *Metal foam*. Wikipedia [cited; Available from: http://en.wikipedia.org/wiki/Metal_foam].
47. Bohnart, R.J.S.a.E.R., *Welding: Principles and Practices*. Third Edition ed. 2005: McGraw-Hill.

48. ***Cambridge Engineering Selector*. 2005, Granta Design Limited: Cambridge, UK.**
49. ***Aluminum Alloys and their Classification*. [cited 12/5/06]; Available from: <http://www.ae.msstate.edu/vlsm/materials/alloys/aluminum.htm>.**
50. ***Machining Kaiser Aluminum*. First ed. 1955: Kaiser Aluminum & Chemical Sales, Inc.**

About the Author

Brian Hohmann was born and raised in Port Monmouth, New Jersey. The youngest of Henry and Barbara Hohmann's three children, he has two sisters, Colleen and Jennifer. Brian attended Port Monmouth Elementary School, Thorne Middle School, and Middletown High School North, where he was involved in numerous clubs and sports. After graduating fifth in his class from Middletown North in 2000, he attended Rutgers University in New Brunswick, NJ. Brian graduated from Rutgers in 2004 with a degree in Ceramic Engineering, winning the Michael A. Zudnick Award for highest cumulative GPA in his major. While at Rutgers the author was very active in Tau Beta Pi and Keramos. Entering into graduate school directly after college, Brian started at MIT in the Fall of 2004. At MIT, Brian has been an active member of the Graduate Materials Council, serving as Vice President in 2005. The author is also in his second year as a Graduate Resident Tutor at Simmons Hall.